

LOUGHBOROUGH
UNIVERSITY OF TECHNOLOGY
LIBRARY

AUTHOR/FILING TITLE

DIRWISH, M. E.

ACCESSION/COPY NO.

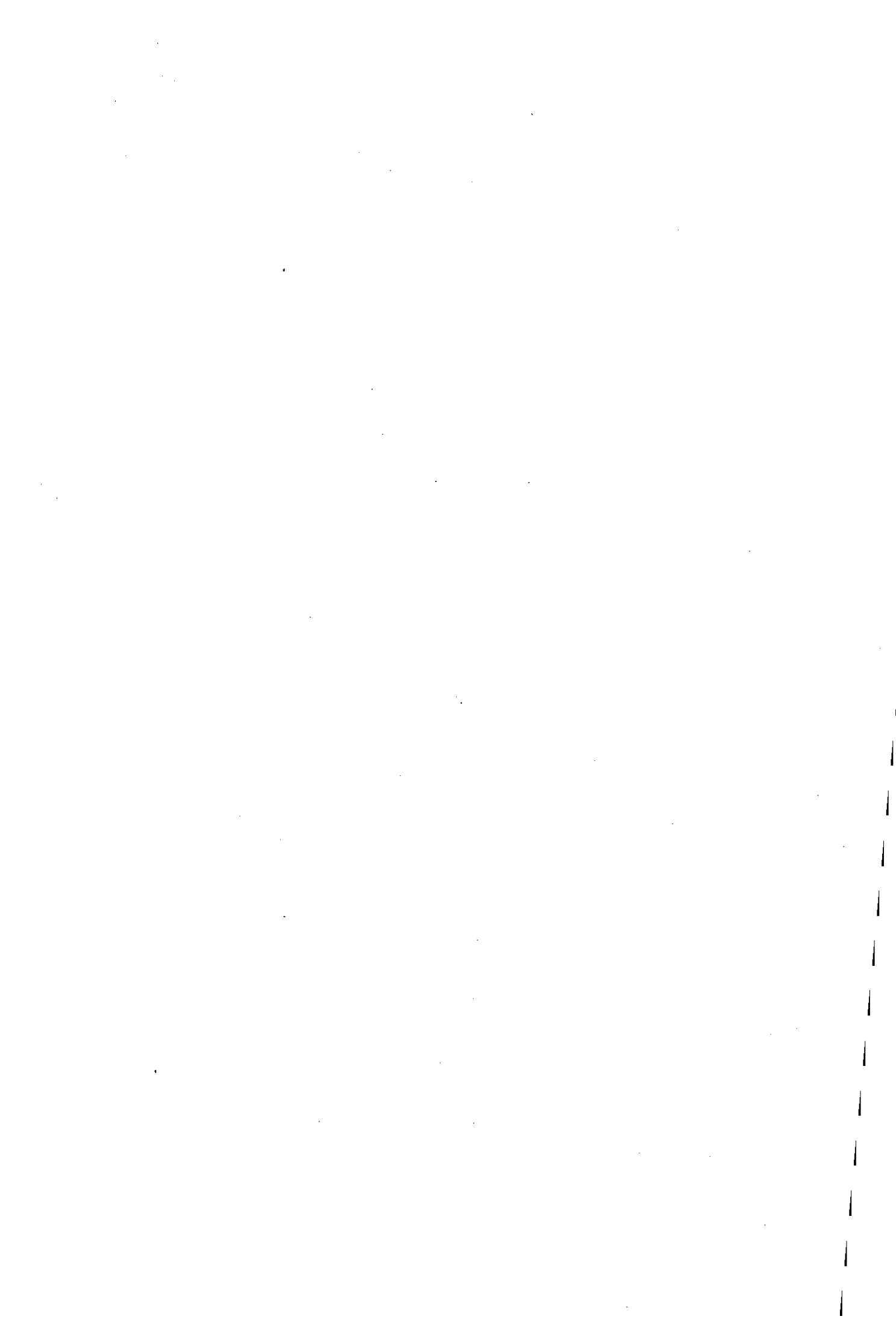
125752/01

VOL. NO.

CLASS MARK

ARCHIVES COPY

FOR REFERENCE ONLY



THE DYNAMIC MECHANICAL CHARACTERISTICS OF
VISCO-ELASTIC MATERIALS AT HIGH RATES OF
LOADING USING CYLINDRICAL SHOCK WAVES
INITIATED BY AN EXPLODING WIRE

BY

MOHAMMED EBDAN DIRWISH

B.Sc., M.Sc. (Aston).

*A Doctoral Thesis submitted in partial fulfilment
of the requirements for the award of Doctor of Philosophy
of the Loughborough University of Technology.*

July 1979.

Supervisor: L.J. Griffiths, B.Sc., Ph.D., M.Inst.P.
Department of Physics.

© by M.E. Dirwish, 1979.

| |
|--|
| Loughborough University of Technology Library |
| Date Oct 1979 |
| Class |
| Acc. No. 125752 01 |

ACKNOWLEDGEMENTS

I am deeply indebted to Dr. L.J. Griffiths for suggesting this project and for his continuing guidance and Dr. D. Parry for his consistent help during the project's period and his invaluable criticism during the thesis preparation. My thanks are also due to Professor J. Raffle for his provision of laboratory facilities and F. Hateley for his help during the project.

My thanks also to the Ministry of Higher Education in Iraq for their financial support.

Finally I would like to thank Mrs. B. Wright and Miss M. Matthews for their indispensable help in typing and preparing the thesis.

SYNOPSIS

A study of the properties of visco-elastic materials has been made by observing their response to large amplitude stress waves propagated in cylindrical specimens. The experimental work has been concerned with the production of shock waves resulting from exploding a wire inside a hollow cylinder; the propagation of these waves radially outwards within the cylindrical specimen and the response of the material to this loading. The explosion produced by discharging a high voltage (20 - 40 kv) capacitor across the ends of the wire creates a high intensity shock wave which propagates radially outwards towards the cylinder wall. Radial symmetry is to be expected in this case and the strong cylindrical blast waves which are produced have been studied by optical methods, mainly the schlieren technique using a high speed image converter camera. The results obtained of the position and velocity of the shock front as a function of time show a remarkably good agreement with results of the blast wave theory for a cylindrical shock wave.

An investigation of the efficiencies of the explosions for discharge voltages in the range 25 - 35 kv for copper wire showed that a diameter of 0.559 mm (i.e. SWG 24) gave the greatest efficiency and also produced the highest blast-wave pressure inside the cylinder. The efficiency drops rapidly as the wire diameter is either increased or decreased.

The blast wave pressure was found by two different methods:

Firstly, by measuring the velocity of the blast wave so that a theoretical value of pressure could be found from a table devised

by Law and Bristow , and

Secondly, by measuring the pressure directly using a pressure bar technique originally devised by Hopkinson. Excellent agreement was found between the experimental and calculated pressure values. In addition the measured rise time of the output signal from the bar compares well with theoretical predictions of Davies.

The pressure-time history found from the experimental results have been used in a theoretical treatment concerned with the calculation of the response of elastic specimens which was developed by Mehta and Davids.

COMMONLY-OCCURRING SYMBOLS

| | |
|------------|---------------------------------|
| a_0 | Velocity of sound in air. |
| a | Pressure bar radius. |
| c | Wave Velocity. |
| E | Young Modulus. |
| I | Current. |
| k | Bulk Modulus. |
| K | Piezo-electric strain constant. |
| M | Mach Number. |
| n | Refractive index. |
| P | Pressure. |
| R | Shock Wave Radius. |
| R_i | Cylinder Inner Radius. |
| t | Time. |
| u | Displacement. |
| U | Shock-wave Velocity. |
| v | Particle Velocity. |
| ρ | Density. |
| μ | Rigidity Modulus. |
| ϵ | Strain. |
| σ | Stress. |
| γ | Specific Heat Ratio. |
| ν | Poisson's Ratio. |

TABLE OF CONTENTS

| | <u>Page</u> |
|--|-------------|
| CHAPTER 1 - INTRODUCTION AND LITERATURE SURVEY. | |
| 1.1 Introduction. | 1 |
| 1.2 Type of Stress Waves. | 1 |
| 1.2.1 Elastic Waves. | 2 |
| 1.2.2 Plastic Waves. | 3 |
| 1.2.3 Anelastic Behaviour. | 5 |
| 1.2.4 Shock Waves in Solids. | 6 |
| 1.2.5 Shock Waves in Gases. | 7 |
| 1.3 Literature Survey. | 9 |
| 1.3.1 Elastic Waves. | 9 |
| 1.3.2 Plastic Waves. | 14 |
| 1.3.3 Shock Waves. | 17 |
| 1.3.4 Viscoelastic Waves. | 20 |
| 1.4 Conclusion. | 24 |
| 1.5 Present Investigation. | 25 |
| CHAPTER 2 - THE EXPLODING WIRE APPARATUS. | |
| 2.1 Introduction. | 27 |
| 2.2 The Charging and Control System. | 28 |
| 2.2.1 The Power Supply. | 30 |
| 2.2.2 The Capacitor and Spark-gap Units. | 30 |
| 2.2.3 Thyatron and Trigger Pulse Generator. | 32 |
| 2.2.4 The Control Units. | 32 |
| 2.3 The Exploding Wire Rig. | 33 |
| 2.4 The Charging and Exploding Procedure. | 34 |
| CHAPTER 3 - CURRENT MEASUREMENTS AND CYLINDRICAL SHOCK WAVE FROM EXPLODING WIRES. | |
| I - Current Measurements. | |
| 3.1 Introduction. | 36 |
| 3.2 Current Characteristics for Exploding Wire. | 37 |
| 3.3 Discussions. | 38 |

| | <u>Page</u> |
|--|-------------|
| II - Cylindrical Shock Wave from Exploding Wires. | |
| 3.4 Introduction. | 39 |
| 3.5 Experiment Equipment. | 41 |
| 3.5.1 The 'Imacon' Camera. | 43 |
| 3.5.2 Imacon Camera Framing Speed. | 43 |
| 3.5.3 Xenon Light Source. | 45 |
| 3.5.4 Schlieren Technique Method. | 45 |
| 3.6 Symmetry of the Exploding Wire. | 46 |
| 3.7 Velocity of the Shock Wave. | 47 |
| 3.8 Blast Wave Theory for the Shock Wave Propagation. | 50 |
| 3.9 Efficiency of the Exploding Wire. | 51 |
| 3.10 Pressure Determination. | 53 |
| 3.11 Conclusion. | 54 |
| CHAPTER 4 - MEASUREMENT OF THE PRESSURE-TIME PROFILE. | |
| 4.1 Introduction. | 56 |
| 4.2 The Hopkinson Pressure Bar. | 56 |
| 4.3 The Pressure Bar Gauge System. | 59 |
| 4.4 Calibration of the Pressure Bar. | 62 |
| 4.5 Pressure Measurements. | 63 |
| 4.6 The Rise-Time of the Output Signal from the Pressure Bar. | 65 |
| 4.7 Conclusion. | 66 |
| CHAPTER 5 - THEORY. | |
| 5.1 Introduction. | 68 |
| 5.2 Analysis of Wave Propagation in Cylindrical Coordinates. | 69 |
| 5.3 Numerical Solution. | 70 |
| 5.4 The Discontinuous Step Analysis. | 71 |
| 5.4.1 Application to Cylindrical Wave Propagation. | 71 |
| 5.4.2 Summary of Discontinuous-Step Analysis. | 74 |
| 5.5 Results and Discussions. | 77 |
| 5.5.1 Variation of Exponential Decay Pressure Pulses. | 77 |

| | <u>Page</u> |
|---|-------------|
| 5.6 Conclusion. | 79 |
| CHAPTER 6 - DISPLACEMENT MEASUREMENTS. | |
| 6.1 The Displacement Measurement System. | 80 |
| 6.1.1 The Calibration Units. | 81 |
| 6.1.2 The Optical System. | 81 |
| 6.1.3 The Light Detector. | 82 |
| 6.2 The Recording System Calibration. | 84 |
| 6.3 The Peak Displacement Measurements. | 86 |
| 6.3.1 Reproducibility. | 87 |
| 6.3.2 Peak Displacement. | 88 |
| 6.4 Wave Velocity Measurements. | 89 |
| 6.4.1 Wave Velocity Measurements from Discontinuities. | 89 |
| 6.4.2 Wave Velocity Measurements using Differences in Transit Times. | 90 |
| 6.5 Conclusion. | 92 |
| CHAPTER 7 - CONCLUSIONS AND RECOMMENDATIONS FOR FUTURE WORK. | |
| 7.1 Conclusions. | 95 |
| 7.2 Recommendations for Future Work. | 98 |
| REFERENCES. | 100 |
| APPENDIX 1 | 106 |
| APPENDIX 2 | 109 |

CHAPTER 1

INTRODUCTION AND LITERATURE SURVEY

1.1 INTRODUCTION.

The mechanical behaviour of materials at high rates of loading is of interest from two points of view. Firstly, the use of the materials under conditions where they may have to withstand sudden impacts, demands a knowledge of how their mechanical properties depend on the rate at which stresses are applied, and secondly, because the variation of the stress-strain diagram with loading rate is related to relaxation processes taking place on a microscopic scale in the material. The behaviour of many materials when deformed at high strain rates differs appreciably from that under conditions of static or quasi-static loading. The importance of studying the ways in which material properties change under dynamic loading conditions needs little emphasis. The engineer designing structures to be subjected to impacts needs some knowledge about the dynamic properties of his materials. The fabrication of metals and other materials by such processes as deep-drawing, deep-punching, high speed rolling, explosive forming, etc., requires similar information. On the other hand, the structural metallurgist concerned with correlating mechanical properties with dislocation theory needs to include a strain-rate term. Hence accurate experimental data relating stress, strain and strain-rate, accompanied by adequate theory, is required in both fields.

In testing the mechanical properties of materials at high rates of loading the rate of change of the parameters involved make it necessary to take into account the inertia of the test experiment and also that of the specimens. Consequently no method of testing can be devised which overlooks the effect of inertia when a large force is applied in a short time-that is the propagation of stress waves. Thus it is necessary to study the propagation of stress waves in solids if a thorough investigation of material properties is to be attained.

1.2 TYPE OF STRESS WAVES.

Three types of stress waves can be propagated in a solid: elastic, plastic and shock waves. These are determined for a particular material by the level of stress associated with the impact. For inelastic materials such as rubbers and plastics, viscoelastic waves can propagate while for many composites any of these four different types of wave may be produced.

1.2.1 Elastic Waves.

The basis for the theory of elastic waves is that the material obeys Hooke's law - i.e. for most solids the strain is proportional to the applied load, provided that the load does not exceed a given value which is known as the elastic limit, and the relation between stress and strain is linear. There are a number of different kinds of elastic waves which can be propagated through the solid at different velocities depending on the medium involved. The velocities of propagation of elastic waves depend amongst other factors, on the elastic constant, and density of the medium, so that the dynamic elastic constants can be determined from the velocity of propagation.

For a fluid it can be shown that only one type of stress wave can be propagated, these have a velocity equal to $(k/\rho)^{\frac{1}{2}}$, where k is the bulk modulus and ρ is the density of the media. A solid is able to withstand shear stresses and as a result it can be shown, Kolsky (1953) that for an unbounded solid two types of elastic waves are possible. 'Dilatational' or 'Irrotational' waves propagate with velocity $[(k + 4\mu/3)/\rho]^{\frac{1}{2}}$, where μ is the rigidity modulus, and 'distortional' or 'equivoluminal' waves which propagate at a velocity $(\mu/\rho)^{\frac{1}{2}}$. Dilatational waves involve changes in volume of the material but no rotation; distortional waves involve rotation but no change in volume. The particle motion in a dilatational wave is along the

direction of propagation (longitudinal wave), whereas in a distortional wave the motion is at right angles to the direction of propagation (transverse wave). In addition to these, Rayleigh waves can travel along the surface of a solid so long as their wavelength is not large compared with the lateral dimensions of the specimen.

1.2.2 Plastic Waves.

Plastic waves occur in media whose stress-strain relation has ceased to be linear. Plastic waves can be produced when the medium is elastic up to a given stress, but for stresses greater than this, flow occurs. Under these conditions an elastic wave is propagated through the medium, and this is followed by a plastic wave which travels with a lower velocity.

The first theoretical analysis of plastic wave propagation was due to Donnell (1930) for a simple impact wave travelling in one direction down an initially undisturbed rod. If the static stress-strain is assumed to apply under the dynamic conditions, each increment of stress in the wave front travels with the speed $\sqrt{E/\rho}$ where E is the tangent modulus at the stress level considered, and ρ the density. Thus for the usual form of the stress-strain relation in tension, concave to the strain axis, such a wave front spreads as it travels, each stress increment travelling more slowly than the previous ones.

The general mathematical theory of plastic wave propagation in one dimension based on an invariant stress-strain relation, devoid of strain rate influence, was developed by Karman (1942). It takes

its simplest mathematical form in terms of Lagrange coordinates based on the displacement (u) from the undisturbed position (x), with the nominal strain $\epsilon = \frac{\partial u}{\partial x}$, and the nominal stress σ . Plastic waves are then governed by

$$\frac{\partial^2 u}{\partial t^2} = c^2 \frac{\partial^2 u}{\partial x^2}, \quad c^2 = \rho^{-1} df/d\epsilon \quad (1)$$

where $\sigma = f(\epsilon)$ is the stress-strain relation. The static relation is used, although it would be possible to replace it by an invariant dynamic relation if one could be determined to provide a closer approximation to the material behaviour during wave propagation. This theory is based on the longitudinal equation of motion only, and since during the stretching of a rod lateral contraction occurs, inertia effects associated with this will modify the motion if appreciable strain variations occur for changes of (x) of the order of the rod diameter. The same theory applies for compression waves in a slab, as shown by Wood (1952), for which the displacement is in the direction of wave propagation and then limitations due to the neglect of lateral inertia do not arise. In this case, since compressibility effects dominate the stress-strain relation in the plastic range, the speed of propagation of plastic waves is much higher than for waves along rods and wires.

Solutions of equation (1) for quite general boundary and initial conditions can be obtained through the theory of characteristics which determines curves given by $dx/dt = \pm c$ along which an integral of the solution can be expressed

$$v \pm \int c d\epsilon = \text{constant}$$

where v is the particle velocity. These relations enable solutions

to be constructed numerically when wave interactions become too involved to permit analytical representation.

1.2.3 Anelastic Behaviour.

Elastic solids are assumed to behave in a completely linear manner where the components of strain are linear combinations of the components of stress. When materials are stressed beyond the elastic limit, the behaviour is then quite different and is termed 'anelastic'. Theoretical predictions are possible only if the anelastic behaviour can be specified mathematically. It is found that the way in which materials deviate from perfect behaviour varies from solid to solid. The deviations are found to be of two types. First, as a result of mechanical yielding or because the magnitude of the strain becomes comparable with unity. The simple Hookean relation between stress and strain is found no longer to be valid and the strain becomes a nonlinear function of the stress. Second, the value of the strain may cease to be a univalued function of the stress, and depends upon the particular path by which the final stress was reached.

Many solids show time dependent stress-strain behaviour. If a constant load is maintained the strain is often found to increase steadily with time; this phenomenon is known as creep. Alternatively, if the material is deformed and the deformation is held at a fixed value, the stress is found slowly to decrease, this is a phenomenon known as stress relaxation.

The theory of wave propagation in such materials is extremely difficult and a comprehensive treatment has yet to be made. However,

many real anelastic solids fall into one or other of two classes. Those whose behaviour is non-linear but time-independent, and those whose behaviour is linear but time-dependent, to close approximations. Metals in the plastic state are typical materials of the first group, and some plastics (e.g. high polymers) fit into the second group and are then known as linear viscoelastic solids.

1.2.4 Shock Waves in Solids.

On the treatment of plastic waves by the Eulerian method, the equations of motion and continuity in a solid rod or wire are similar to the equation of a wave of finite amplitude in a fluid. The velocity of propagation of disturbance is given by $(c + v)$ in

$$\frac{\partial \epsilon}{\partial t} + (c + v) \frac{\partial \epsilon}{\partial x} = 0 .$$

If the elastic modulus $S = \frac{\partial \sigma'}{\partial \epsilon}$ is ^{not} constant, large compressive disturbances will travel faster than smaller ones so that any finite compression pulse will eventually acquire a steep front as it travels through the medium. In solids the particle velocity, even for intense disturbances, is very small compared with the velocity of propagation so that, if S is constant, stress pulses can travel for considerable distances without change in form, and it is changes in the value of this elastic modulus S with strain that are principally responsible for the distortion of pulses of finite amplitude. For most solids S decreases beyond the proportional limit, and plastic waves rather than shock waves are set up in rods of the material when the deformations are sufficiently large.

Another type of shock wave can occur in tension when the stress-strain curve is concave upwards, i.e., when the tangent modulus increased with increasing strain. Lee and Tupper (1954) have discussed the theoretical basis for such shock wave generation in steel where at large amplitudes the stress-strain curve becomes concave. Kolsky (1953) points out that similar behaviour might be expected in rubber, which also has a dynamic stress-strain curve that is concave upwards.

The theory of shock waves in solids has been studied intensively by a number of theoretical and experimental schools, and a review of this work by Duvall (1962) summarize the advances made in this field.

1.2.5 Shock Waves in Gases.

A sound wave is propagated through a gas in the form of a weak isentropic adiabatic compression. Only small amplitude longitudinal displacements of the molecules are involved in this process. There is no net **transport** or flow of gas in the direction of propagation of the wave. The changes in the physical state of the gas due to the wave are minute, and the process is reversible. The rate at which the sound is propagated is called the speed of sound in the gas.

The sound wave is transmitted in the gas by collisions between gas molecules; consequently, it is not surprising that a wave of very different nature is set up in a gas when a disturbance is forced through it with a speed greater than the characteristic sound speed at which the molecules communicate a weak compression.

The nature of such a wave is all that the term given to it implies - a shock wave. When a shock wave is generated the pressure, density and temperature must build up in the wave, since the gas molecules in its path can only move away from the front with the characteristic sound speed. Due to this effect the molecules will be carried along in the shock wave, and a flow in the direction of propagation results. This property and the large changes induced in the physical state of the conducting gas, distinguish a shock from a sound wave.

The simplest picture of the formation of a plane shock wave was that given by Becker (1922). Consider a long tube having a piston at one end as in Figure 1.1a, and the piston be capable of acceleration to a constant velocity v which is greater than the sound speed of the gas: let the velocity v be reached by small increments dv in a short but finite time. The first increment dv from rest causes a weak compression wave to propagate in the gas at the speed (a) as in Figure 1.1b.

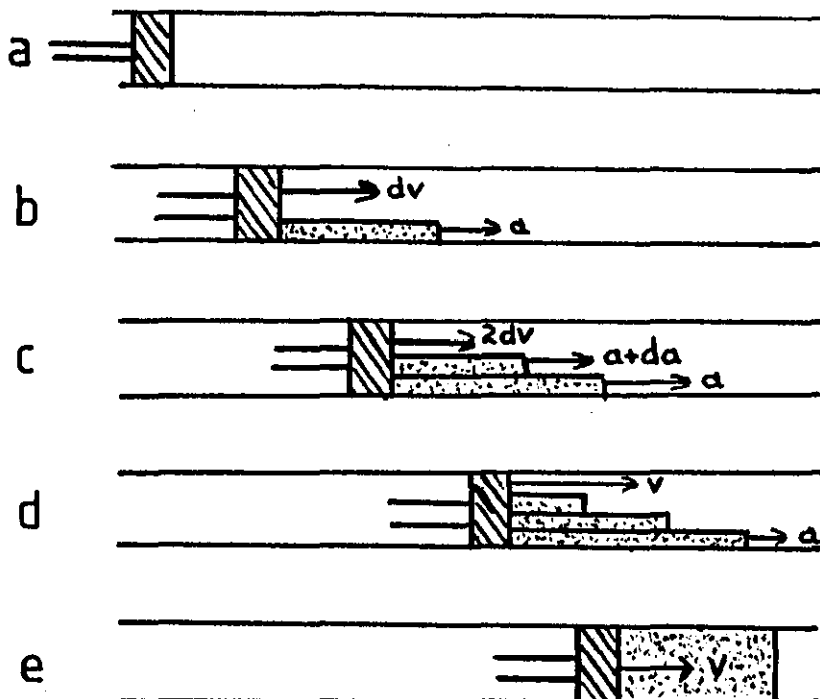


FIG. 1.1 Formation of a plane shock wave

At this stage the gas between the piston and the wave front has been compressed uniformly and adiabatically and has acquired the velocity dv , while that on the other side of the wave front is unchanged and stationary. Now let the piston acquire another velocity increment dv as in Figure 1.1c, a second compression wave is sent out through the moving gas in pursuit of the first, since it travels at a higher velocity relative to the tube. After many such increments the piston reaches its final velocity v . At this stage series of waves of increasing strength exist between the initial wave and the piston, as in Figure 1.1d. The flow velocity of the gas in the individual waves increases from dv for the front wave to v at the piston face; the separation between successive waves is thus decreasing with time. It is physically impossible for them to over-take one another, since as weak compression waves they travel at the local speed of sound in the gas, and due to the differing degree of adiabatic heating in each successive compression this quantity increases from the front to the piston.

Consequently, the train of waves must ultimately coalesce to form a single steep wave front, as in Figure 1.1e across which exist large gradients of pressure, density and temperature. This is called the shock front. Between the front and the driving piston is a column of gas of continually increasing length flowing with the velocity of the piston.

1.3 LITERATURE SURVEY.

1.3.1 Elastic Waves.

Mechanical disturbances propagate through an infinite elastic

medium as dilatational waves and distortional waves, i.e. alterations in volume and alterations in shape of any elementary volume. The velocity of the waves depends on the elastic constants and the density of the medium as described in section 1.2.

Wave propagation through a finite, bounded medium, e.g. a specimen, is a much more complex matter because reflections and refractions occur at the surfaces. A complete presentation of this is given in the treatise by Love (1927).

Application of the theory to practical situations where boundaries are present in the medium gives rise to equations which often become mathematically intractable for the particular boundary conditions applied. The elementary theory of the propagation of elastic disturbances along a cylindrical bar predicts that dispersion will occur with fluxural pulses, whilst longitudinal and torsional pulses will be propagated along a bar without change in form. The exact treatment of this problem for an infinite bar was obtained by Pochhammer (1876) and separately by Chree (1889), and is known as the Pochhammer-Chree theory. This theory shows that the velocity of propagation of longitudinal sinusoidal waves depends on their wavelength, and it is only when torsional waves are travelling in their fundamental mode that dispersion is absent. This theory also shows that for all three types of waves the elementary theory applies only when the wavelength is large compared with the radius of the bar.

An important characteristic of the propagation is the phenomenon of dispersion. The treatment of pulse propagation is complicated by this dispersion and methods based on Fourier techniques, coupled with the use of exact dispersion curves, have produced approximate

solutions. In discussing the cause of this dispersion, Davies (1948) called attention to Pochhammer and Chree theory which proved for sinusoidal waves that a condition of zero stress at the lateral surface of a bar leads to an equation connecting phase velocity and frequency. Because of this dependence a pulse composed of Pochhammer-Chree waves of all frequencies would be expected to change shape during travel.

The Pochhammer-Chree theory applies to infinite long cylinders, and attempts at describing propagation in finite or semi-finite bars have resorted to approximate theories (for a description of these see for example Green (1960)). A good review of the developments in elastic wave propagation is given by Miklowitz (1960). Here studies of torsional and flexural waves are included along with a large number of references. It will be concluded from this review that the bulk of modern day studies of wave propagation is concerned with problems involving boundaries and dispersion.

The experimental work in elastic waves has been concerned with confirming established theories or comparing the adequacy of approximate treatments. One of two approaches is usually adopted investigations in which continuous waves are excited or those involving the propagation of pulses. Techniques used in the former investigations consist essentially of setting a bar into resonant longitudinal vibration using piezo-electric crystals in conjunction with frequency oscillator, or by methods based on magnetostriction. Nodal points in the vibrations are located by means of an indicator such as lycopodium powder; wavelength, and hence the velocity of propagation can be determined.

Experiments on the propagation of pulses in bars usually employ some form of the 'Hopkinson pressure bar'. Hopkinson (1914) investigated the propagation of stress pulses in order to study the nature of the pressure-time relations when an explosive was detonated or when a projectile impinged on a hard surface. His apparatus, which has become known as the 'Hopkinson pressure bar', is an application of the simple theory of stress propagation of elastic pulses in a cylindrical bar where the length of the pulse is great compared with the radius of the bar. The apparatus consisted of a cylindrical steel bar with a short piece of the same diameter and material wrung on to the end of it. When the bar was subjected to an impulsive force at the opposite end, the end-piece flew off and its momentum was determined using a ballistic pendulum. Modern experiments, whilst using the same principle, employ more sophisticated electronic measuring techniques. Davies (1948) devised a pressure bar in which the measurements are made electrically.

Experiments on propagation in two and three dimensions have been performed using plates and blocks, employing ultrasonic techniques ^{and} the use of explosives. Davies (1948) devised a pressure bar in which a continuous record was produced of the longitudinal displacement at the free end of the bar. The displacement was measured by using the bar as the earthed conductor of a parallel-plate condenser. The isolated conductor consisted of a metal plate held in a frame attached close to the free end. When the pressure pulse reached the free end of the bar, the small movement of the earthed side of the condenser caused a change in

the capacity of the condenser, and this change was measured on a CRO as a changing potential difference; a photographic record was then taken of the signal. Displacement-time records were obtained in this way, and they demonstrated the existence of the so-called Pochhammer-Chree oscillations at the end of the pulse, and showed the effects of dispersion in increasing the pulse length. Davies also used cylindrical condensers, in which an isolated metal tube was held with its axis parallel to the axis of the bar. Measurements of the radial and longitudinal displacements of the bar surface were possible, although these units were only useful for measurements with long pulses.

More recent techniques involve resistance strain gauges mounted on the surface of the pressure bar, so that direct measurements of the strain-time profile may be obtained. Since the pressure bar remains elastic, the relationships for longitudinal elastic stress waves can be used to reconstruct the applied stress loading.

A major use of the Hopkinson pressure bar has been in the dynamic testing of materials. The general principle of the method is to have the specimens in the form of thin discs which are placed between the flat end faces of two cylindrical steel bars (Kolsky, 1949). A transient stress pulse is initiated at one end of the incident pressure bar, and the pulse propagates along the incident bar, through the specimen and into the transmitter pressure bar. The experiment consists of measuring the dynamic stress-strain characteristic of the specimen material. Further applications of Kolsky's original technique have been given by: Krafft, Sullivan

and Tipper (1954) and Campbell and Duby (1956) for the yield behaviour of mild steel; Davies and Hunter (1963) for various annealed metals and polymeric materials; Chiddister and Malvern (1963) for aluminium at elevated temperatures; Lindholm (1964) for three annealed face centered cubic metals; Hauser, Simmons and Dorn (1961) for high purity aluminium at temperatures below ambient, and Tennyson, Ewert and Niranjana (1972) for the dynamic viscoelastic response of bone.

1.3.2 Plastic Waves.

The time dependence of the stress-strain relation for most metals is very much less marked than it is for high polymers. As a first approximation, the assumption that the stress-strain relation is time-independent is perfectly satisfactory for most purposes. The first treatment of the problem of wave propagation along a material with such characteristics was published by Donnell (1930). He considered the propagation of a longitudinal wave along a thin rod of a material which had a bilinear stress-strain curve, the first part of the curve was assumed to correspond to the elastic behaviour, and the second part to strain-hardening associated with plasticity.

A large amount of research was performed by Taylor (1946), Von Karman and Duwez (1950), White and Griffis (1947), and Rakhmatulin (1945), who independently developed theories for the propagation of plastic waves in wires. This theory was based on the assumption that the stress-strain curve for a material was independent of strain rate, and is known as the strain-rate-

independent theory.

The examination of the results of Duwez and Clark (1947), by Lee (1955) has shown that the distribution of permanent plastic strain does not quantitatively agree with that observed experimentally. Malvern (1951) developed a theory to account for such deviations and has shown that the original calculations were subject to computational error. This observation is in accord with the experimental observations of many workers including Duwez and Clark (1947), Douch and Kolsky (1962), observed similar effects with aluminium and copper specimens.

Bell (1951) tested the rate-independent theory in another way. He stretched a copper specimen and, while it was being drawn, propagated an additional incremental tensile pulse. According to the rate-independent theory such incremental pulses should travel at a velocity proportional to the square root of the tangent modulus; Bell found they travelled at a velocity proportional to the square root of Young modulus, because the copper was well in its plastic range. These results were confirmed for copper by Sternglass and Stuart (1953), and for lead by Alter and Curtis (1956). In the work with lead both the preload and the incremental load were dynamic, because this metal is rate-dependent and almost viscoelastic in its behaviour.

A weakness of Malvern's theory of (1951) is that it did not predict the presence of a strain plateau at the impact end of the bar observed by many experimenters. Malvern (1965) has since indicated that a strain plateau may in fact be deduced from his theory.

Since these earlier experiments, controversy has continued between the proponents of the strain-rate independent theory and those of the strain-rate dependent theory. Bell (1951) put forward results supporting Malvern's theory and he devised an elegant technique for making dynamic strain measurements. His method depends on a diffraction grating ruled on the specimen; he measured the angle of the diffracted beam and thus inferred the values of the strain.

Most of the experiments on plastic behaviour have been based on forms of the Hopkinson bar, consisting of two long elastic bars with a specimen sandwiched between them as described earlier.

Experimental data obtained are usually analysed by using simplifying assumptions that ignore the effects of longitudinal inertia caused by the specimen. Average stress-strain are obtained in this case, and it is only by the use of thin wafer type specimens that inertia effects become negligible. The use of thin specimens however, introduced complications due to radial movements and the accompanying frictional effects. These cannot be ignored and must be corrected for, Davies and Hunter (1963) included axial, radial, and tangential corrections in their work and concluded that the behaviour of a number of metals is strain-rate sensitive.

Conn (1965), Bell (1966), and Dillon (1967) have emphasised that the validity of all Hopkinson bar data is suspect until these wave interactions and their effects have been accounted for. Characteristic of the work of Bell (1966) is his measurement of strains at points along the length of a long specimen. In this way he claims to overcome some of the problems inherent in the thin wafer methods. However as pointed out by Karns and Rupperger (1966),

in whose experiments both stress and strain were directly measured, his calculations of corresponding stresses in the bar are based on the assumption that the propagation of a given strain increment was proportional to the square root of the tangent modulus at that strain. In other words, Bell uses part of the strain rate-independent theory to prove itself. The results of many years work by Bell is presented in his (1968) monograph.

1.3.3 Shock Waves.

It has been known for some time that the "linear" treatment of sound waves no longer applies when the amplitude of disturbance becomes large. The linear differential equations are responsible for the properties of reflection, refraction and superposition which are characteristic of sound waves. In case of very violent disturbances, it is therefore to be expected that these simple laws are invalid.

However, an even more remarkable feature of non-linear wave motion is the appearance of shock fronts. Shock fronts are extremely rapid changes in the thermodynamic state of the fluid medium which can be approximated in the simple theory by mathematical discontinuities. They can occur at some later time in a flow which was initially continuous and are then able to propagate without further change. Under different circumstances, an initial discontinuity may eventually give rise to continuous motion. It is the propagation of the shock front through the medium which is usually referred to as the shock wave.

The early measurements of the speed of sound showed that intense sound waves from explosions travelled at more than the normal speed,

and as early as 1848 Sir George Stokes discussed the instability of a sound wave of finite amplitude.

Although it had been observed some years earlier that the differential equations of motion need not necessarily possess a unique solution for the velocity, the realization that shock waves are physically possible can be attributed to Earnshaw (1860). Two years later, a theory describing the propagation of such waves, which assumed an adiabatic, reversible transition, was derived independently by Riemann (1876) using an elegant treatment which has since become known as the method of Riemann invariants. Rankine (1870) examined this theory further and showed that the process could not be adiabatic as Riemann had assumed. However, the nature of the process still remained uncertain until Rayleigh (1910) and Hugoniot (1889) both demonstrated that such transitions must involve a change of entropy and therefore could be neither adiabatic nor reversible.

The first experimental study of ^{shock} wave motion was attempted by Sir Humphrey Davy in 1816. However little progress was forthcoming until the pioneer work of Vicille (1899) in the design of the shock tube. Vicille made measurements of the speed of the pressure pulse in a 6.0 m cylindrical tube using a series of mechanical pistons along the tube and a rotating drum. In his first work he burst under pressure, spherical glass bulbs placed at the end of the tube, but later divided the tube into two sections with a thin diaphragm; he experimented with diaphragms of steel foil, glass, paper and collodion, finding the last the most satisfactory. With air at 27 atm expanding into air at one atm he obtained speeds of over 600 m/s, showed that the decay of the speed was slow.

Between 1934 and 1941 Michel-Levy and Muraour (1936, 1937, 1938) carried out a series of observations on the luminosity from the shock waves produced by the detonation of solid explosives. In some of their work the detonator was placed at the end of a long tube and the luminosity was recorded with a recording-drum camera. Spectroscopic studies were also made, and metal spectra were excited by placing powder on a piece of foil in the path of the wave.

Payman, Shepherd and colleagues at the Safety in Mines Research Board commenced a series of investigations on the ignition of explosive gas mixtures by shock waves. They used the rotating-drum camera developed by Dixon (1903) employing it with a Schlieren system to study the propagation of shock waves from solid detonators into gases.

Reynolds (1943) had used the instrument during the second world war to calibrate piezoelectric gauges which were to be used in blast wave studies. Smith (1945) adapted the technique to a study of the reflection of shock waves at oblique surfaces; these investigations have since been developed to a high degree of sophistication by Bleakney and his co-workers (1949) at Princeton University using a Mach-Zehnder interferometer to show density distributions in the gas at a particular time.

After the second world war the shock tube was rapidly developed, especially in America, as a tool for aeronautical research, Weimer et al. (1949) used a Mach-Zehnder interferometer to study supersonic flow over a body. Hertzberg and Kantrowitz (1950), Resler, Lin and Kantrowitz (1952), Petschek et al. (1955) and independently Laporte

investigated the use of the shock tube as a source of high-temperature thermal radiation.

1.3.4 Viscoelastic Waves.

Metals in the plastic state have a non-linear but time-independent behaviour, whereas polymers and rubbers may have a linear but time-dependent behaviour, and are then known as linear viscoelastic solids. Interest in the behaviour of these materials under dynamic loading conditions is very recent and most work has occurred over the past twenty years or so. The subject of viscoelastic wave propagation is of the interest to the applied mathematician in that it leads to problems in which both the dispersion and absorption of waves are involved. It is of interest to the engineer, who needs to know the transient response of structures which include viscoelastic members (e.g. isolation mounts), and it is of interest to the experimental physicist who is measuring the mechanical properties of high polymers under conditions of very rapid loading, since at high frequencies (where the wavelength becomes comparable with the dimensions of the test specimen), only a wave treatment will lead to a proper interpretation of the experimental observation.

An excellent review of viscoelastic waves has been given by Hunter (1960), which includes references to the earlier important papers describing the mechanical behaviour of rubbers, plastics and metals. These describe the investigations on the propagation of continuous sinusoidal waves along filaments or thin rods of the material, and those using ultrasonic pulses. Photoelastic methods

have also been used to observe the passage of stress waves through transparent plastics. Also there have been several reviews on stress waves in viscoelastic media and of their application in determining the dynamic mechanical properties of rubbers and polymers. Among the notable are those of the works of Kolsky (1953, 1958, 1960, 1967), Hillier (1960, 1961) and Hunter (1960, 1967).

Hillier (1949) has considered the propagation of longitudinal sinusoidal waves along a viscoelastic filament and has derived the relation for a Maxwell solid, a Voigt solid, and a 3-parameter solid. Kolsky (1954, 1956) has measured the change in shape of an initially sharp longitudinal pulse travelling along thin rods of various plastics using a form of Hopkinson bar. He has shown that the pulse assumes an asymmetric shape as a result of dispersion and that Fourier synthesis can be used to accurately predict the pulse shape if the response of the material to continuous waves of various frequencies is known. Further, he has derived a generalised pulse shape from theory which fits observed results for polymers having a coefficient of internal friction that is essentially constant over a frequency range.

From experiments on lead bars Bodner and Kolsky (1958) have shown that whilst this metal is not linearly viscoelastic the change in pulse shape with distance is very similar to that observed for polymers.

Davies and Hunter (1963) report a comprehensive study of pulse propagation in a number of metals and polymers using a split Hopkinson pressure bar, with corrections for inertia and frictional effects. For a number of polymers a linear relation between stress

and strain was confirmed.

In attempting to obtain analytical expressions for pulse propagation in viscoelastic solids, Laplace transforms have been employed to obtain solutions for longitudinal propagation in rods. Berry and Hunter (1956) have combined Boltzmann for the stress-strain relation with the equation of motion, and then used Laplace transform methods for obtaining general solutions for longitudinal disturbances propagated along semi-infinite and finite rods. Lee, et al. (1954, 1953, 1956a, 1956b) have used instead the operator form of the stress-strain relation and obtained explicit solutions for pulses propagated in solids which behave like two, three and four-parameter models. Berry and Hunter (1956) have shown that their treatment leads to the solution given by Lee and Kanter (1953) for a Maxwell solid, when the appropriate memory function is used in the Boltzmann equation.

Lee and Kanter (1953) explored the unidirectional pulse propagation in a Maxwell solid under constant velocity impact and demonstrated the delay of the wave front as it travels along the rod. They have also shown that solutions to boundary-value problems in finite rods may be then obtained by a method of superposition. For Voigt solids, transform methods have been used by Zverev (1950), Eubanks, et al. (1955), and Morrison (1956). Glawz and Lee (1954) employed the method of characteristics for treating a four-parameter model, while Dunwoody (1966) used the same method in conjunction with a Maxwell solid.

More general treatments of wave propagation in linear viscoelastic solids which do not depend on the assumption of idealized

model behaviour have been given by Charles (1951), Berry and Hunter (1956), Berry (1958), and Bland (1958). Norris (1967) has attempted a spectral material representation for polyethylene; however, it appears from Kolsky's work (1960), in this case of a rather hard plastic, an even more limited characterization might have produced equally good results. Arenz (1964) employed an approximate method involving the Laplace transform in an effort to predict wave propagation in soft viscoelastic materials involving the complete spectrum of material response. His treatment indicated an oscillatory disturbance following the glassy wave front. Although this oscillatory behaviour can be argued qualitatively on the basis of Fourier synthesis through cancellation and reinforcement of Fourier components travelling at different velocities, their existence is doubtful and could be as a result of the approximate method used. Similar oscillations may arise in an exact or approximate model analysis such as proposed by Valanis (1966) when series truncation occurs too early. Approximate methods such as those above are important for predictions of wave propagations when geometries are complicated and their accuracy has been examined by comparison with an exact solution by Knauss (1968). Knauss analysis, using real material properties, showed an initial glassy wave front of approximately 1070 m/s which vanished for practical purposes and the bulk of the disturbance travelled with a velocity less than this value. The comparison of the exact solution with the approximate methods indicated good agreement and the conclusion that approximate transform solutions may be useful if interpreted correctly. It thus appears that only limited characterization of a viscoelastic material

is required for wave propagation problems for both hard and soft materials, with the caution that such a limited characterization needs to be further explored either through the calculations outlined by Knauss (1968) or through experiments as performed by Kolsky (1956) and Liftshitz and Kolsky (1965).

More recent wave propagation studies included that of Walsh (1971), who considered the decay of stress waves in one-dimensional polymers rods with the concept of acceleration waves, and obtained good correlations with Kolsky's work (1956).

McNiven and Mengi (1971) used the method of characteristics in their investigation of cylindrical waves in an infinite viscoelastic solid, while Arenz (1965) and Liftshitz and Kolsky (1965) have investigated two and three-dimensional propagation respectively.

1.4 CONCLUSIONS.

In the study of stress-wave propagation in solids, the theoretical complexities of the problem usually require geometric restrictions to allow mathematical tractability. Such restrictions have somewhat limited the study of stress-wave propagation to the propagation of waves in rods and wires—the one-dimensional stress configuration, and the propagation of waves through the thickness of a plate—the one-dimensional strain configuration. The review of Kolsky (1953), Gragg (1961) and Hopkins (1961) reveal that most of the experimental work has been concerned with the propagation of longitudinal waves in wires and rods. Experimentally, it is quite a simple matter to impact a rod or wire axially, but unfortunately the stresses produced

are not one-dimensional while the appropriate tractable theory is being based on the expected negligible effects of the radial stresses. On the other hand the one-dimensional strain theory is a close approximation to the propagation of a plane wave through the thickness of a plate if the measurements are made prior to the disturbances which propagate in from the edges of the plate. However, it is quite difficult to generate a known disturbance uniformly over the surface of a plate of sufficient area to effectively eliminate the edge effects. A geometric configuration that is also mathematically tractable is one-dimensional displacements in a cylindrical geometry, with the disturbance propagating radially outward from the axis of the cylinder. The disturbances to cause such deformation must be uniform along the axis of the cylinder and also symmetric at any point about this axis.

From the above survey it will be apparent that the present disagreement between the two schools of thought on the role of strain-rate in the dynamic behaviour of materials arises largely from the difficulties inherent in the measurements that are made.

1.5 PRESENT INVESTIGATION.

It has been recognised by a number of workers in the field that other methods not beset with the same difficulties must be sought to obtain similar data. Ensminger and Fyfe (1966) emphasised this need and reported results of their feasibility study on the utility of a cylindrical stress wave configuration for determining constitutive relationships for various materials. In this work cylindrical stress waves were produced in a hollow cylindrical specimen of aluminium by

electrically exploding at high energy a copper wire aligned along the axis of the specimen. The outward propagation of these waves was shown to be radially symmetric (Fyfe and Ensminger (1964, 1966)) and accurately reproducible. The response of the specimen to this loading was obtained by a measurement of the time variation of the outer surface displacement using an optical method. Good agreement with the corresponding theory for the case of elastic waves confirmed the validity of this type of measurement and the authors have since used the method to study the propagation of plastic waves (Fyfe and Swift, (1969)).

As emphasised by Fyfe and Ensminger (1964), the advantages of using a cylindrical geometry are (i) the ability to directly observe the specimen response, (ii) a greater area of the specimen is available for measurements, and (iii) there is a closer approximation to one-dimensional displacements.

Ensminger and Fyfe (Ensminger, (1964)) spent a considerable period developing a method for a measurement of the pressure variation on the inner surface of the specimen for use as a time dependent boundary condition using piezo-electric probes, but met a number of difficulties that forced them to abandon the method (Ensminger and Fyfe, (1968)). Instead, for their plastic wave studies they computed the pressure variation by an 'inverse method' based on elastic free surface displacement measurements (Fyfe, (1968)).

In the work described in this thesis the method proposed by Ensminger and Fyfe (1966) was adopted for the experimental investigation and a method similar to theirs was used to measure the displacement of the outer surfaces of the cylinder subjected to an internal pressure

wave due to the reflection of the blast-wave from an exploding wire. However, it was decided to use the Hopkinson pressure bar to determine the pressure-time profile of the pressure curve.

One part of this thesis is concerned with the production of shock waves resulting from exploding a wire inside a hollow cylinder and determination of the pressure from the explosion - directly measured using the Hopkinson pressure bar technique. The other part of this thesis is concerned with obtaining theoretical predictions of the response of cylinders of various dimensions subjected to the type of loading pressures met in the experimental situation.

CHAPTER 2

THE EXPLODING WIRE APPARATUS

2.1 INTRODUCTION.

Investigation of stress wave propagation (as described in the literature survey in Chapter 1) in short or long bars employ some means of producing and applying a longitudinal pressure pulse (bullet, striker bar etc.), accompanied by some means of measuring the time variation of stress and strain at some point in the specimen. In the cylindrical stress wave system described below, the cylindrical pressure pulse is produced by means of an exploding wire technique. The fundamental circuit for investigating exploding wire phenomena (Chace and Moore, (1959)), consists of a capacitor charged from a power supply and discharged through the wire. Since the wire itself has very low resistance and inductance, the circuit parameters are extremely important in any study of wire explosions. Special precautions are therefore usually taken in designing equipment. Esminger and Fyfe (1966) designed a simple technique to accomplish three basic objectives. These were:

(a) To provide a rapid loading pulse on the inner surface of a cylindrical specimen, with the requirement that the pulse be uniform along the axis of the cylinder and symmetric about this axis. A configuration of this type would result in deformations which varied only in the radial direction giving a biaxial state of strain.

(b) To measure the pressure-time history of the applied pulse on the inner surface of the specimen. This measurement was necessary as a time-dependent boundary condition to determine uniquely a theoretical prediction of the response.

(c) To measure the response of the specimen to the aforementioned loading. This was a direct measurement of the free surface displacement of the specimen to avoid introducing any unnecessary assumptions. This displacement provided the experimental results which could be compared with those predicted by the theory.

The experiments described below are based upon exploding wire phenomena. A wire placed along the axis of a hollow cylindrical specimen is made to explode by discharging a high energy capacitor bank through it. The response of the cylinder to the stress wave passing radially through it is obtained by a direct measurement of the outer surface displacement with time. This is achieved by means of an optical arrangement based on a variable light gap method.

The experimental work^{is} also concerned with the production of shock waves resulting from the explosion have been studied by optical methods, mainly the schlieren technique using a high speed image convertor camera.

Another method of measuring the pressure-time history of the loading pulse from the exploding wire at the inner surface of the specimen is that of the Hopkinson pressure bar technique.

2.2 THE CHARGING AND CONTROL SYSTEM.

The basic circuit commonly used in exploding wire studies (Chace & Moore, (1959)) is essentially simple, and as shown in Figure 2.1. A capacitor C, charged to a high potential by power supply P, is discharged by a fast switch S through the wire W which explodes. The current during the discharge is monitored using a low resistance R.

The object of the arrangement is to discharge a given energy into the wire in as short a time as possible, and since the arrangement is an LCR circuit factors which need to be taken into account in achieving a fast discharge are:

- (a) inherent self-inductance of the capacitor,
- (b) the self-inductance of the leads,
- (c) the self-inductance of the switch S,
- (d) the capacitance of C,
- (e) the characteristics of the wire,
- (f) the total resistance of the circuit.

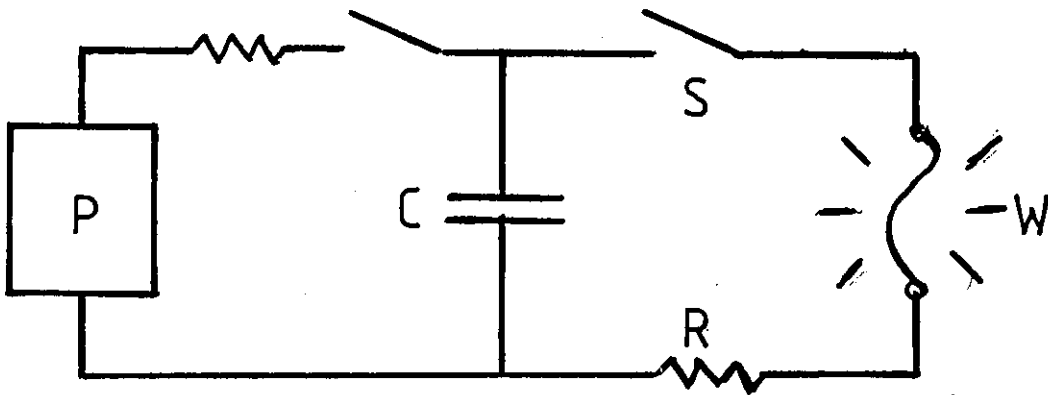


Figure 2.1. The basic circuit of exploding wire.

Examination of the equations for an LCR circuit given in Appendix 2 shows that L, C and R must be kept as low as possible for low current rise-time. The magnitudes of (d), (e), and (f) above are easy to control, the main problem lying in the reduction of the inherent self-inductances. Choice of high voltage capacitors with high natural ringing frequencies helps reduce the magnitude of (a), and the use of coaxial lines as short as possible reduces the

magnitude of (b). Accurately controlled timing and relatively low inductances suggest the use of a thyatron or spark gap as switch S.

Description of the Apparatus.

A block diagram of the apparatus used in the exploding wire is shown in Figure 2.2. The major components of the system consists of a bank of high voltage capacitor, charging power supply, switching and control units, and transmission lines. Figure 2.3. shows a general view of these units.

2.2.1 The Power Supply.

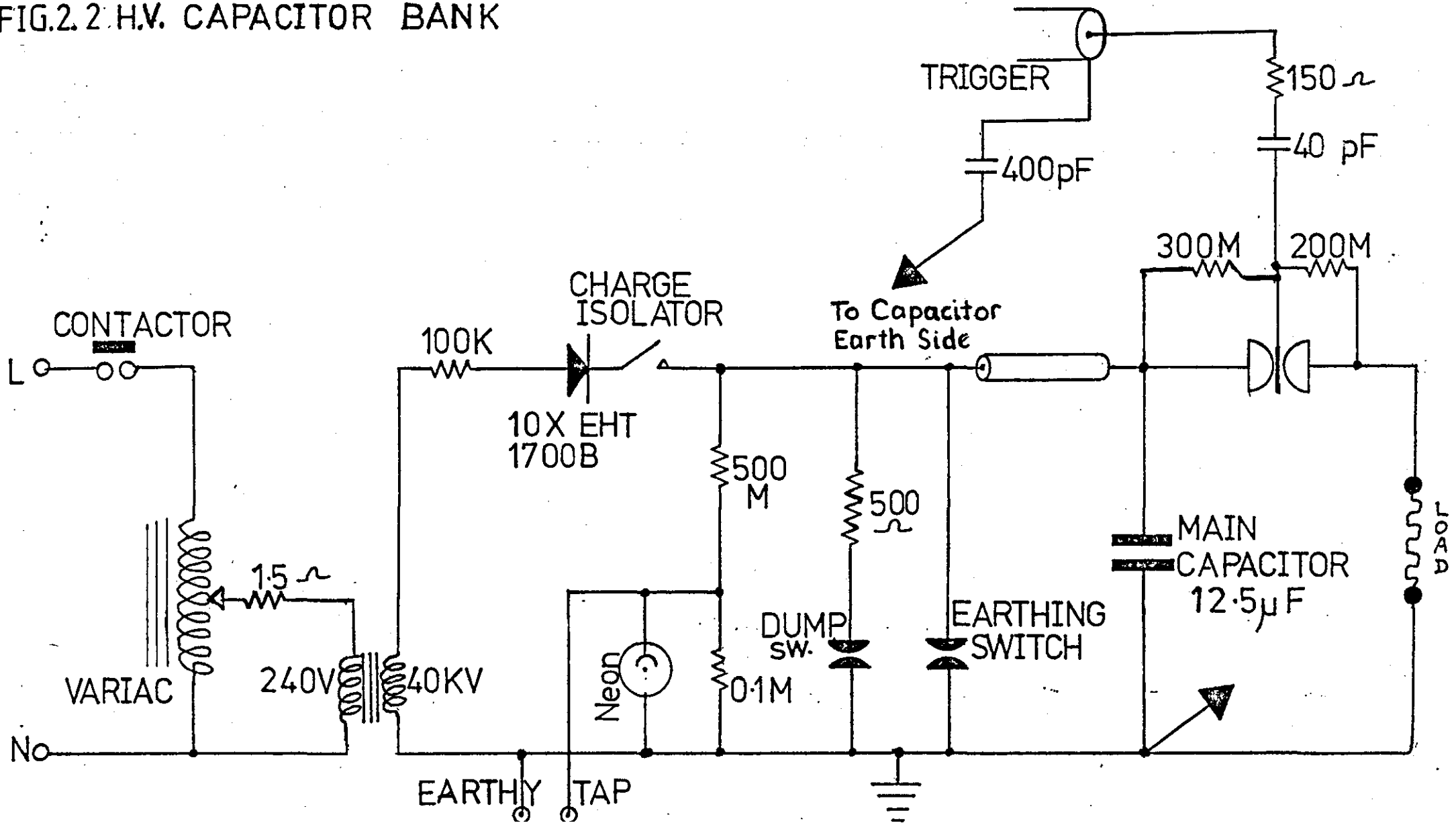
The power supply is a variable DC output supply comprising variac, transformer (0-40) KV charging rectifier, Neon and earth switches (pneumatically operative) as shown in Figure 2.2. The output voltage can be set manually using the variac in the primary of the E.H.T. transformer.

A safety feature of the unit is the ability to discharge or 'dump' the capacitor charge by short circuiting the capacitor through a low resistance (500 Ω). This can be done at any stage of the firing procedure.

2.2.2 The Capacitor Unit.

In order to utilise the inherent low inductance of the unit, connections are of the parallel-plate transmission line type with the smallest insulation separation possible. It is essential that connection be made to both sides of the case. The connection to the case not only surrounds and effectively screens the high voltage

FIG.2.2 H.V. CAPACITOR BANK



connections but also forms a rigid mechanical structure to withstand high magnetic forces.

The spark gap switches are mounted at the end of the capacitance to form an integral assembly, and an additional transmission line is placed between the case and high voltage connections. This allows the spark gap to be placed at the end remote from the load connections to give good accessibility.

Culham Laboratory in collaboration with BICC Ltd., have developed this unit, the 12.5 μF capacitor/spark gap unit has a combined inductance of 30 nH and a maximum current rating of 500 KA peak. This capacitor is supplied as 10 KJ, 40 KV.

The capacitor winding elements use an oil/paper dielectric system and are housed in a rectangular metal case of dimensions (1.12 \times 0.4 \times 0.39 m) as shown in Figure 2.3. The elements are connected in parallel to H.T. terminals in the centre of an insulating lid such that a low inductance configuration can be obtained by using external parallel plate transmission lines. The spark-gap switches used are three-electrode field distortion pressurised air gaps of various sizes having ratings of 5-100 coulombs per pulse and inductances of 15-50 nH. This spark-gap arrangement was developed for rapid transference of energy to the wire.

The Spark Gap.

The spark-gap arrangement, developed when the need for a quicker transference of energy to the wire became apparent, is shown in Figure 2.4B. The triggered spark gap consists essentially

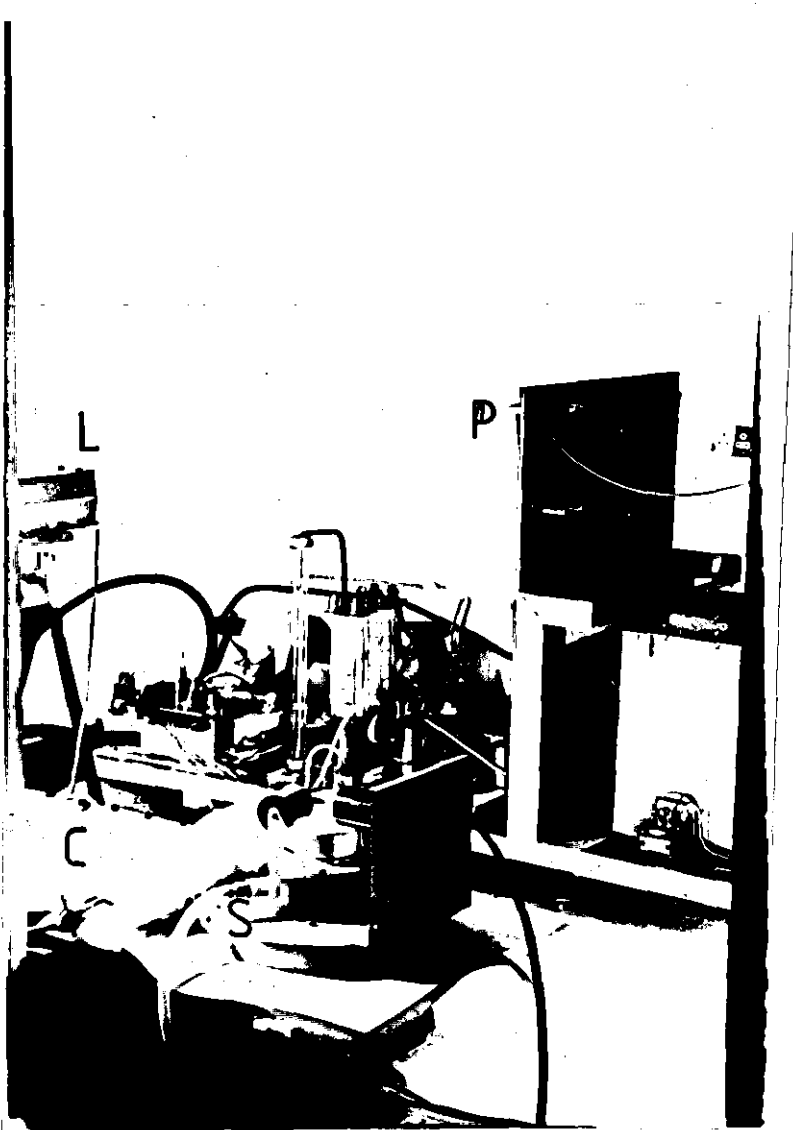


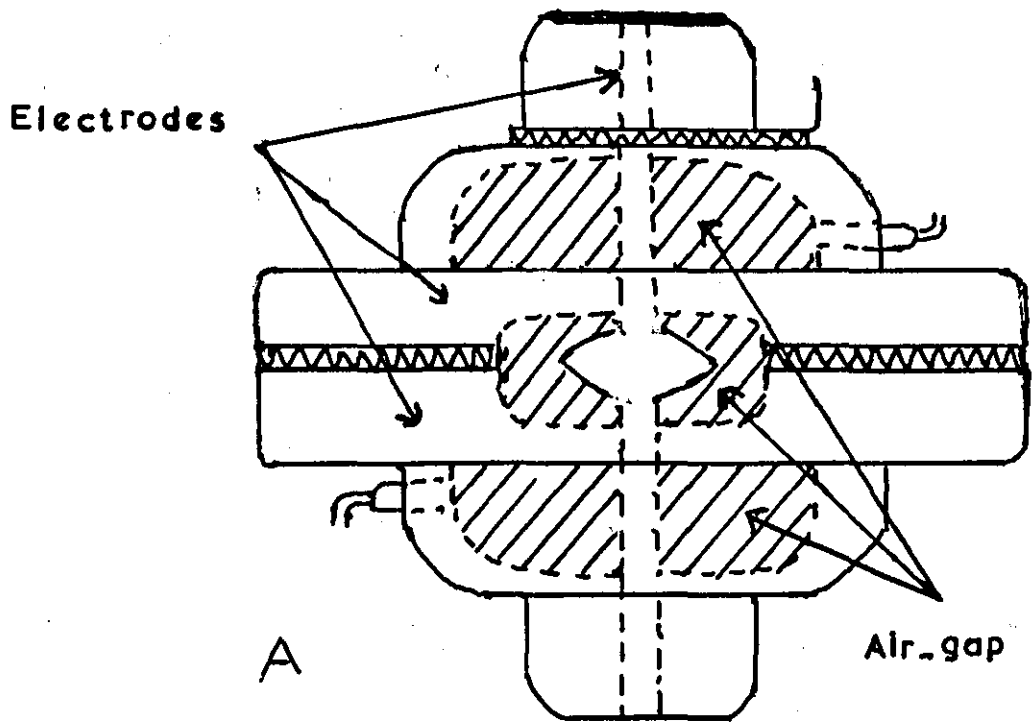
FIG. 2.3 GENERAL VIEW OF THE OPERATION ROOM

C - CAPACITOR

L - LASER

P - POWER SUPPLY

S - SPARK-GAP



B



FIG. 2.4 THE SPARK-GAP UNIT

of three electrodes, two as discs separated by insulation sheets but joined in the centre by air gap and the third electrode inserted through the discs all separated by a pressurised air gap as shown in Figure 2.4A. The electrodes are covered by two insulating lids. When a voltage pulse is applied to the trigger electrode, spark breakdowns take place between the two main electrodes and the capacitor bank is discharged. The trigger pulse of 10 KV required to initiate the discharge is obtained from the thyatron unit.

2.2.3 Thyatron and Trigger Pulse Generator.

The single thyatron unit is of type 8004.1 and is connected to the spark gap by driving the cable doubler for triggering the spark-gap. The thyatron operates as a controlled rectifier control signal to start conduction. Conduction is achieved when a suitable current pulse is passed through the thyatron. The output pulse from the triggering unit generator is + 150 V for about one microsecond followed by - 150 V for one and half microsecond driving into a 100 Ω load connected to the thyatron.

The pulse generator and the thyatron are shown in Figures 2.5 and 2.6 respectively.

2.2.4 The Control Units.

The control panel is situated outside the operation room as shown in Figure 2.7. This controls all procedures for the exploding wire. The panel has an interlocking system, which is necessary for safety, and should any part of the exploding test malfunction, then the interlocking system will operate to show exactly the type of

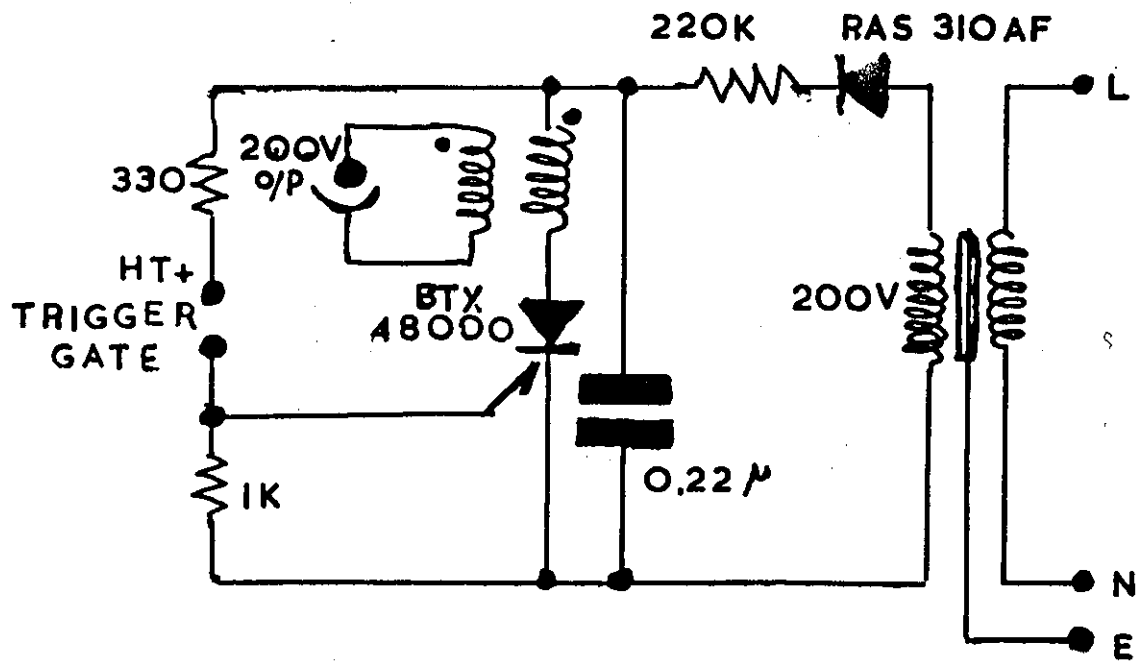


FIG. 2. 5 TRIGGER PULSE GENERATOR

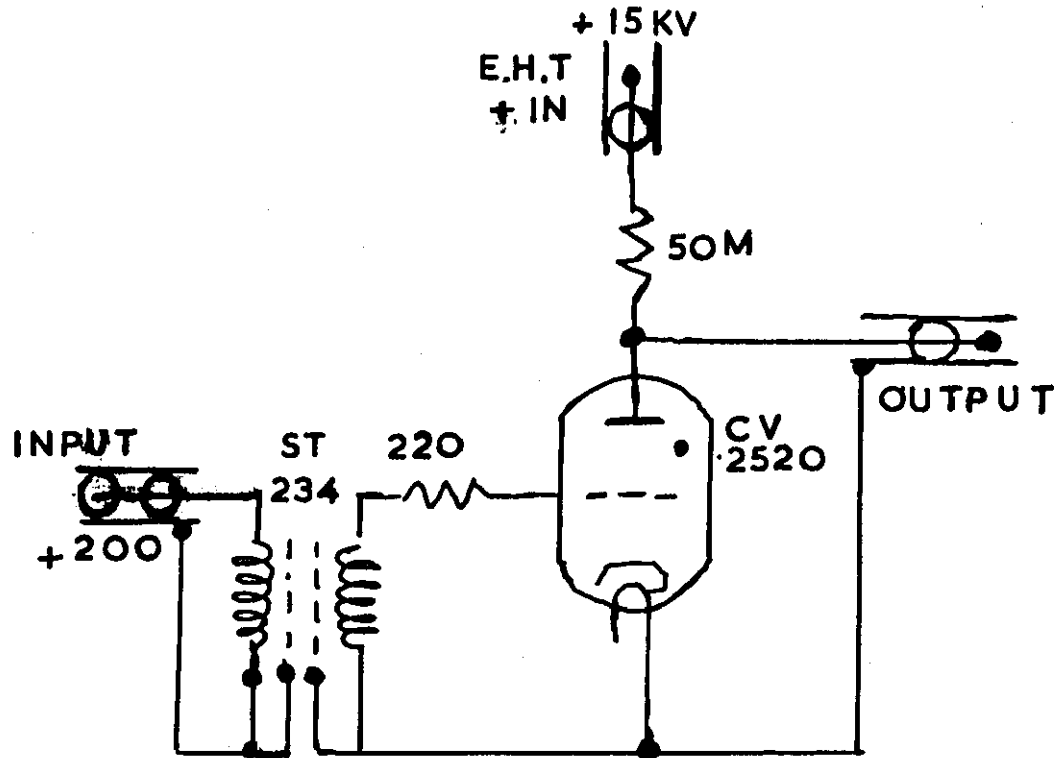


FIG. 2. 6 SINGLE THYRATRON UNIT TYPE 8004.1

- A- CONTROL UNIT
- B- DELAY-TIME UNIT
- C- GAS CYLINDER
- D- PRESSUR GAUGE
- E- THYRATRON & PULSE
GENERATOR

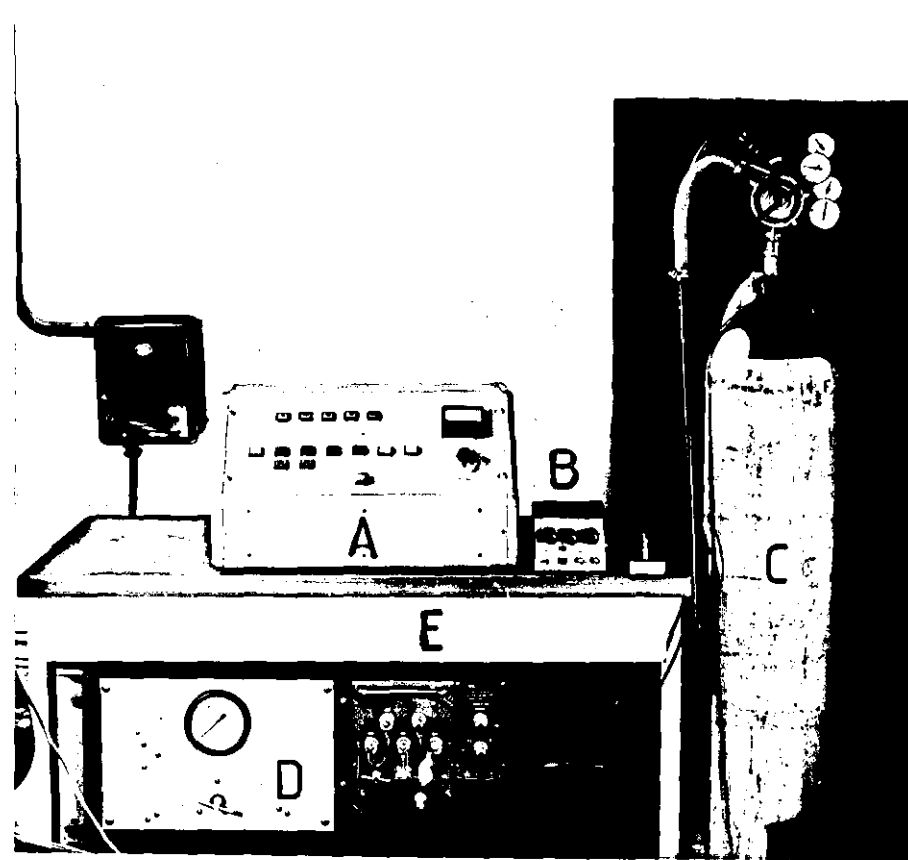


FIG.2.7 GENERAL VEIW OF THE CONTROL SYSTEM

malfunction. These are designated as:

- (1) Air fail,
- (2) Emergency stop,
- (3) Earth sticks,
- (4) Door open, and
- (5) Its indication the interlocks are complete or fail.

The block diagram of the control system is shown in Figure 2.8.

The control units have the following functions:

- (a) Ensure by means of a small spark-gap that the bank is not charged above a certain pre-set voltage.
- (b) Introduce an interlock between the power supply and voltage switch of power supply.
- (c) Lower and raise earth in case of emergency.
- (d) Start and stop charge.

The circuit diagram of control units, the key to charger interconnections and the diagram of the charger interconnections are shown in Figures 2.9, 2.10 and 2.11 respectively.

2.3 THE EXPLODING WIRE RIG.

The structure developed to accommodate the cylindrical specimen relative to the exploding wire and optical displacement measurement system was designed to meet the following requirements:

- (1) rigid accommodation of cylindrical specimens of various diameters (3-8 cm) and lengths up to 15 cm,
- (2) accurate alignment of the wire along the axis of the cylinder,
- (3) reasonable ease of changing specimen and replacing wire,

INTERLOCKS

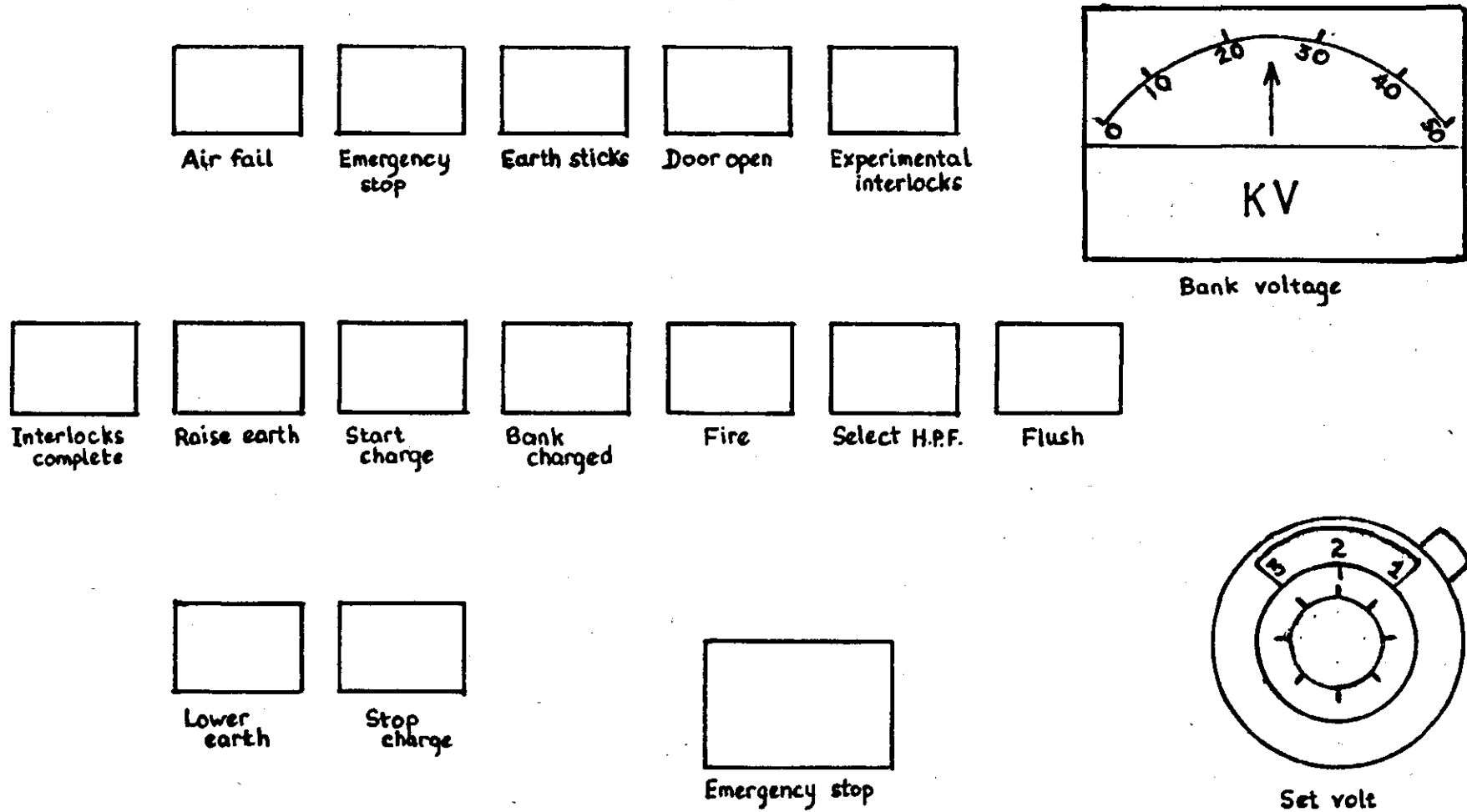


FIG.2.8 DIAGRAM OF THE CONTROL SYSTEM

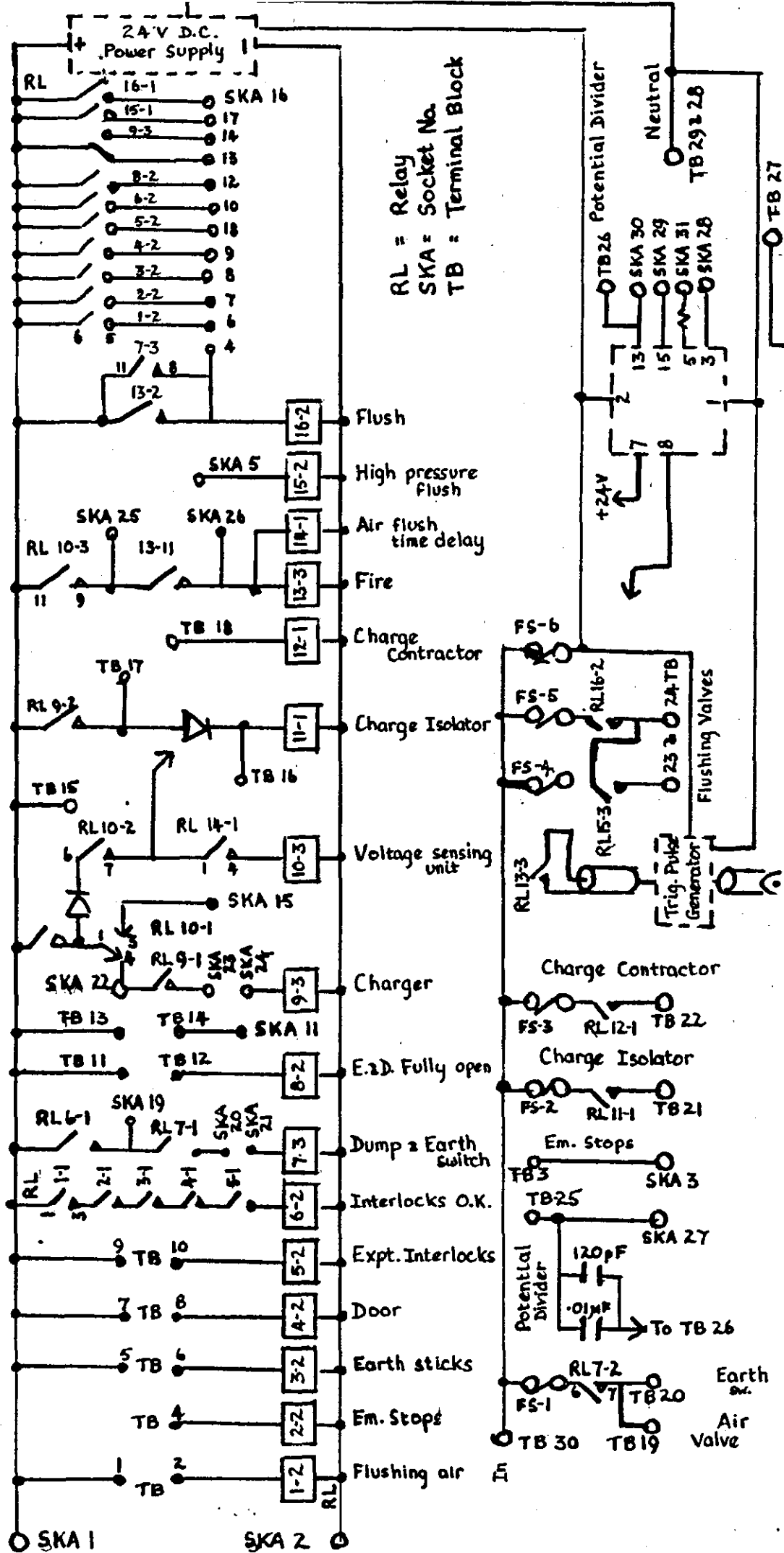


FIG. 2.9 CIRCUIT DIAGRAM OF THE CONTROL UNITS

| FROM CONTROL UNIT | | TO | |
|--------------------------------|--------------------------------|----------------|----|
| <u>REAR TERMINAL BLOCK L-R</u> | | | |
| 1. | AIR PRESSURE SWITCH | AIR PANEL | 4 |
| 2. | AIR PRESSURE SWITCH | AIR PANEL | 5 |
| 3. | EMERGENCY STOPS | | |
| 4. | EMERGENCY STOPS | | |
| 5. | EARTH STICKS | | |
| 6. | EARTH STICKS | | |
| 7. | DOOR SWITCH | | |
| 8. | DOOR SWITCH | | |
| 9. | EXP. INTERLOCKS | | |
| 10. | EXP. INTERLOCKS | | |
| 11. | EARTH & DUMP SWITCH OPEN | CHARGER | 9 |
| 12. | EARTH & DUMP SWITCH OPEN | CHARGER | 10 |
| 13. | EARTH SWITCH CLOSED | CHARGER | 9 |
| 14. | EARTH SWITCH CLOSED | CHARGER | 11 |
| 15. | CHARGE CONTACTOR (AIR CONTACT) | CHARGER | 6 |
| 16. | CHARGE CONTACTOR (AIR CONTACT) | CHARGER | 5 |
| 17. | CHARGE ISOLATOR MICRO-SWITCH | CHARGER | 7 |
| 18. | CHARGE ISOLATOR MICRO-SWITCH | CHARGER | 8 |
| 19. | AIR INPUT CONTROL VALVE (COIL) | AIR PANEL | 3 |
| 20. | EARTH SWITCH SOLENOID | CHARGER | 13 |
| 21. | CHARGE ISOLATOR SOLENOID | CHARGER | 12 |
| 22. | CHARGE CONTACTOR (COIL) | CHARGER | 4 |
| 23. | 4.P. VALVE SOLENOID | AIR PANEL | 2 |
| 24. | FLUSHING VALVE SOLENOID (LIVE) | FLUSHING VALVE | |
| 25. | POTENTIAL DIVIDER (TAP) | CHARGER | 15 |
| 26. | POTENTIAL DIVIDER (EARTHY) | CHARGER | 14 |
| 27. | CHASSIS | EXP. EARTH | |
| 28. | MAINS NEUTRAL | CHARGER | 2 |
| 29. | MAINS NEUTRAL | AIR PANEL | 1 |
| 30. | MAINS LIVE | CHARGER | 1 |

FIGURE 2.10. THE CHARGER INTERCONNECTIONS KEY.

Experimental Interlocks

Select H.P.F.

Flush

Fire (1)

Bank Charge

Start Charge

Stop Charge

Earth Switch Open

Earth Switch Closed

Interlocks O.K.

Door Open

Earth Sticks

Emergency Stops

Air Fail

Select H.P.F.

Flush

Emergency Stop

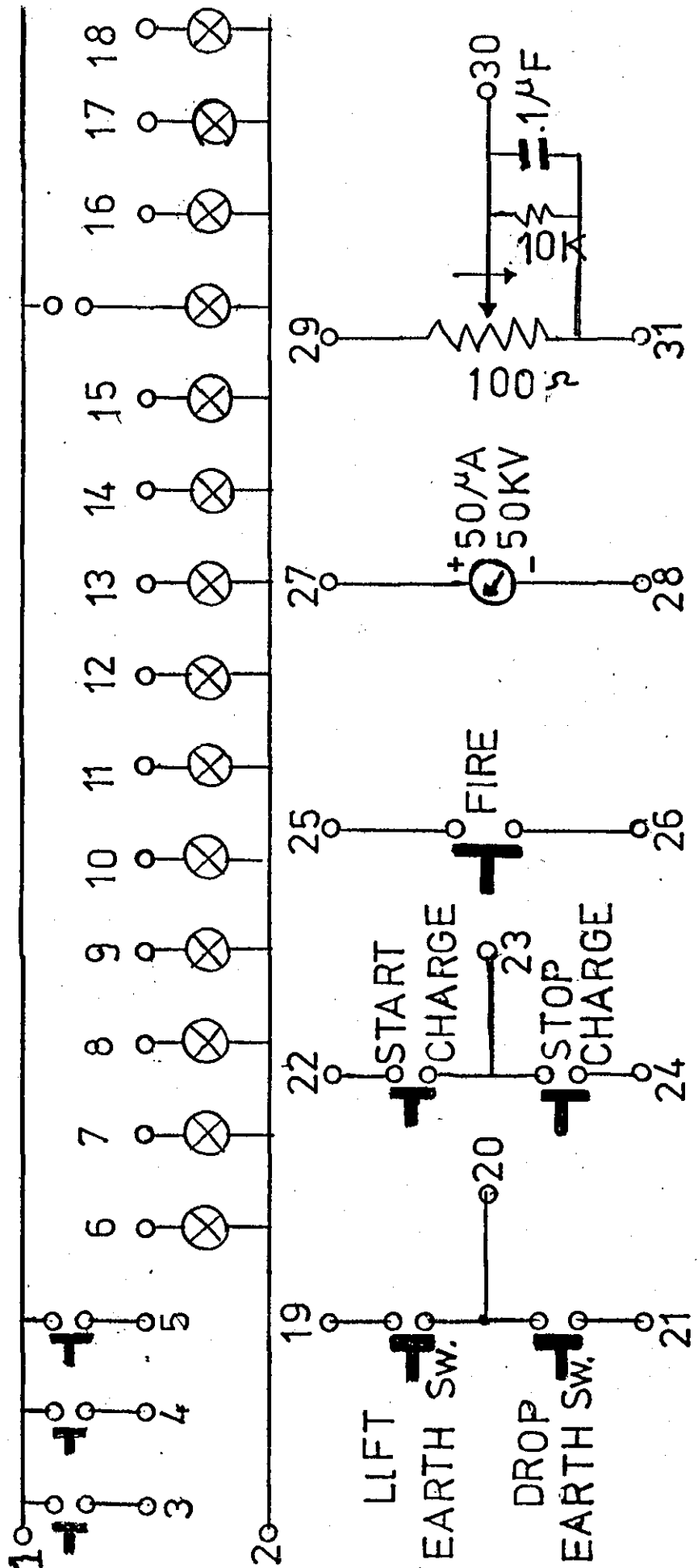


FIG.2.11 THE CHARGER INTERCONNECTIONS

- (4) adequate insulation between incoming transmission lines,
- (5) minimum contact resistance at points of connection of the wire,
- (6) facility to accurately vary the gap between wedge and specimen by known amounts during calibration.

Figure 2.3 shows the position of the rig in relation to the optical system (described in Chapter 6), and Figure 2.12 show detail of the electrodes and incoming transmission lines. The rig is fabricated from steel and insulation is of tufnol sheet. Each solid aluminium electrode has a vertically adjustable and replaceable brass holder, (Figure 2.13), for firmly gripping the wire. The electrodes are connected to the transmission lines by means of brass bolts located in slits machined in the tufnol insulation. This enables the horizontal position of the electrodes to be varied to accommodate different specimen lengths. The transmission lines lie beneath the base plate and are fully insulated by sandwiches of tufnol sheet.

2.4 THE CHARGING AND EXPLODING PROCEDURE.

The sequence of operation of the control panel is as follows:

- 1 - The experimental interlocks are complete and are shown by the panel light.
- 2 - The required voltage is set from the "Set Volt" and this shows on the bank voltage meter.
- 3 - The 'Earth' is raised. This disconnects the live capacitor connection from earth.
- 4 - Charging is started. This is achieved by closing charge isolator connection.

- A. Cylinder support
- B. Electrode support
- C. Electrode
- D. Optical bench
- E. Wire holder

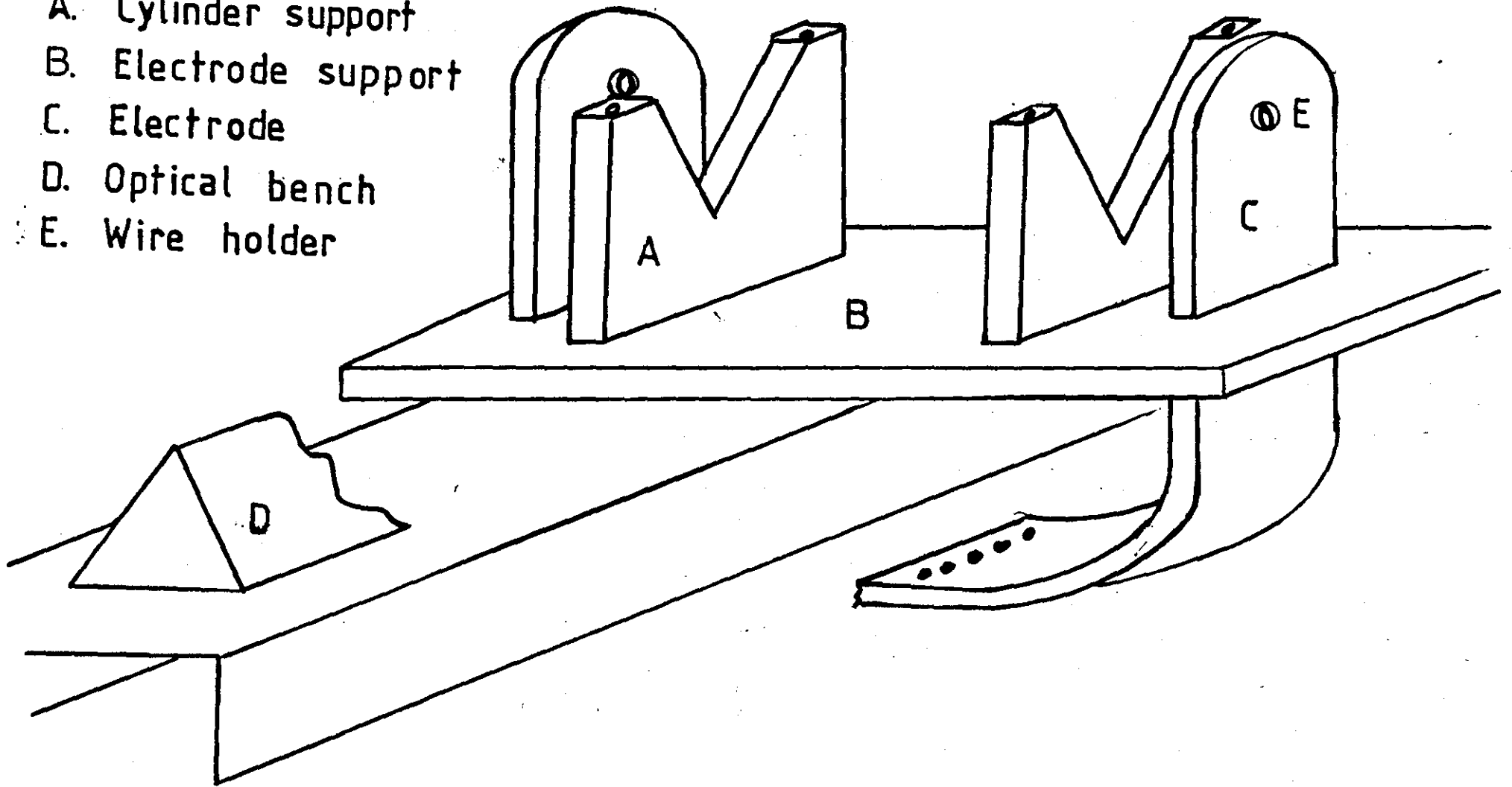


FIG. 2.12 GENERAL ARRANGEMENT OF EXPLODING WIRE RIG

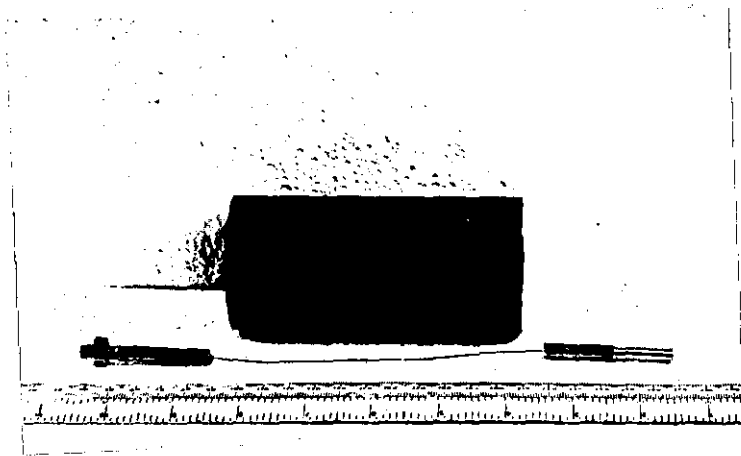


FIG. 2.13 THE WIRE HOLDER

5 - When the bank is charged the panel light indicates 'Bank charged'.

6 - 'Fire', this discharges the capacitor bank through the wire by triggering the spark-gap.

7 - If any fault occurs during charging the capacitor, an emergency stop switch is available to dump this charge on the capacitor and to lower the earth.

CHAPTER 3

CURRENT MEASUREMENTS

&

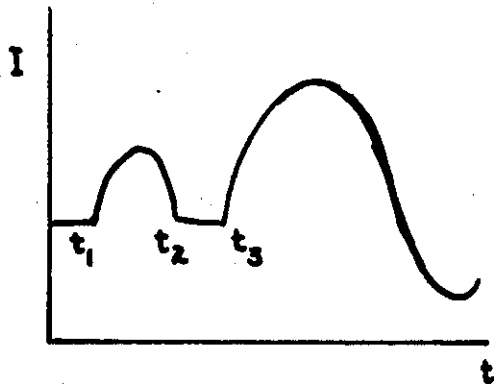
CYLINDRICAL SHOCK WAVE FROM EXPLODING WIRES.

I CURRENT MEASUREMENTS.

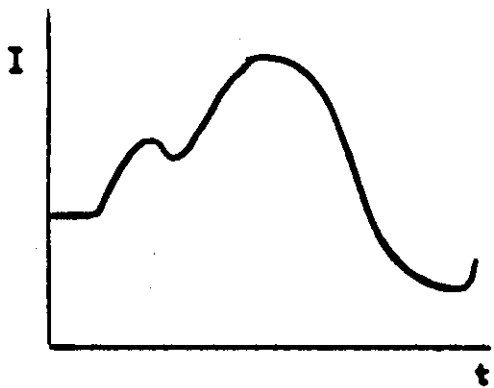
3.1 INTRODUCTION.

It is necessary to be able to measure the pressure-time history at the inner cylinder surface for use as a time-dependent boundary condition. It is reasonable to assume (Ensminger and Fyfe (1968)) that the form of the pressure pulse created by the exploding wire bears some relationship to the characteristics of the discharge current. Hence a measurement of the current would give a ^{very} rough indication of the nature of the pressure variation, and more important a record of the current provides a convenient time maker for relating different displacement traces.

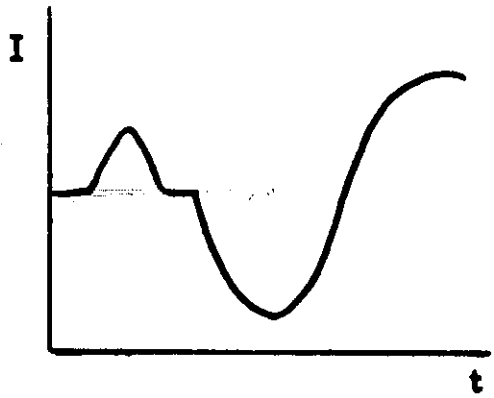
Much effort has been directed towards study of the exploding wire phenomenon (Chace and Moore (1959-1967)). One of the main measurements made in such studies is of the time variation of the current through the wire during the explosion, and a good account of instrumentation problems involved is thus given in Chace and Cullington. Depending on the nature of the wire itself and on circuit parameters, the current waveform for an exploding wire may be of several forms. Typical waveforms for wires exploding under different conditions are shown in Figure 3.1. The mechanisms involved during the explosion have been described by a number of theories (Chace and Moore (1957-1963)), it being relevant here to describe only the general form of the current-time history. Referring to Figure 3.1, the current initially rises as though following a damped sine wave until a 'transplosion' occurs, after which the conductivity drops. This pause or so-called "dwell-time" ($t_2 - t_3$) is characteristic of most explosions and is followed usually by a 'restrike' or 'reignition' when the current again



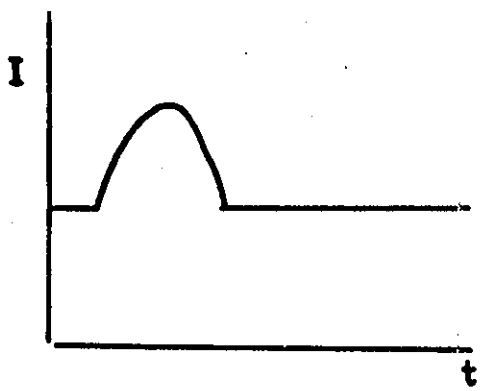
Typical case
($t_2 - t_3$) dwell time



Short dwell with
fast re-strike



Rare case



Single burst

FIG. 3.1 CURRENT WAVEFORMS FOR
EXPLODING WIRES.

rises controlled by LCR constants of the circuit.

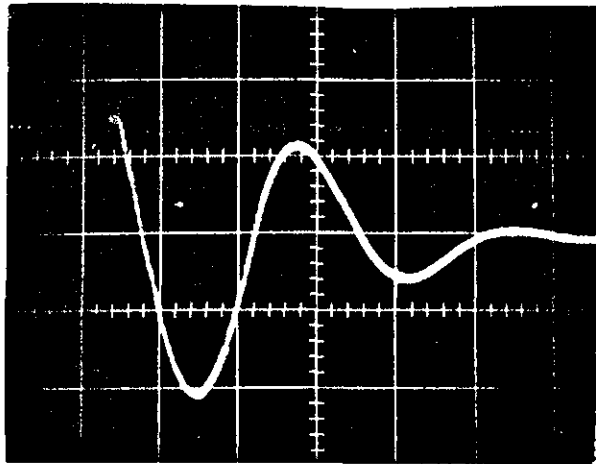
Oscilloscopes have been used to record the time histories of current in exploding wires and the voltage developed across the wire. To examine the current-time and voltage-time response of an exploding wire system Fyfe and Swift used a dI/dt pick-up loop attached to the system and fed back to an oscilloscope through an integrator and voltage divider respectively. Butler (1970) obtained current waveforms by using two methods, a Rogowski coil pick-up placed near the circuitry and a low series resistance in the exploding wire circuit across which the potential difference was measured. The voltage was discharged through 20 cm lengths of copper and Phosphor-bronze wires of different sizes. He found that 20 SWG copper wire gave the optimum current.

For the purpose of this work it is important to produce a simple current pulse in which most of the electrical energy is discharged through the wire in a single short burst, i.e. the restrike does not occur, the dwell time being infinite.

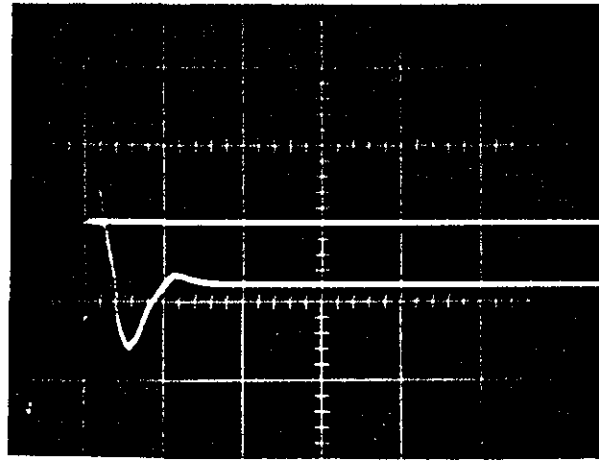
The method used for the measurement of the current in an exploding wire involves a pick-up coil (Rogowski coil) placed near the circuitry in which a signal proportional to the rate of change of current is induced.

3.2 CURRENT CHARACTERISTICS FOR EXPLODING WIRE.

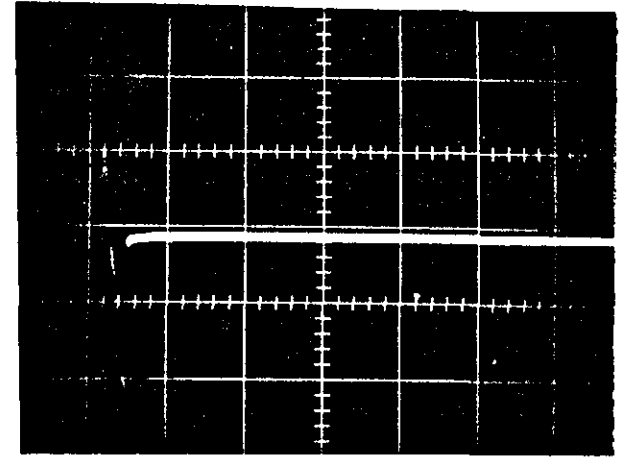
To find the wire giving the optimum amplitude and variation, a number of copper and Phosphor-bronze wires of various diameters were exploded in air. Figures 3.2 and 3.3 illustrates a series of current waveforms for 20cm wires having the following diameters.



20 SWG
25 SWG
10V/cm
5 μ s/cm



22 SWG
26 SWG
20V/cm



24 SWG
31 SWG
20V/cm

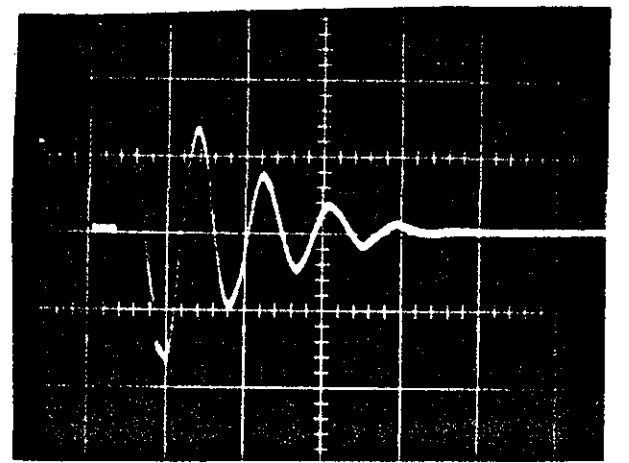
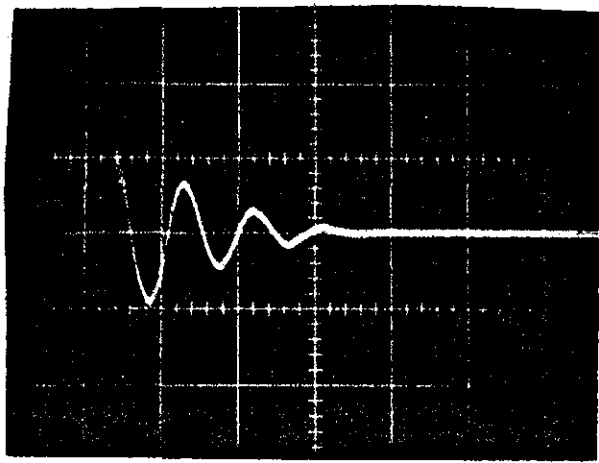
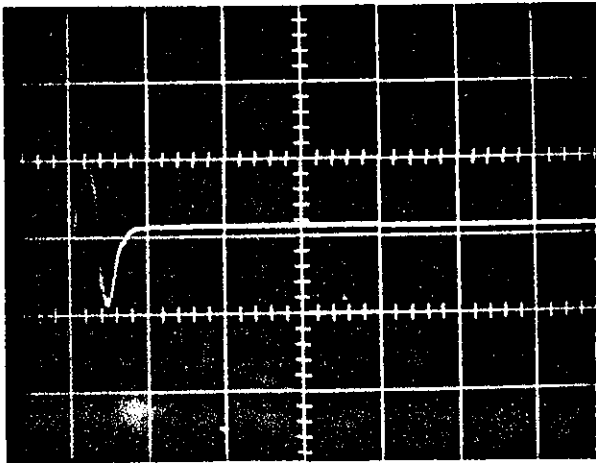
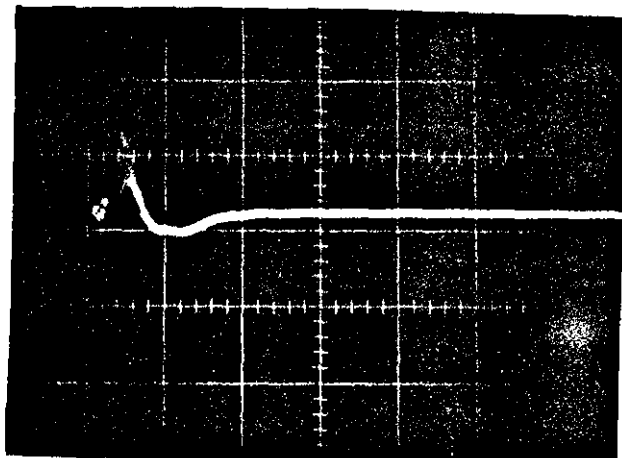
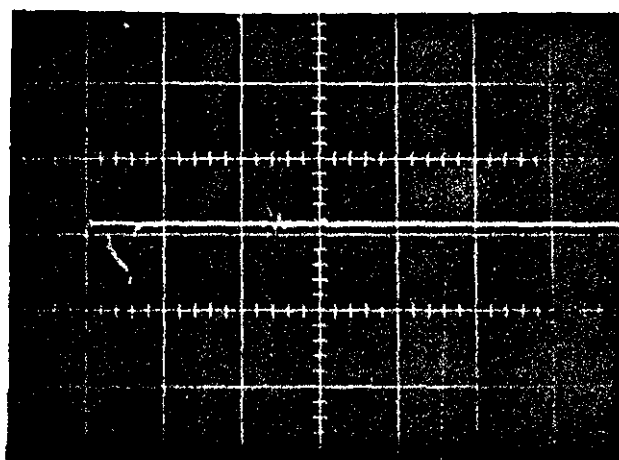


FIG. 3.2 CURRENT WAVEFORMS FOR COPPER WIRE
Sweep: 10 μ s/cm

24 SWG
20V/cm
5 μ s/cm



25 SWG
10 μ s/cm
10V/cm



29 SWG
10V/cm
10 μ s/cm

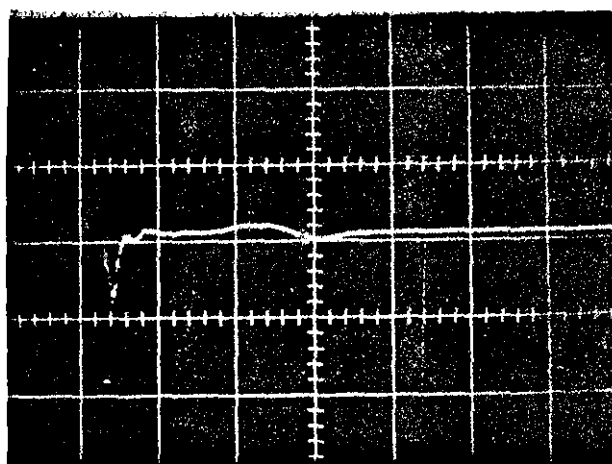


FIG. 3.3 CURRENT WAVEFORMS FOR PHOSPHO-BRONZE WIRE

| <u>Standard Wire Gage (SWG)</u> | <u>Diameter in mm.</u> |
|---------------------------------|------------------------|
| 20 | 0.914 |
| 22 | 0.711 |
| 24 | 0.599 |
| 25 | 0.508 |
| 26 | 0.457 |
| 27 | 0.417 |
| 29 | 0.345 |
| 31 | 0.295 |

In Figure 3.2 it seems that the current variation for the thickest and thinnest wires, i.e. (20, 22, 27, 29 and 31 SWG) are of the form of heavily damped sine wave and it shows the effect of successively increasing the wire diameter. Also the wire response shows that no 'restrike' occurs in any of the copper wire traces, i.e. the dwell-time was infinite. Figure 3.3 shows the current waveforms for Phosphor-bronze, the traces are not uniform and in some of them bursts of noise are recorded. Current wave forms of copper and Phosphor-bronze wires show that the nature of the current discharge depends on the material of the wire.

All tests were carried out with a capacitor bank voltage of 20 KV. It was found after these tests that no charge remained on the capacitor bank which was completely discharged. This was tested by connecting an electrostatic voltmeter of range 0-40 KV to the high voltage tube in the power supply with the earth switch disconnected. The voltmeter indicated that no voltage remained after exploding the wire.

3.3 DISCUSSIONS.

With the aim of producing a single burst of current, as much

energy as possible is discharged during the explosion. From the above investigation it was found that the 24 SWG copper wire produced a simple current pulse in which most of the electrical energy is discharged in a single short burst. Further comparison of various diameters of copper wires is discussed in Section II.

The inductance and the ringing frequency of the exploding wire system measured from the records are about $0.4 \mu\text{H}$ and 60 KHz respectively.

II CYLINDRICAL SHOCK WAVE FROM EXPLODING WIRES.

3.4 INTRODUCTION.

When a fine cylindrical wire is exploded in air by the passage of heavy current pulse, a complex flow with closely cylindrical symmetry is induced in the surrounding medium. The explosion is accompanied by a shock wave which is responsible for the loud noise present in the explosion.

Measurements of exploding wire phenomena have been studied in several laboratories by various methods. Optical methods commonly used include, schlieren-Kerr cell technique used by Müller (1937) for investigation of the shock system. In these experiments an energy of up to 12 joules per centimeter of wire was used and the shocks were followed out to distances of 3 cm from the wire axis. Bennett (1958) used high resolution rotating mirror streak camera photography to follow the primary shock trajectory for several centimeters. In this case about 60 joules per centimetre of wire is expended in the explosion. For the investigation of strong

cylindrical shock waves, Jones and Gallet (1962) used microwave Doppler technique. They transmitted three independent microwave frequencies with wavelengths of 0.84, 1.20 and 3.0 cm normal to the expanding shock front. Their input energies were 282, 361 and 500 Joule per cm discharged through 4 inch copper wire of different sizes. They found a wire of size 26 SWG gives the most energy output for all pressures. They used 10 μ F, 20-KV condenser bank, and the pressure inside the chamber ranged between 10-50 cm Hg.

Fyfe and Ensminger (1964) have investigated the symmetry of exploding wire inside a cylinder. The apparatus they used consisted of two 20-KV, 15 μ F capacitors connected by parallel plates with either spark-gap or mechanical switch initiating the discharge. They imbedded two probes into varying depth holes located around the centre of a polyethylene cylinder (2 inches in diameter, 4 inches long) at the same depth and 90° apart. They also used a second method by examining the deformation in aluminium cylinders initiated by exploding the wire inside the cylinder.

Ensminger and Fyfe (1966) have used an exploding wire technique to produce a high amplitude stress wave incident on the inner surface of a hollow cylindrical specimen. This technique requires the measurement of the outer surface displacement and the stress incident on the inner surface in order to produce a stress-strain relationship. They used probes to obtain the pressure-time history on the inner surface and measure the arrival of the shock wave at the probe location. The probe was a brass tube with an internal conductor running down the axis. To one end of this system a small pzt-4 crystal was connected to the tube and rod. The coaxial arrangement

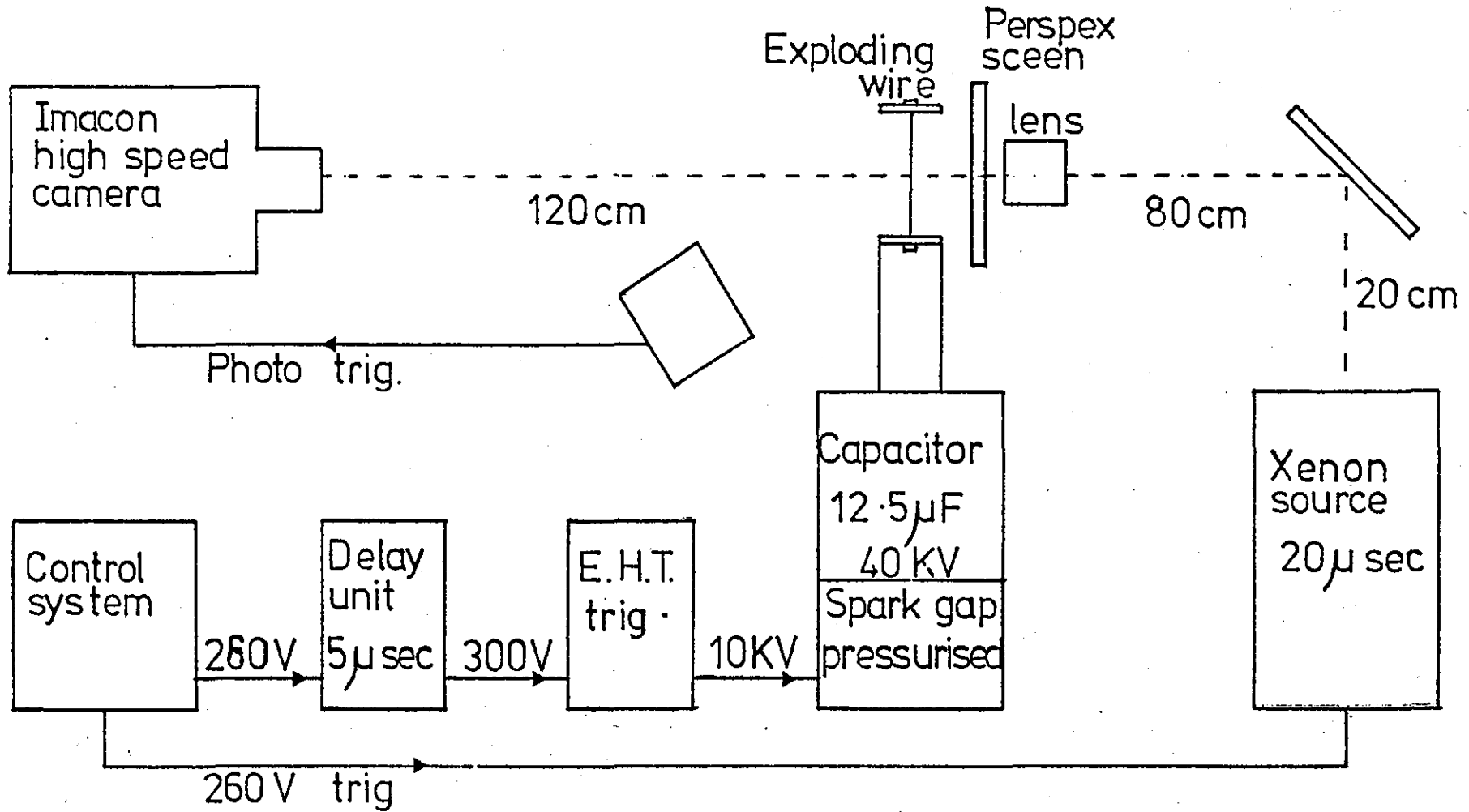
reduces the electromagnetic noise level to tolerable limits when the probe is mounted flush with the inner surface of the cylinder. A voltage-time response from the probe was recorded, and it was reported that the time variation was consistent with the characteristics of the pressure pulse. The output of the probe was combined with the separately measured value for the peak pressure to give the complete pressure-time profile. The peak pressure was calculated by using the Rankine-Hugoniot conditions and considering air as a real gas, the measured shock speed was converted into a value of the peak reflected pressure.

3.5 EXPERIMENT EQUIPMENT.

High-speed photography of the exploding wire has been carried out using a simple single lens Schlieren system in conjunction with a Hadland Imacon image-converter camera operating at nominally 10^6 frames S^{-1} , the frame exposure being 0.2μ sec. The axis of the Schlieren system is perpendicular to the wire, and the knife-edge is set to record density gradients perpendicular to the wire. The light-source and the camera are each about 1.2 m from the wire while the Schlieren lens is just 10 cm away. To protect the lens a perspex sheet is placed between it and the wire. The light source is a Xenon flash (HL 103, J.Hadland) of flash duration $\sim 20 \mu$ sec.

The capacitor is $12.5 \mu F$ with a maximum operating voltage of 40 KV giving a maximum stored energy of 10 KJ. The discharge system is of low inductance ($< 0.5 \mu H$), and gives a time $< 10 \mu$ sec. for the first half-cycle of the discharge. The triggering set-up is shown in Figure 3.4. The capacitor is fired by triggering a

FIG. 3.4 Schematic diagram of exploding wire triggering and recording system.



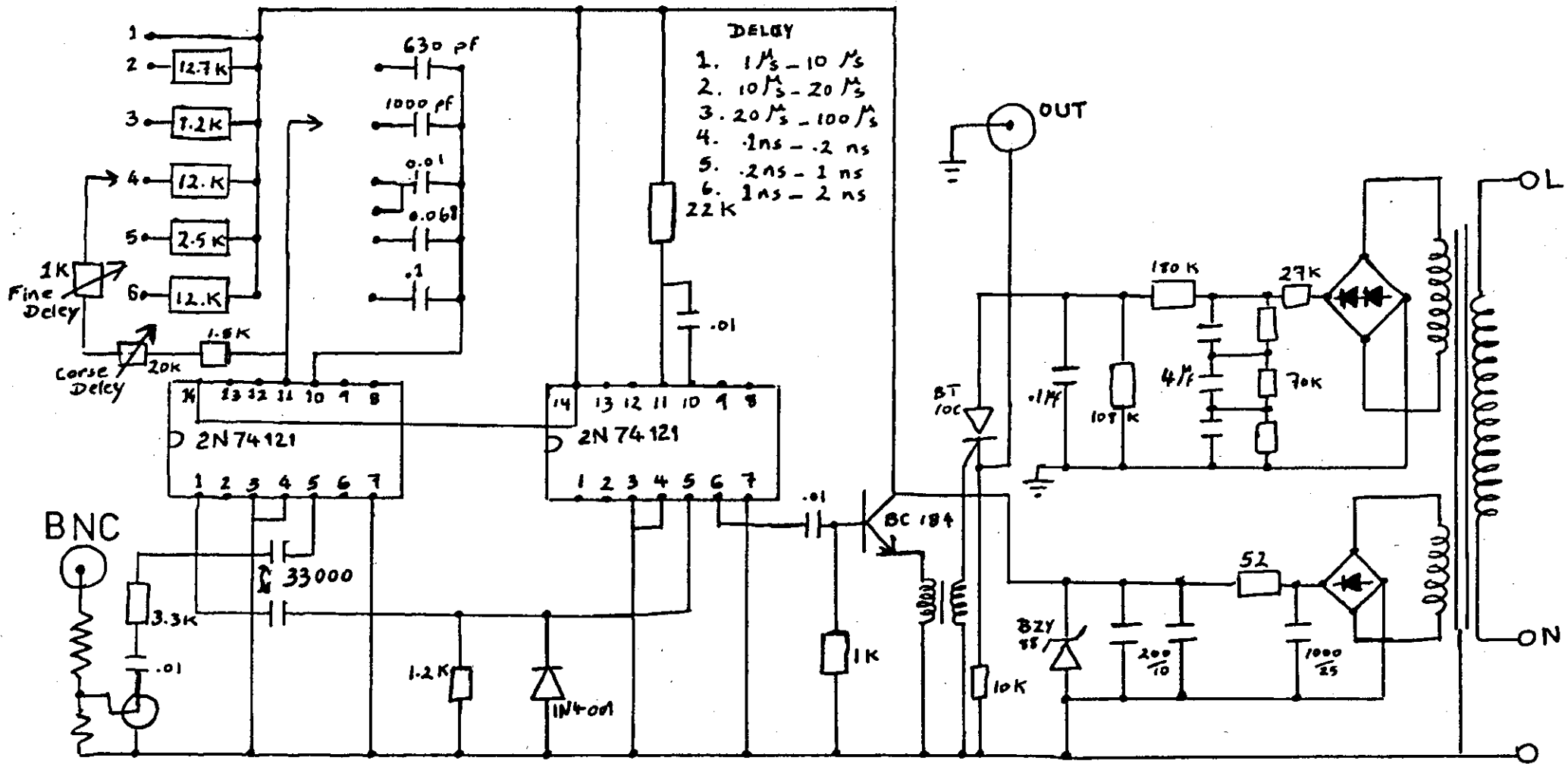


FIG.3.5 CIRCUIT DIAGRAM OF THE DELAY-TIME UNIT.

pressurised dry-Nitrogen-filled asymmetric spark-gap with a 10 KV step pulse initiated by a 250V pulse from a control unit. The 250V pulse is delayed by 5 μ sec. (a circuit diagram of the delay-time unit is shown in Figure 3.5) before reaching the EHT trigger, but is fed undelayed to the Xenon light-source. This is necessary to allow the light source output to reach a suitable level for photography before the explosion occurs. (Figure 3.6 shows an exploding wire without using delay-time unit). The camera is triggered by a photodetector (circuit diagram of the Imacon trigger unit is shown in Figure 3.7) positioned to detect light from the exploding wire itself and not from the Xenon source. The inherent delay between the firing of the capacitor and the camera being triggered is $\sim 1 \mu$ sec.

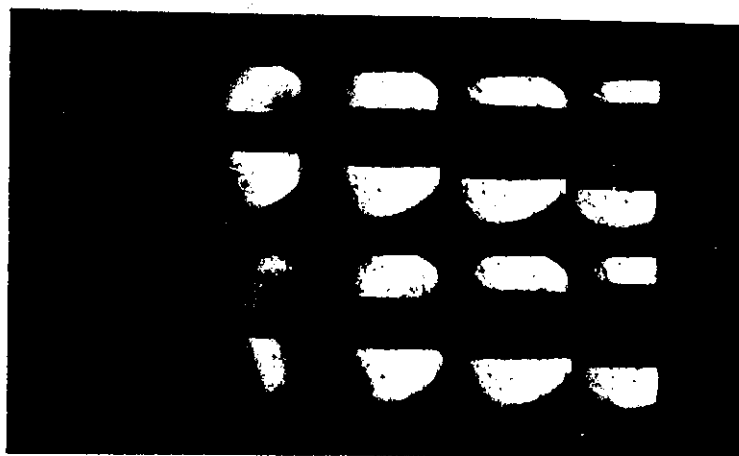


FIGURE 3.6 EXPLODING 34 SWG AT 25 KV
WITHOUT USING DELAY-TIME UNIT.

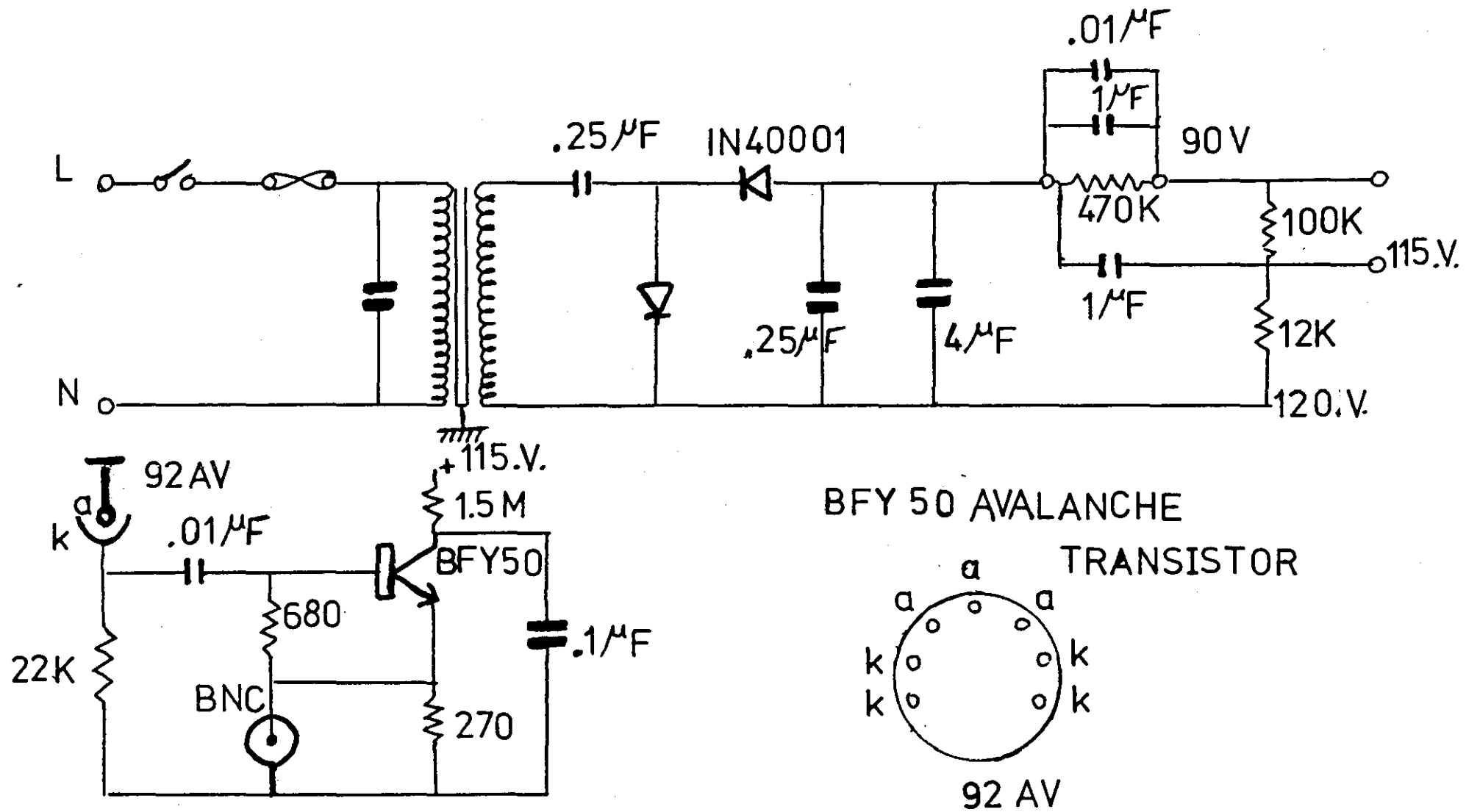


FIG.3.7 IMACON CAMERA TRIGGER UNIT.

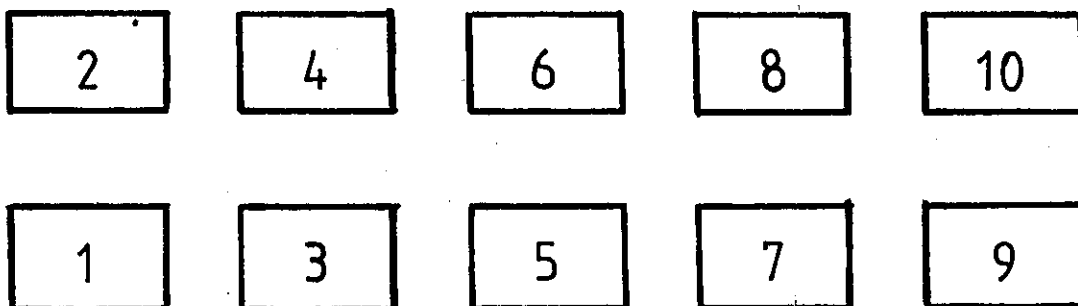
3.5.1 The 'Imacon' Camera.

The Imacon is an ultra high-speed image convertor tube camera operating in both multiple framing and streak modes. In the multi-frame mode a sequence of pictures is produced at rates determined by interchangeable plug-in modules. Rates available cover the range 2.5×10^4 to 2×10^7 frames/second being selected by simple external adjustment. In the streak mode, an image of a line in the event is swept across the film at a constant rate thus producing a record of light intensity distribution against a known time base. The range of sweep rates is from one millisecond/cm to one nanosecond/mm. Much higher recording speeds up to 6×10^8 frames/sec and streak rates of 75 mm/nanosec. (3 picosecond time resolution) are available with the Imacon 600.

The basic advantages of the image converter are: greatly increased optical aperture, the ability to trigger the camera by an electrical signal derived from the event, and intrinsically higher time resolution capability.

3.5.2 Imacon Camera Framing Speed.

The nominal framing speed was 1×10^6 frames/sec. which should give one microsecond separation between two successive frames. The sequence of frames is



This timing interval was checked by using the output from a standard 1 Mhz crystal oscillator as in Figure 3.8. The upper trace of the oscilloscope picture shows this standard 1 Mhz signal while the lower trace is the monitor output from the Imacon camera. The monitor pulses coincide with the frames, 1, 3, 5, 7, 9, etc. By comparing these time intervals with the standard 1 Mhz, the true frame interval was observed. From the lower trace the pulses should be 2 μ sec. apart but the time measured between the frames 3-5, 5-7, and 7-9 are 1.94, 1.93 and 1.90 μ sec. respectively. This difference in time should increase the blast-wave velocity by a factor of 4% and the reflected pressure by 10%.

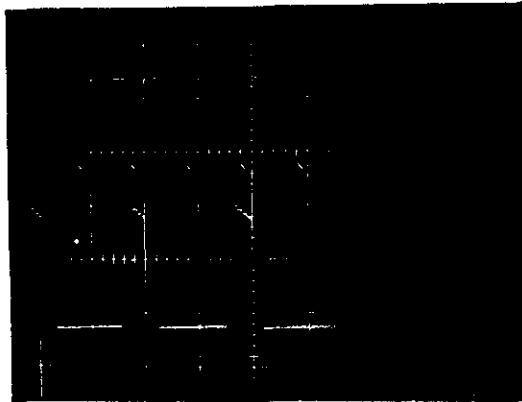


FIGURE 3.8 CRYSTAL OSCILATOR 1 Mhz.

SWEEP : 1 μ s/cm

a : 2 V/cm

b : 10 V/cm

3.5.3 Xenon Light Source.

The flash source is of type HL 103 (20 μ sec. duration). This unit contains high voltage capacitors, these capacitors can be discharged by flashing the lamp. Maximum working voltage is 2.5 KV and maximum energy per flash is 240 Joules. The main transformer and rectifier circuit is shown in Figure 3.9.

There is an intrinsic delay from the trigger pulse to flash. This delay does not depend on the duration of the flash but only on the operating voltage. At 2.5 KV intrinsic delay is 4 μ sec., at 2 KV is 9 μ sec. and at 1.75 KV intrinsic delay is 15 μ sec. The lamp can be triggered by a positive pulse 20-200 volts applied to the "pos-pulse" socket or by pressing the 'test' button. The trigger unit circuit is shown in Figure 3.10.

Variable bias control to alter the trigger voltage level when low amplitude positive trigger pulses discriminate against noise and spurious. Signals can be obtained by backing off the sensitivity until the circuitry does not fire and then slightly increasing. Maximum sensitivity is maximum clockwise. The Xenon flash discharge circuit is shown in Figure 3.11.

3.5.4 Schlieren Technique Method.

The method enables the shock speed to be followed continuously over the entire length of the shock wave. The refraction of a light beam at a density gradient is used to produce a focused image representing the shock front on a film which is displaced rapidly in a direction at right angles to the shock front. The record obtained is thus a graph of distance moved by the shock front

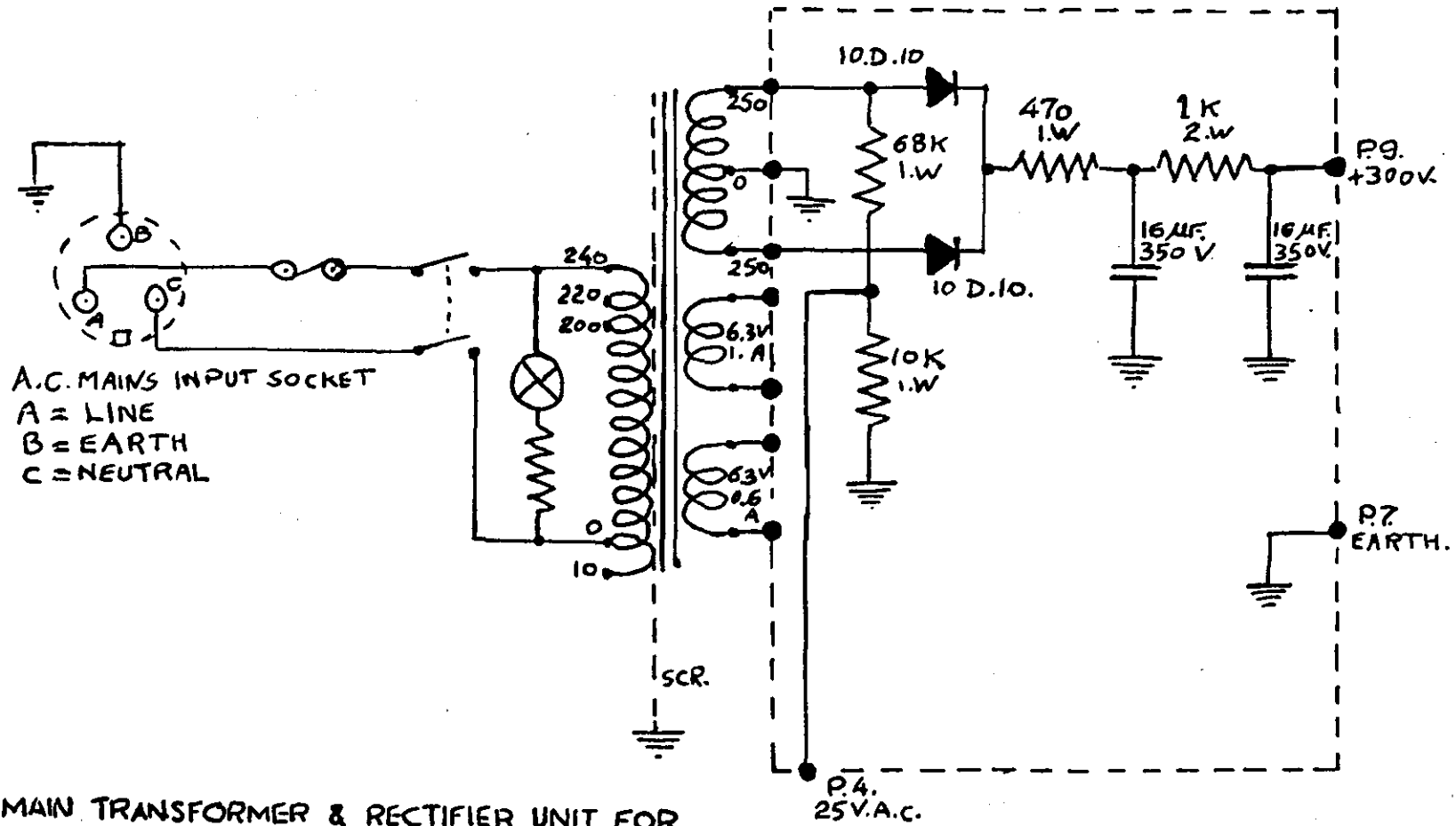
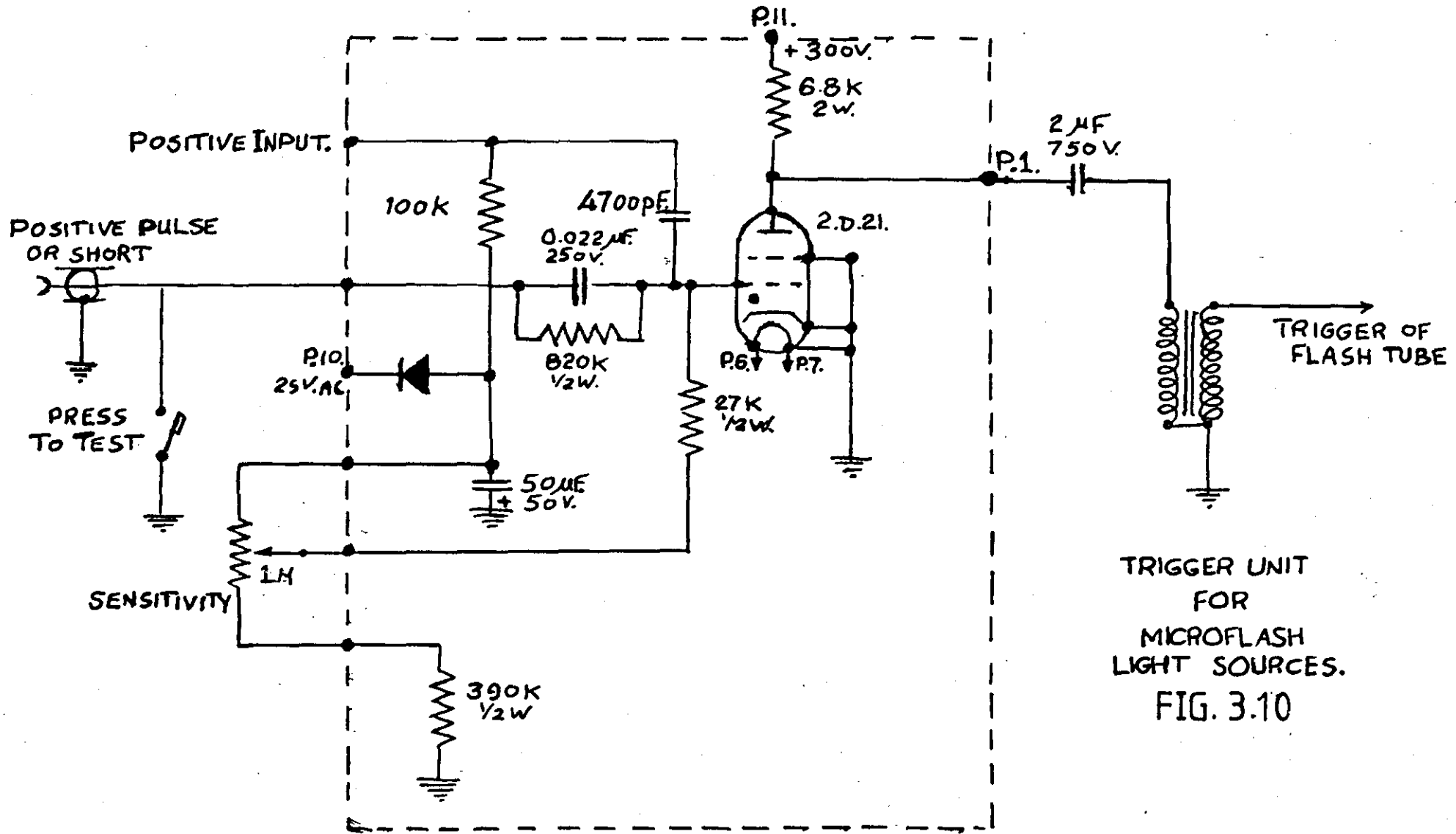


FIG. 3.9 MAIN TRANSFORMER & RECTIFIER UNIT FOR MICROFLASH LIGHT SOURCES.



TRIGGER UNIT
 FOR
 MICROFLASH
 LIGHT SOURCES.
 FIG. 3.10

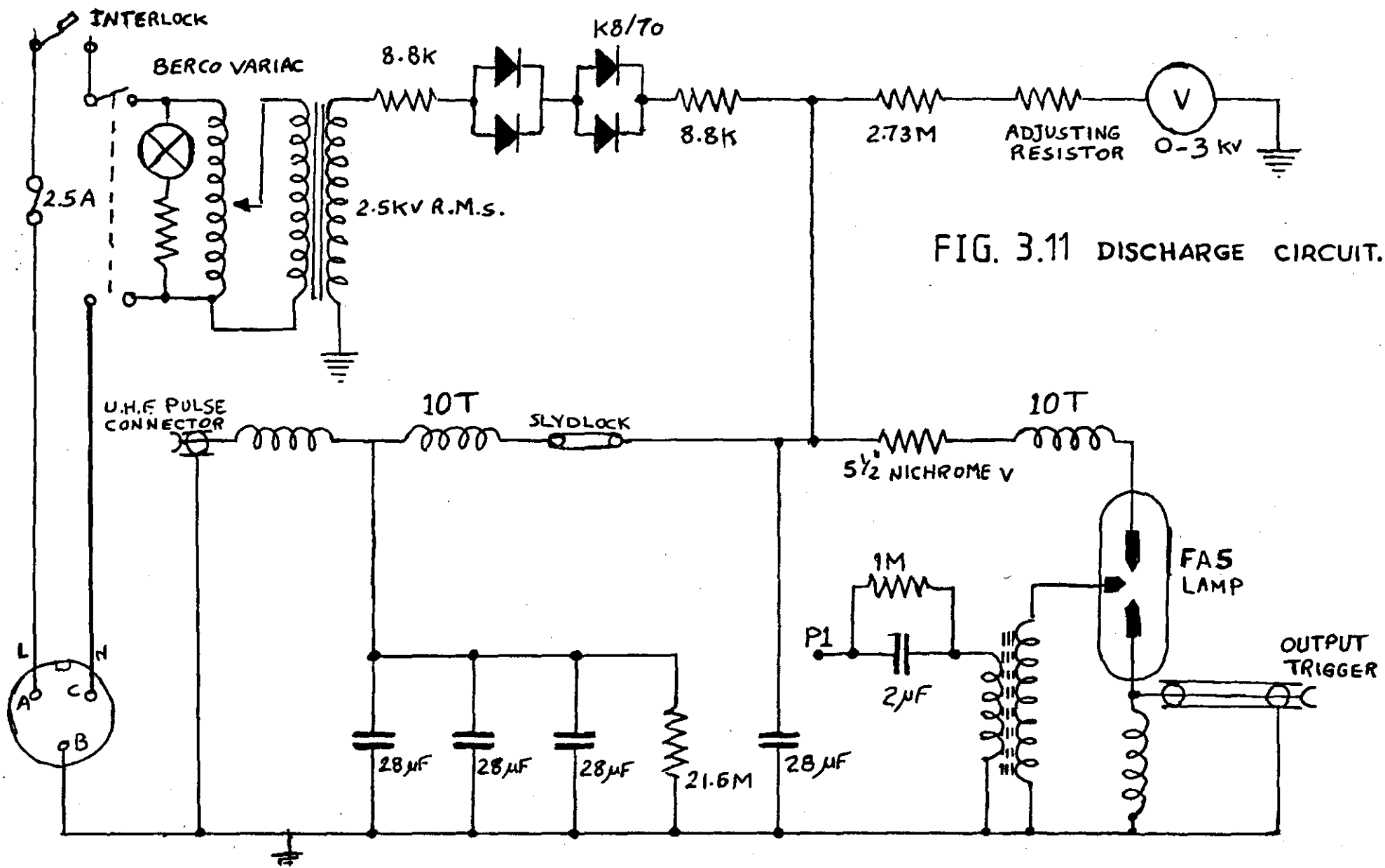


FIG. 3.11 DISCHARGE CIRCUIT.

versus time, and the speed is measured from the slope of the line image.

The refractive index (n) for a gas or vapour was found by Gladstone and Dale to be related to its density (ρ) by the law

$$k\rho = (n-1)$$

where k is Gladstone-Dale constant.

The light travels at a speed inversely proportional to the refractive index of the medium through which it is passing. Thus if a light-wave of given form enters a region in which the density varies, it will travel more slowly through zones of high density, and high refractive index. If the change in direction is great enough, the variation in illumination over a screen placed in the light-beam will be different. This effect is utilised in the shadow graph method for determining the positions and shapes of shock waves. The simple schlieren system is shown in Figure 3.12.

3.6 SYMMETRY OF THE EXPLODING WIRE.

The very nature of an exploding wire would indicate that radial symmetry is to be expected. However, the two most desirable properties are the lack of variation along the length of the wire during and subsequent to the vaporization, and the resulting high pressures generated. This geometric configuration is important in the cylindrical wave propagated from exploding wires inside a cylindrical specimen.

The circuit used in this study is similar to the usual exploding wire circuitry, except that the Xenon flash and high speed camera have been used to measure the cylindrical shock wave produced from

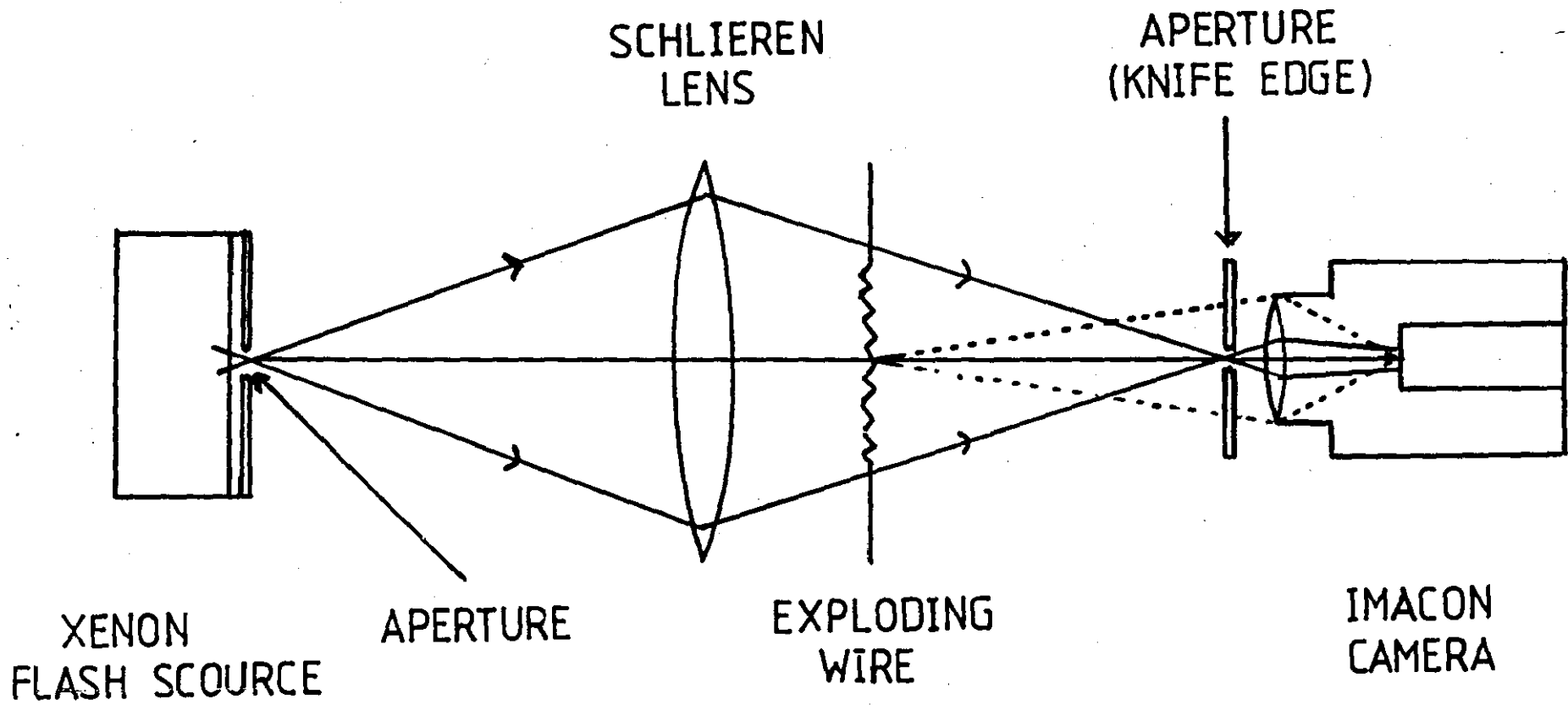


FIG. 3.12 SIMPLE SCHLIEREN ARRANGEMENT.

the explosion of copper wire. The schlieren technique has been used in this experiment by discharging a 3920 Joules at 20 KV through wire of size 24 SWG.

A double exposure was used enabling the wire to be photographed before and during the explosion. The double exposure photograph shown in Figure 3.13 establishes the fact that the wire explodes in cylindrical symmetry.

3.7 VELOCITY OF THE SHOCK WAVE.

The theoretical equilibrium state of a gas in a shock wave can be obtained solely from a knowledge of the speed of the shock, relative to the explosion, and the conditions of the gas into which it propagates. For this reason, a measure of the velocity of shock wave is highly desirable in exploding wire applications, since it enables a theoretical determination of the pressure induced from wire explosions inside a cylinder.

The method of shock wave velocity measurement involves the detection of the shock front relative to the explosion, and this is facilitated by the large and rapid changes in pressure, density and temperature with which the shock front is associated.

Voltages of 25, 30 and 35 KV have been discharged through copper wire of sizes 22, 24, 26, 27, 29, 32 and 34 SWG (Standard wire gauge) of length 14 cm. The shock waves were followed out to a maximum distance 28 mm from the wire axis. High speed photographic records of a typical exploding wire demonstrating the axially symmetric wave front in air are shown in Figures 3.15 - 3.24. For subsequent analysis the distance scale of the records was

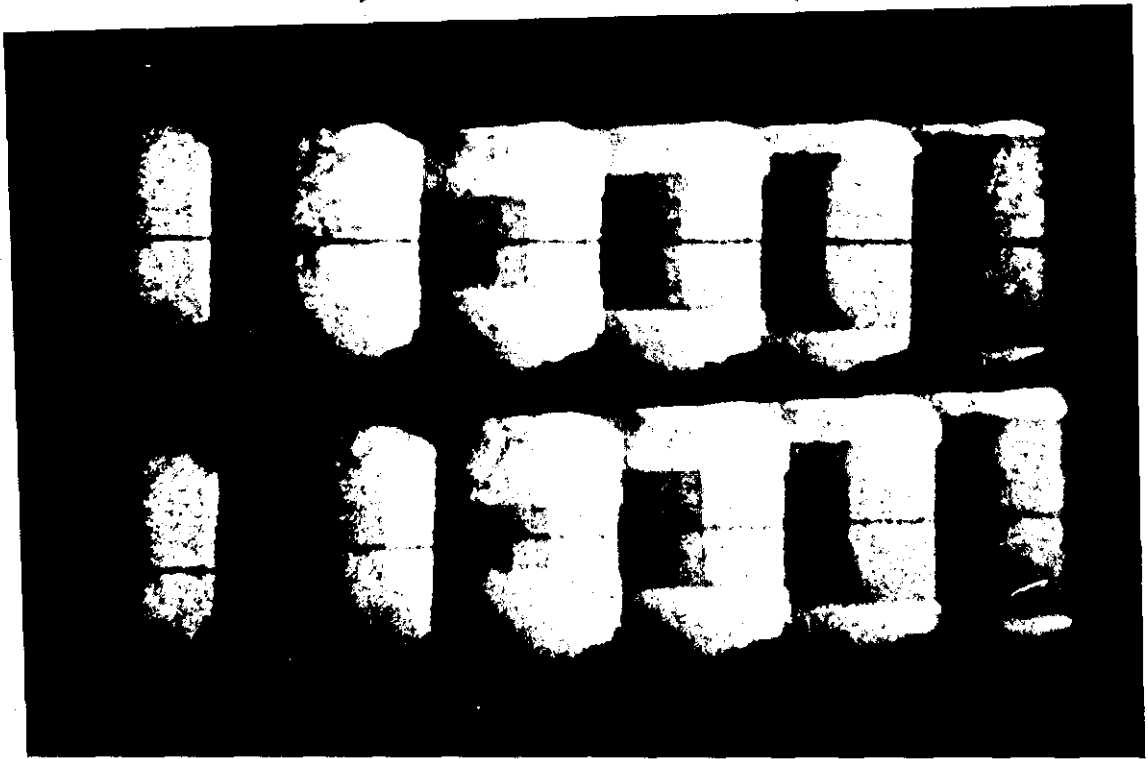


FIG. 3.13 DOUBLE EXPOSURE

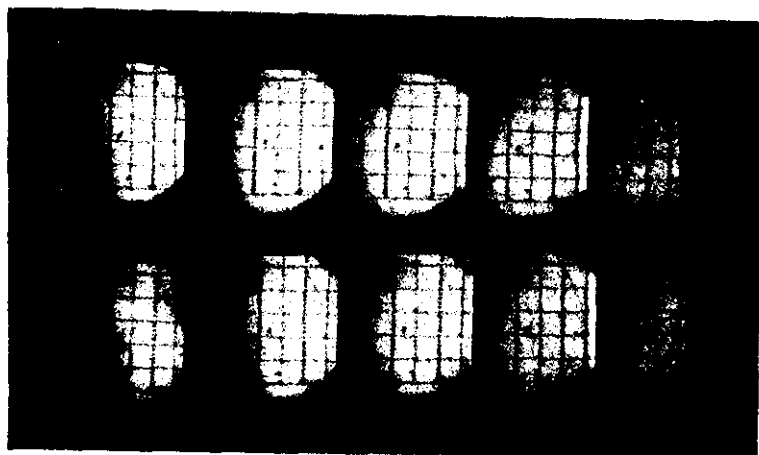


FIG. 3.14 CALIBRATION RECORD

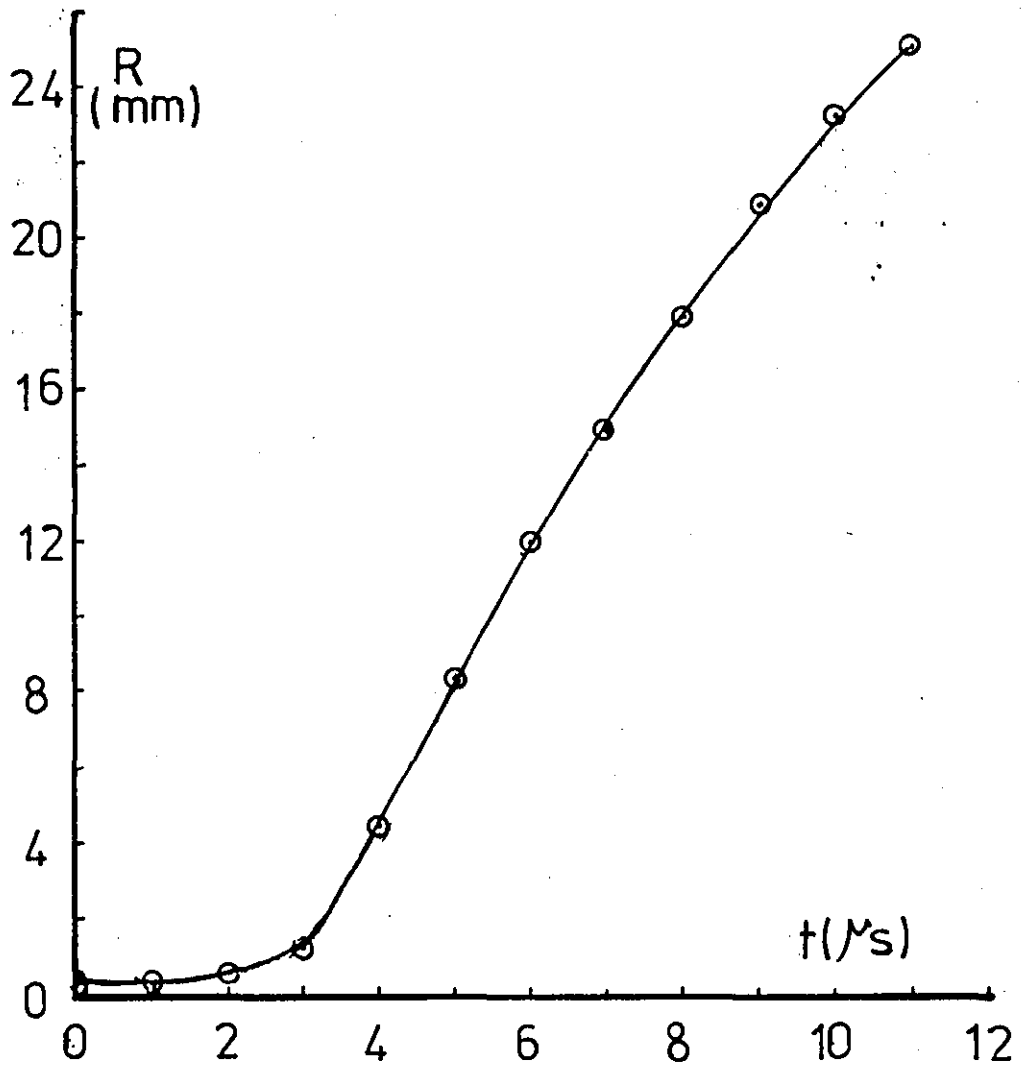
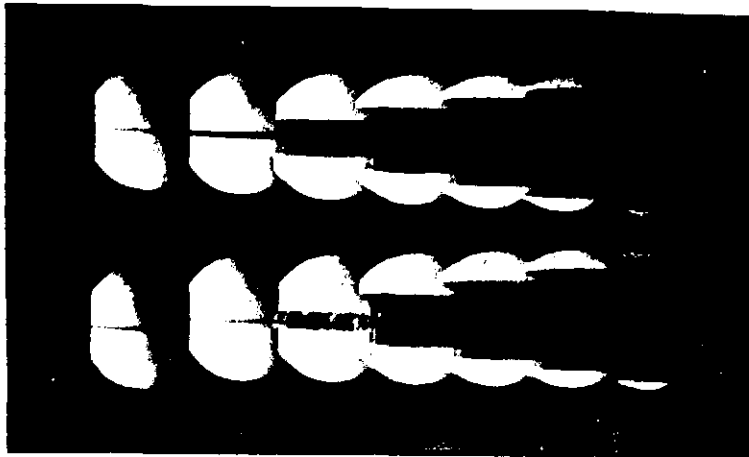


FIG. 3.15 Radius of shock-front against time for 22 SWG at 30 KV.

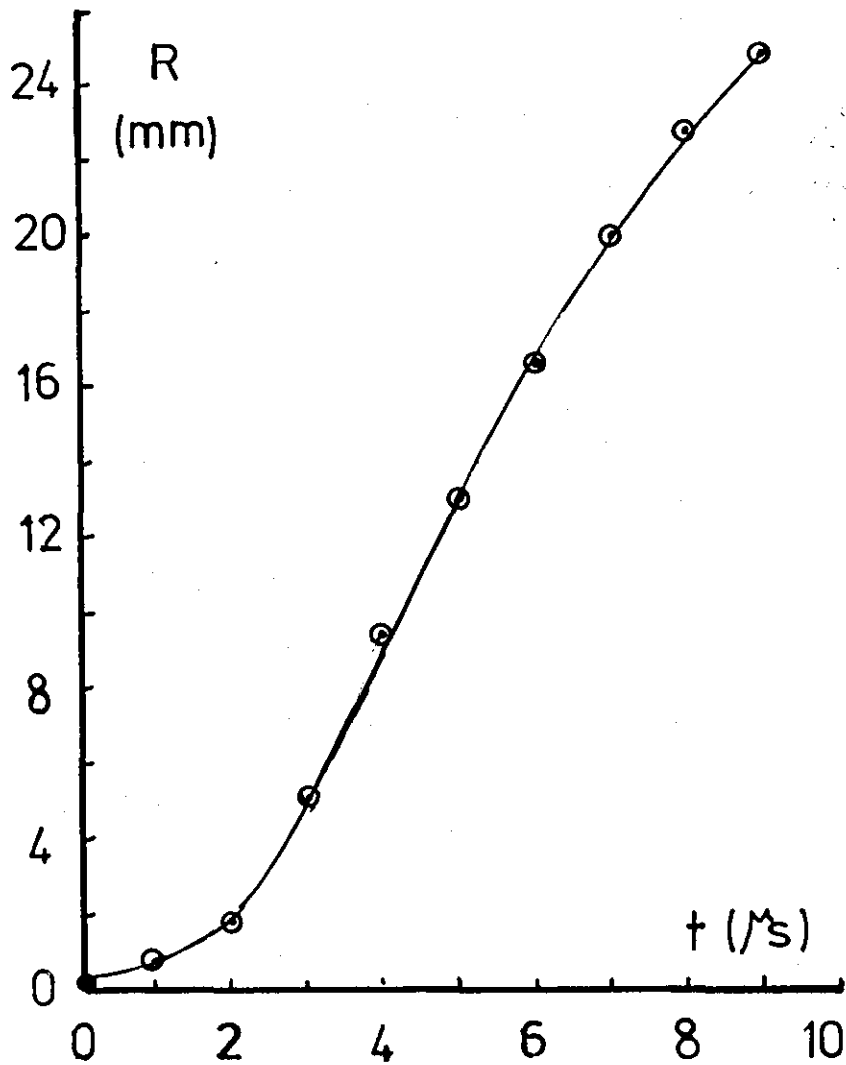
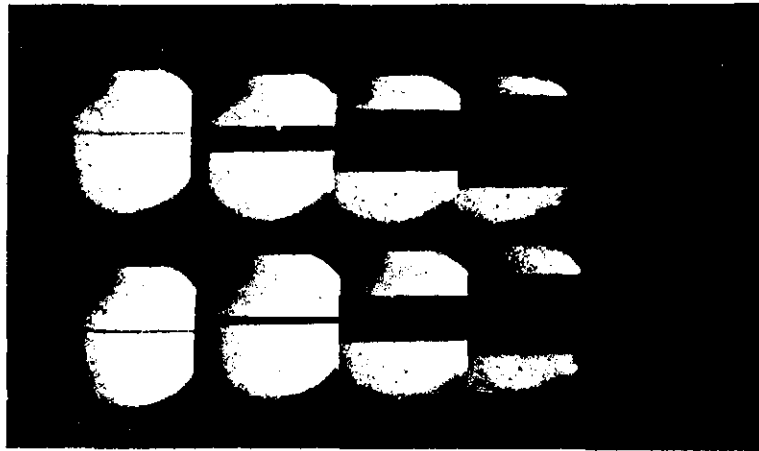


FIG. 3.16 Radius of shock-front against time for 24 SWG at 30 KV.

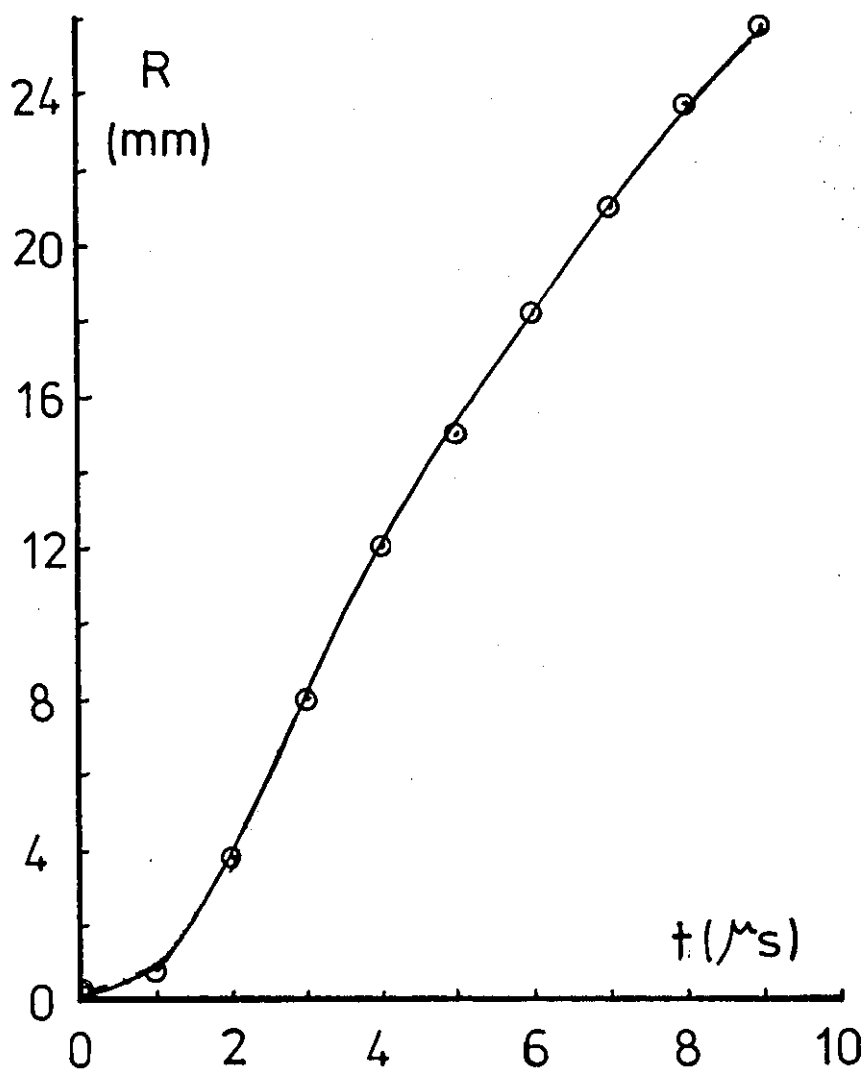
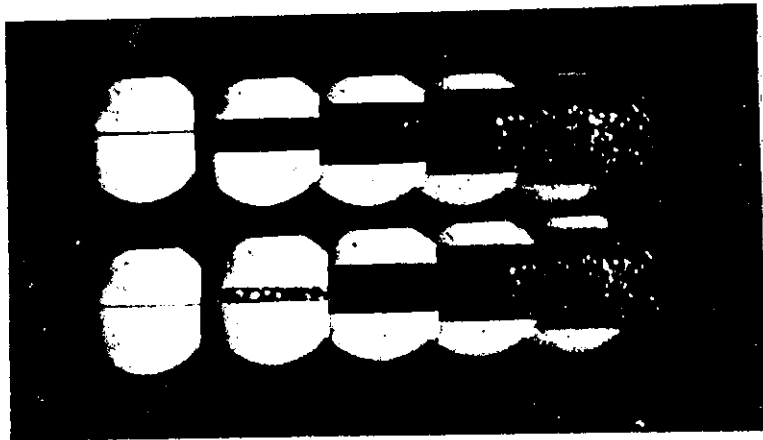


FIG. 3.17 Radius of shock-front against time for 26 SWG at 30 KV.

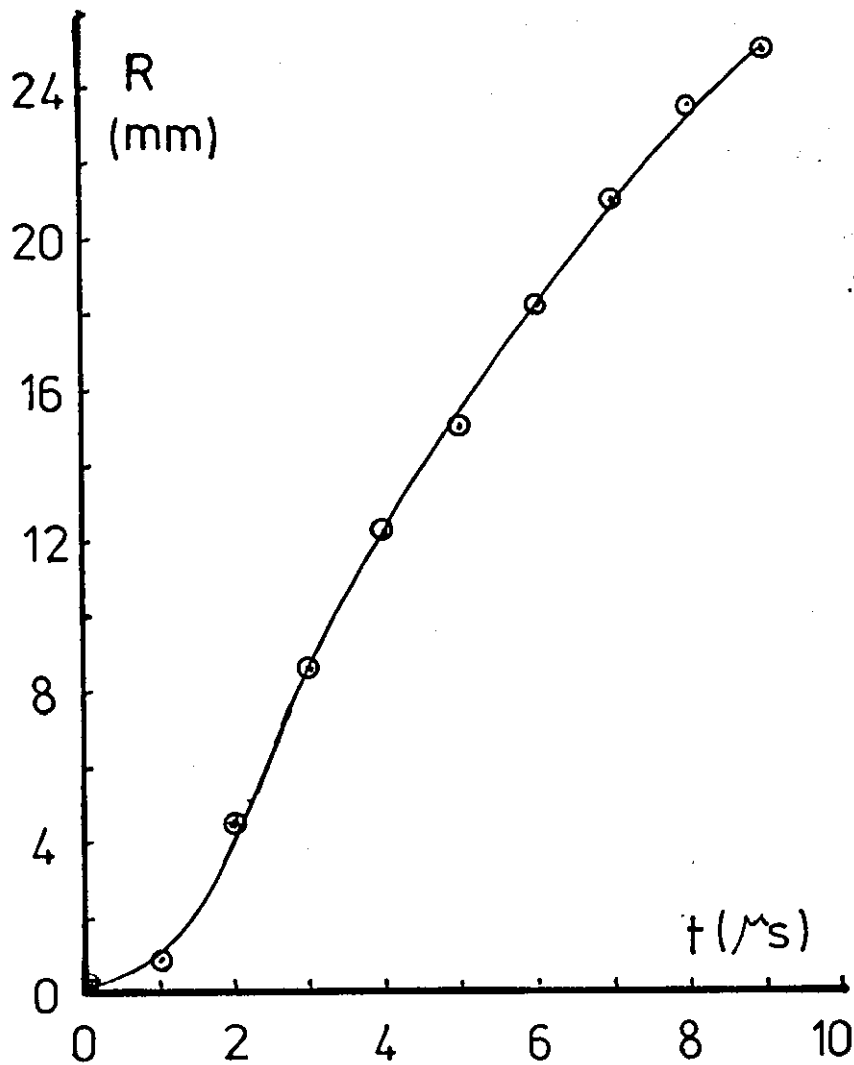
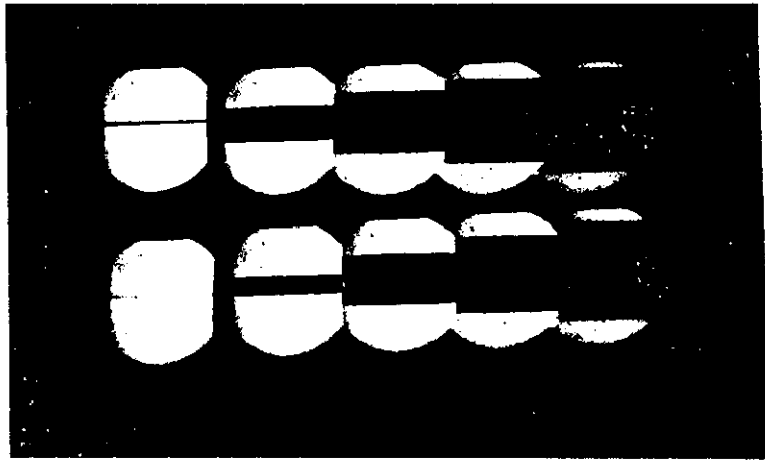


FIG. 3.18 Radius of shock-front against time for 27 SWG at 30 KV.

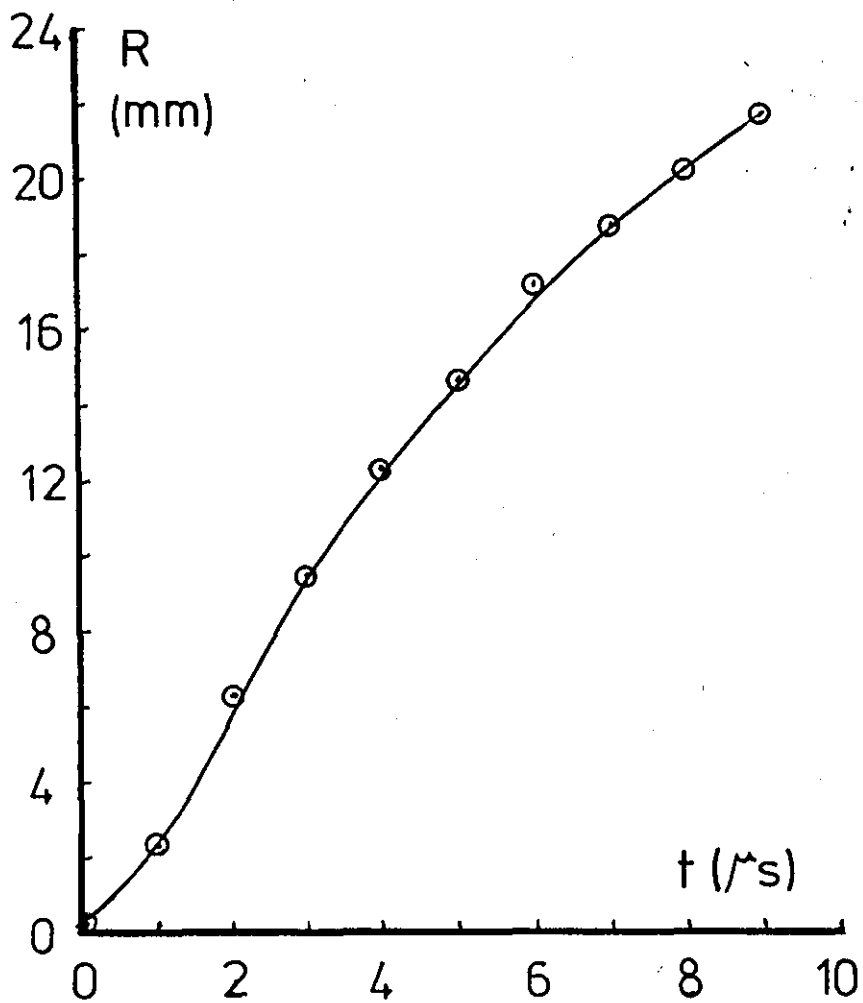
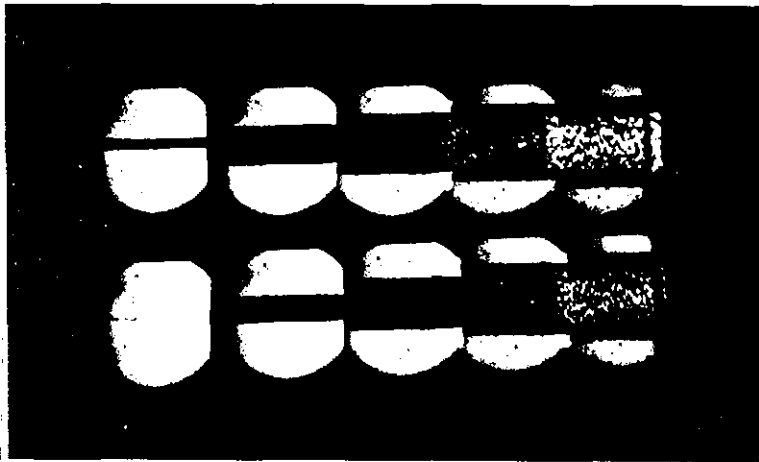


FIG. 3.19 Radius of shock-front against time for 29 SWG at 30 KV.

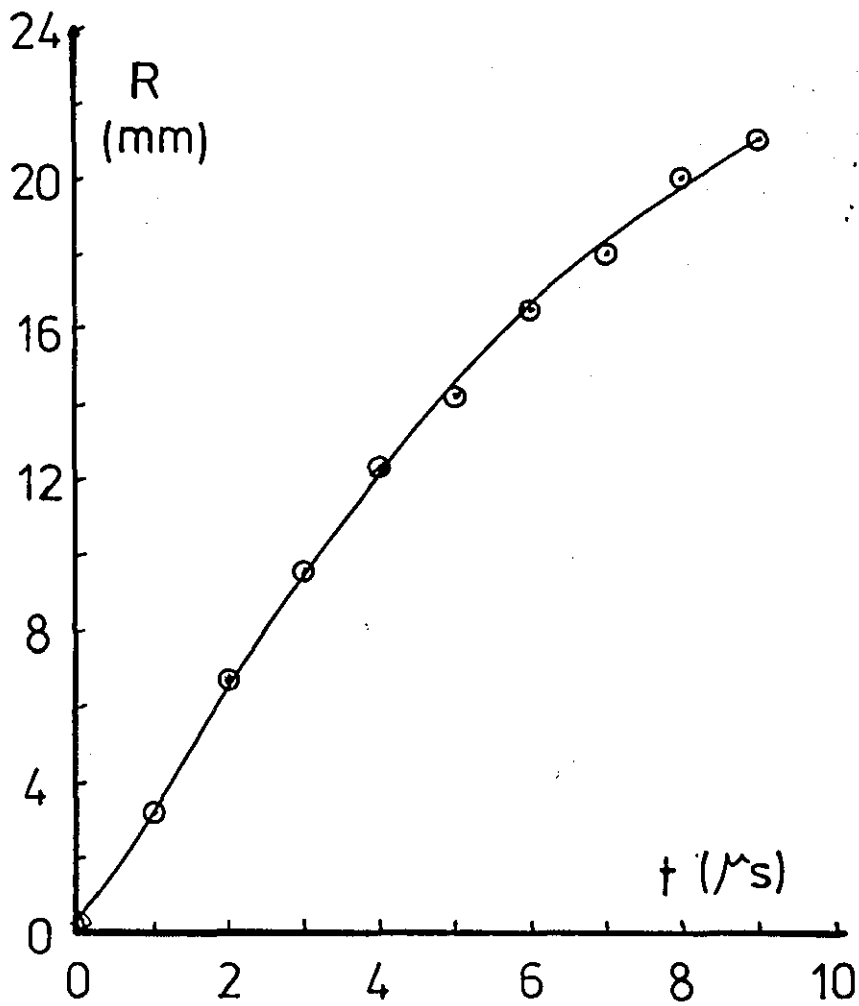
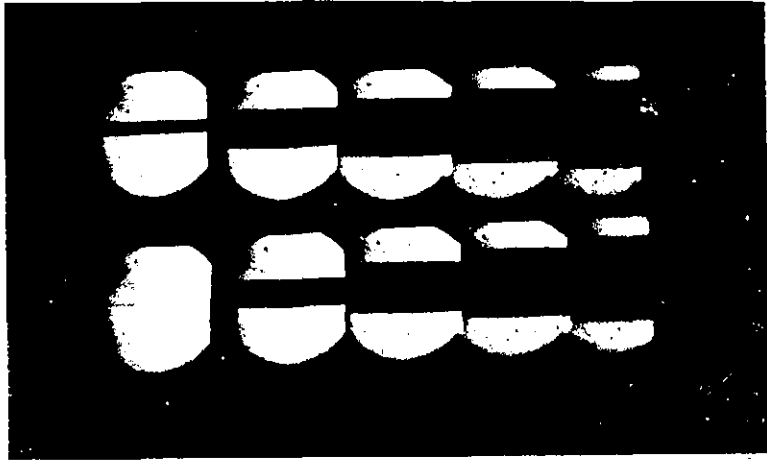


FIG. 3.20 Radius of shock-front against time for 32 SWG at 30 KV.

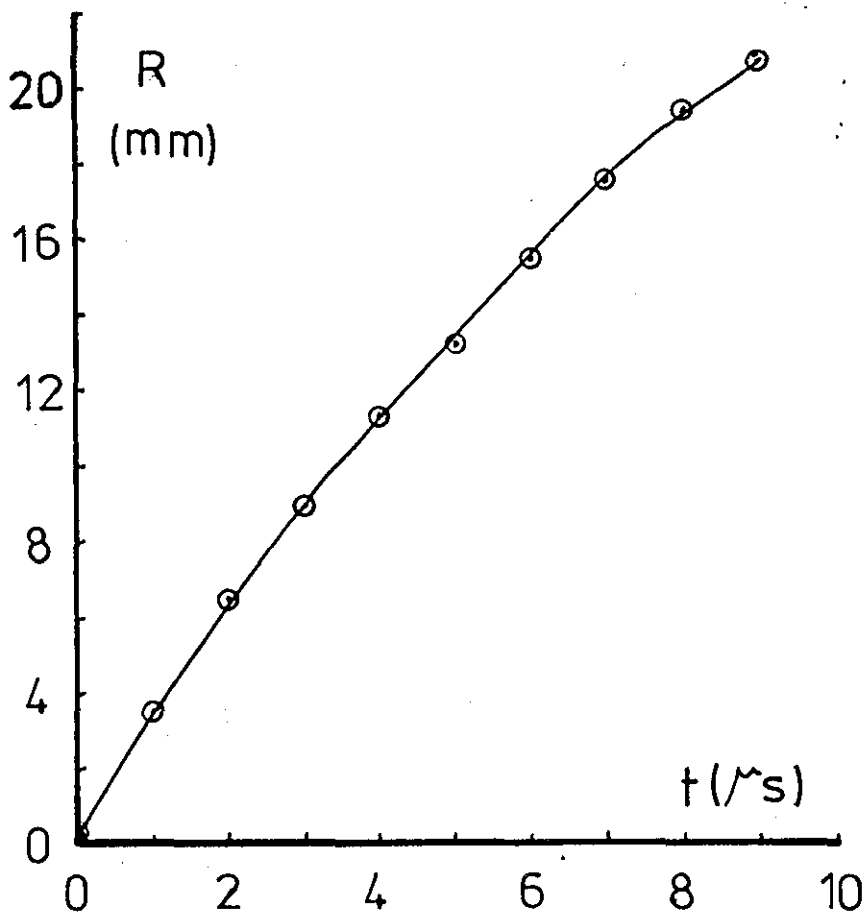
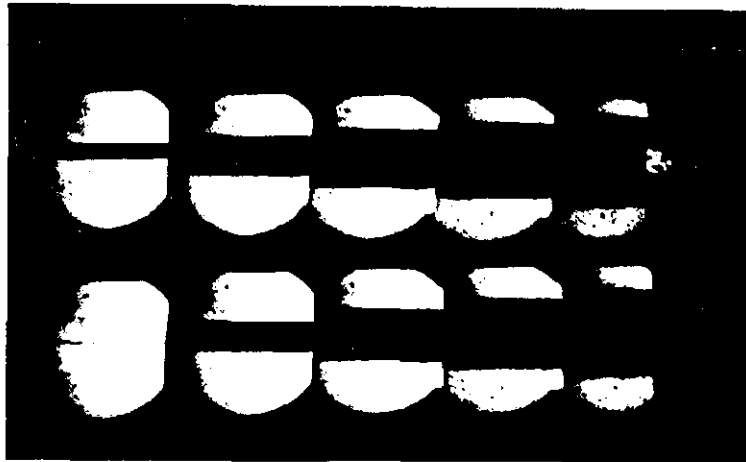


FIG. 3.21 Radius of shock-front against time for 34 SWG at 30 KV.

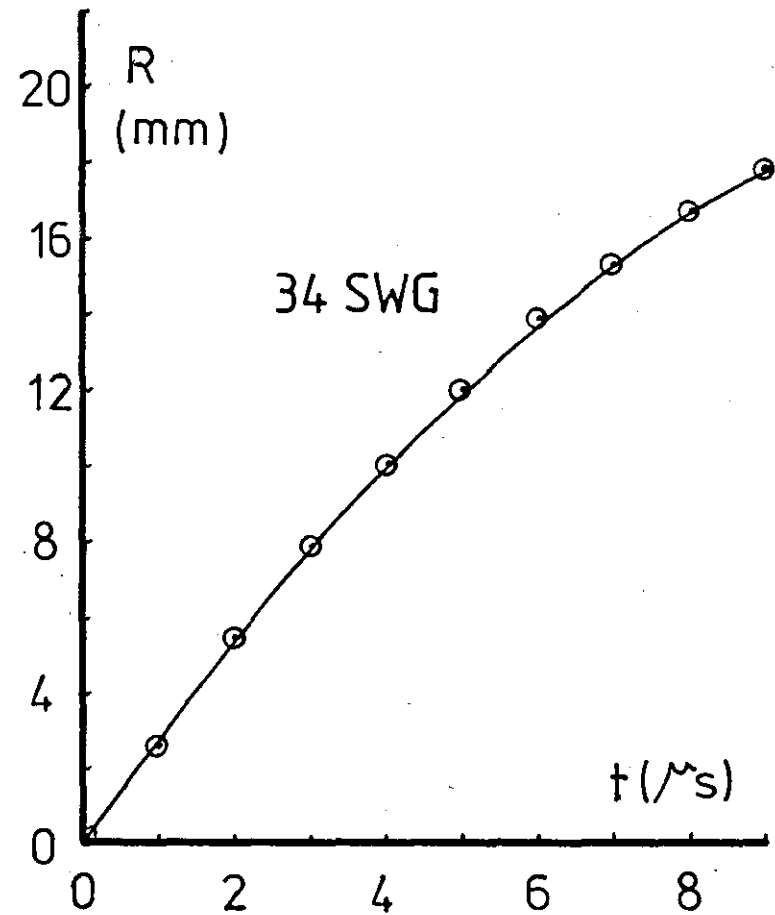
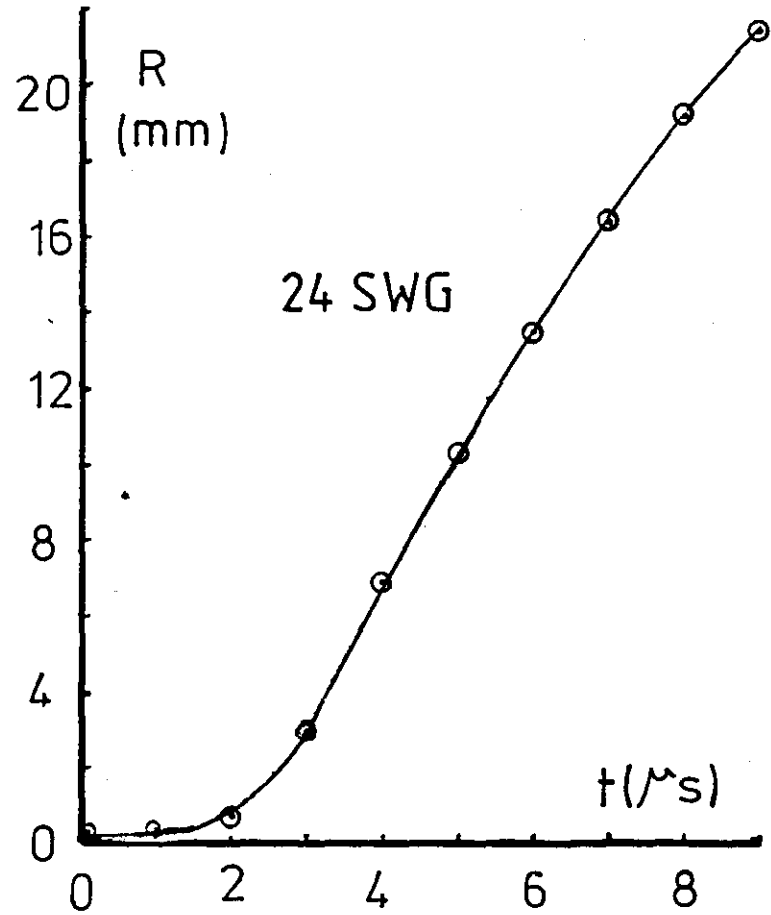


FIG. 3.22 Radius of shock-front against time for 24 & 34 SWG at 25 KV.

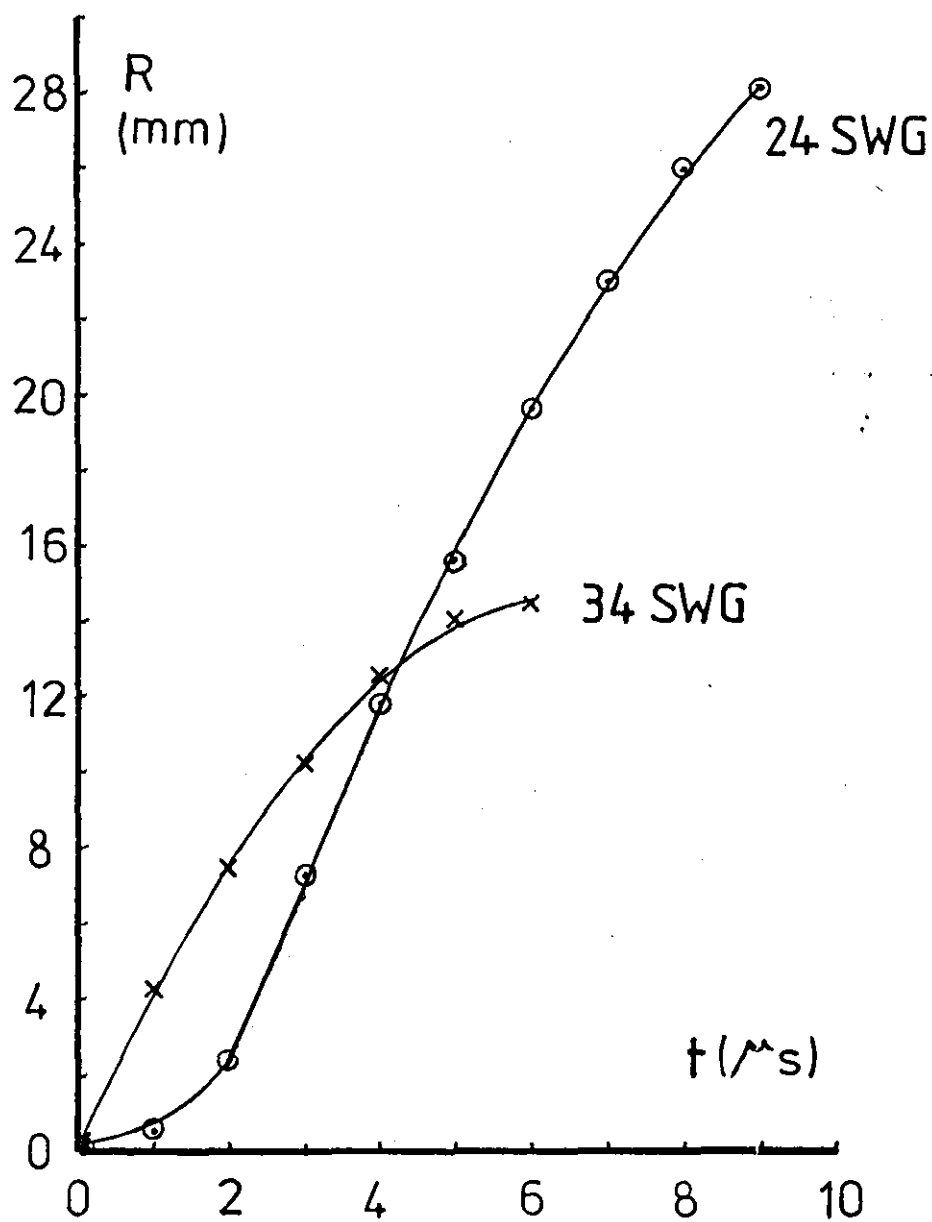


FIG.3.23 Radius of shock-front against time for 24 & 34 SWG at 35 KV.

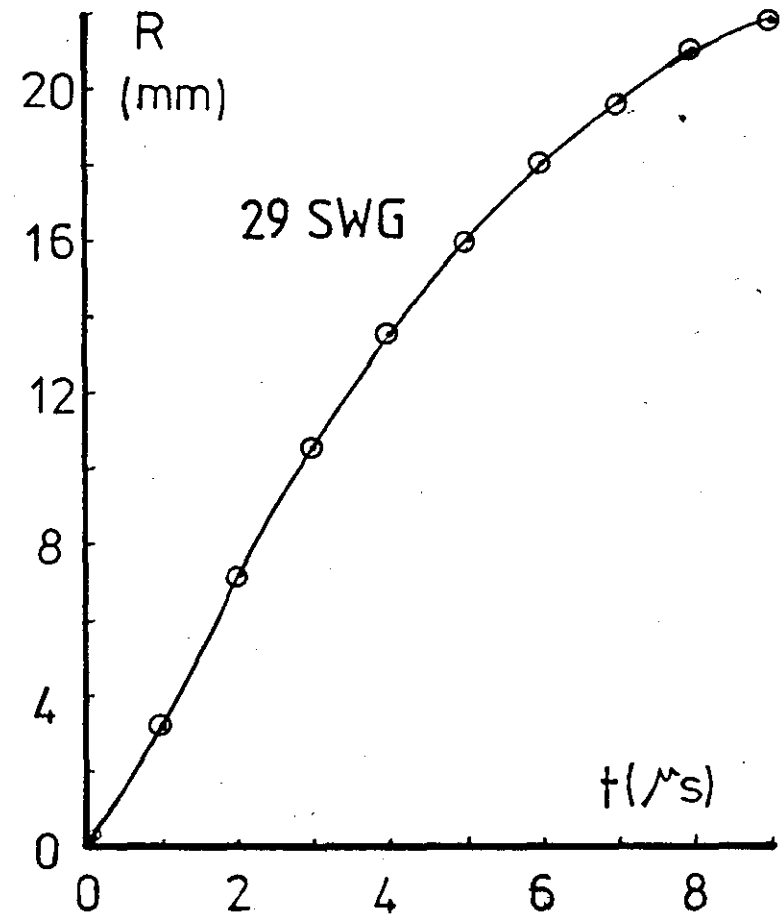
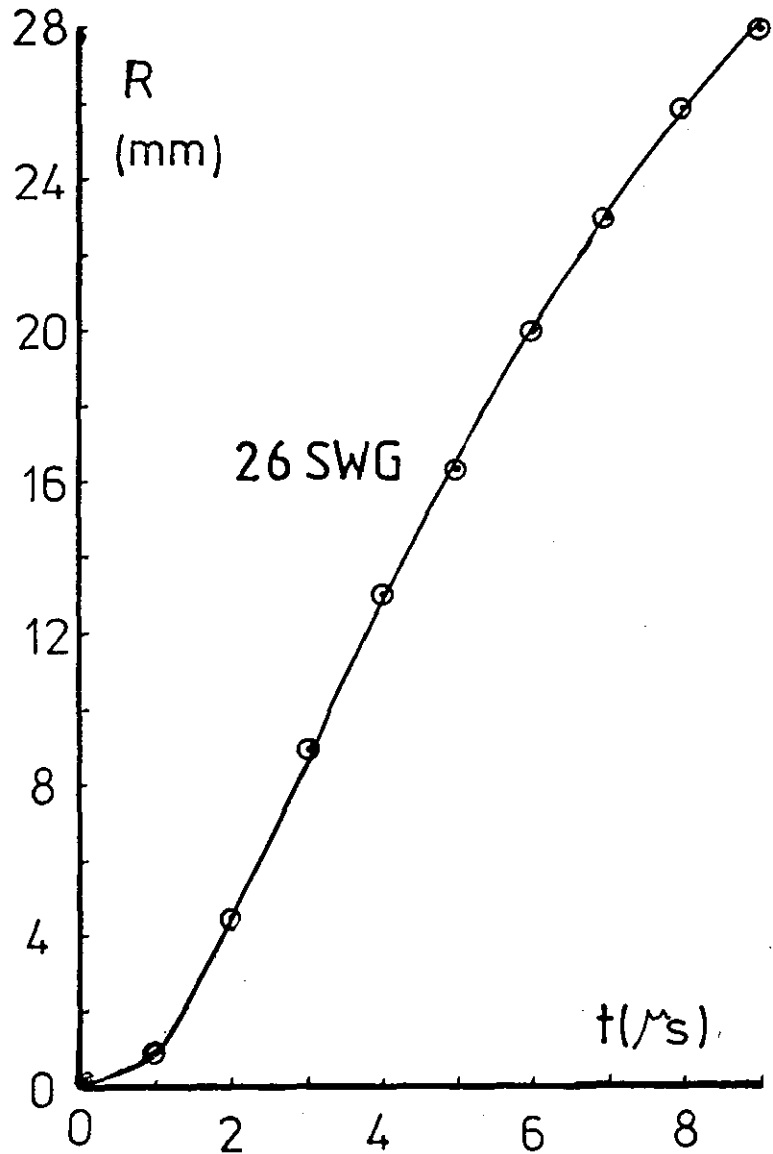


FIG.3.24 Radius of shock-front against time for 26 & 29 SWG at 35 kV.

obtained by photographing a graticule placed in the wire position prior to firing, as shown in Figure 3.14.

The radius of the shock front against the time have been drawn for each wire. The velocity of the shock wave was measured by calculating the slope from the graphs.

The graphs in Figures 3.15 - 3.21 for exploding different wire sizes at 30 KV show that thin wires explode quicker than thicker wires, but the expansion of the wire vapour is shorter; for example in exploding 24 SWG (Figure 3.16) the explosion is slow in the first two microseconds but after this time the vapour expands more rapidly and reaches the maximum velocity in one microsecond whereas in exploding thin wire (34 SWG in Figure 3.21) it took only one microsecond to reach its maximum velocity and slowed down much quicker than the thicker wire.

Figures 3.22 and 3.23 shows a comparison between the exploding of 24 SWG and 34 SWG wires at 25 KV and 35 KV respectively. The representative records obtained from the high speed camera are attached on the same graphs. Figure 3.24 shows the differences in the initial rate of expansion of exploding 26 SWG and 29 SWG at 35 KV.

In all of the records, the shadow of the wire at constant diameter is shown in the first frame of the photograph and is followed by an expansion of the shock waves. The detached vapour **can be** observed in thin wires after six microseconds, **The** shock wave and the contact surface can be seen to separate after which the cloud of dispersed vapour expands more slowly than the shock wave.

Meanwhile the shock propagates outward and

weakens rapidly until the Mach Number, originally higher at the point of separation, drops to less than three at the end of the traces.

The velocity of the shock waves have been measured for each thickness of wire in each of the three input voltages. Values of shock wave velocities obtained from the curves of Figures 3.16, 3.21, 3.22 and 3.23 by measuring the variation of gradient with radius are drawn against radius with the Mach Number printed on the same graphs as shown in Figures 3.25, 3.26 and 3.27. The cylindrical shock wave formed by an exploding wire behaves like an ideal cylindrical blast wave. Mach Number (M) calculated as $\frac{U}{a_0}$, where a_0 is the velocity of sound in air at the room temperature and equal to 345 m/sec.

In Figure 3.25 the velocity of the strong shock wave of 24 SWG wire shows that it rises slower than that of 34 SWG but has higher values and it decays slowly to a further distance of about 18 mm. In the same figure the velocity of the shock wave due to the 34 SWG wire increases rapidly very quickly and decays faster than that of 24 SWG.

The Mach Number for 24 SWG wire at 30 KV is about 12.7 but in the finest wire (34 SWG) at the same energy input is about 9.9.

From these curves, and from those of other wire diameters in Table 3.1 it is seen that: (a) after the explosion there is an initial acceleration phase during which the blast-wave velocity reaches a maximum and then decreases smoothly; (b) this acceleration distance increases with increasing wire diameter; (c) the greatest velocities are obtained with the 24 SWG wire.

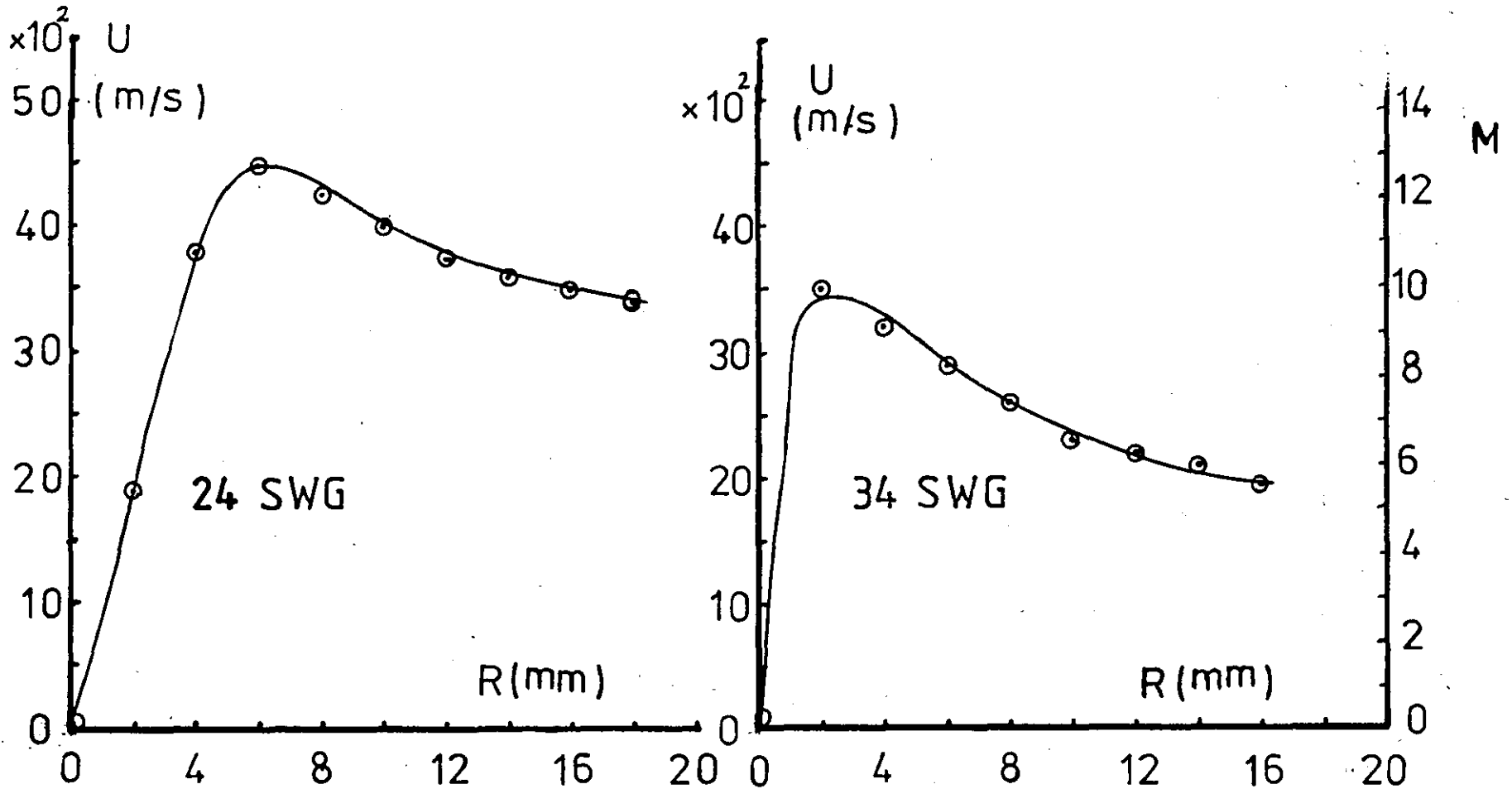


FIG.3.25 Shock-front velocity U and Mach number M against shock-front radius R for 24 & 34 SWG at 30 KV.

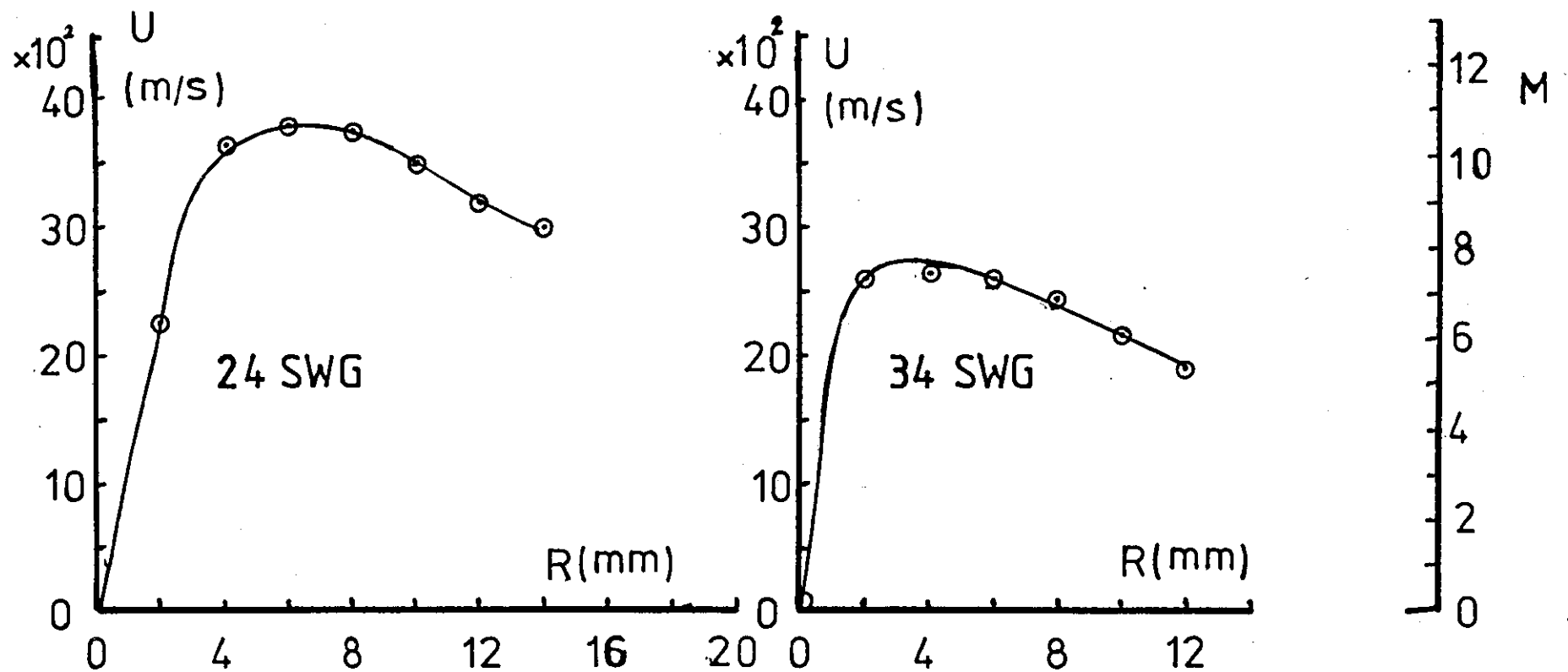


FIG. 3.26 Shock-front velocity U and Mach number M against shock-front radius R for 24 & 34 SWG at 25 KV.

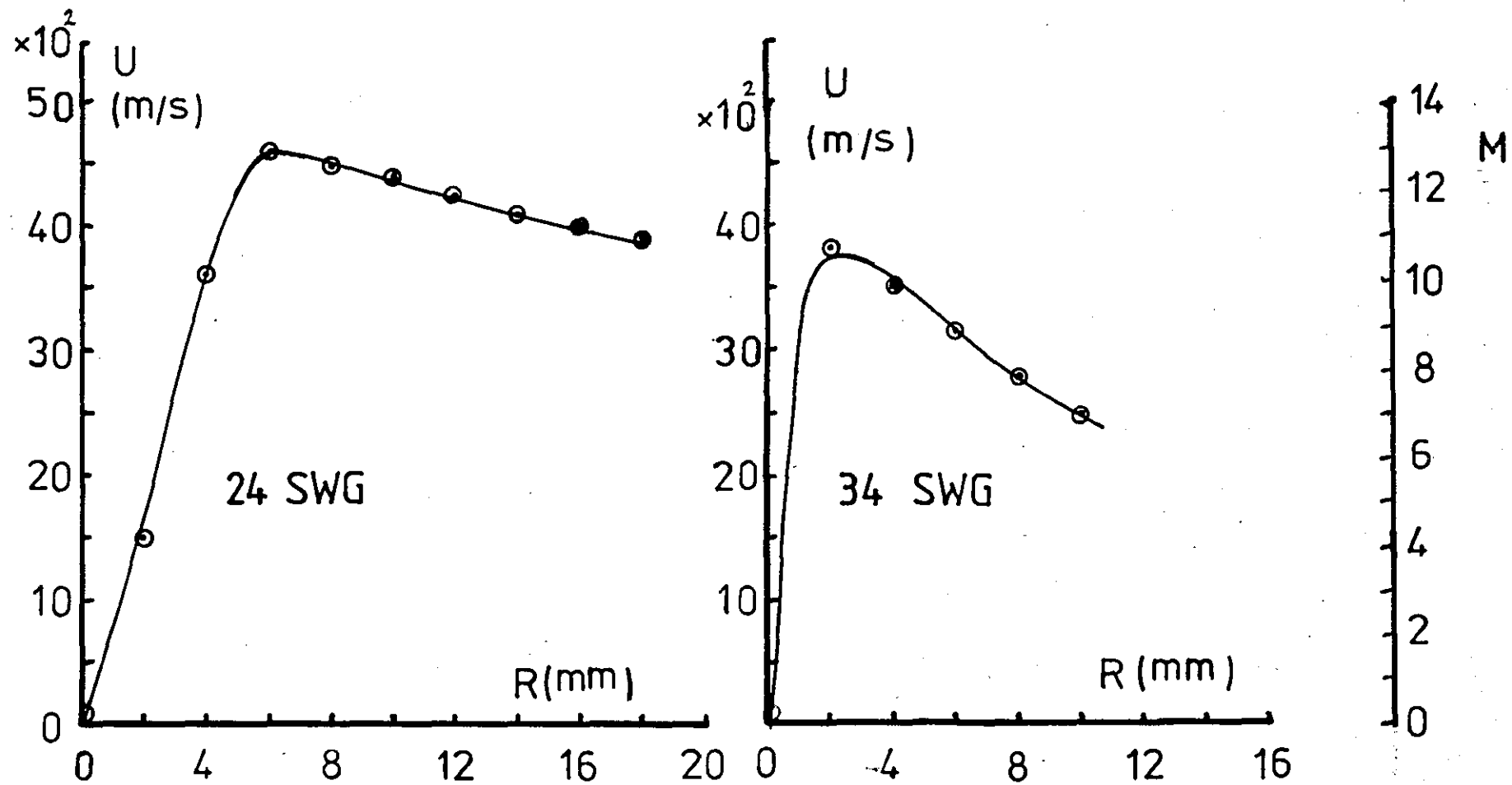


FIG. 3.27 Shock-front velocity U and Mach number M against shock-front radius R for 24 & 34 SWG at 35 KV.

3.8 BLAST WAVE THEORY FOR THE SHOCK WAVE PROPAGATION.

In the theoretical treatment of strong blast waves from wire explosions S.E. Lin (1954) arrived at the following relation between the time and position of the cylindrical shock front:

$$t = \frac{1}{2} \left(\frac{B\rho_0}{E} \right)^{1/2} R^2 \quad (1)$$

where t is the time, R is the distance from the explosion to the shock front, ρ_0 is the density (of air) ahead of the shock, E is the energy in the explosion per unit length, and B is a dimensionless energy parameter (of value 3.94 for air) dependent upon γ , the ratio of specific heats.

The conditions for the validity of this equation are the following:

The energy is assumed to be suddenly released and the shock disturbance is similar at all time, changing only its linear dimensions with increasing time. The gases are supposed to be perfect with constant specific heat ratios. The energy losses from ionization and radiation are neglected.

If equation (1) applies to shock waves from exploding wires, the energy per unit length in the shock can be calculated directly from the measurements of the time and radius of the shock front. When R^2 versus t is plotted it is known that a straight line should be obtained with a slope m given by

$$m = 2 \left(\frac{E}{B\rho_0} \right)^{1/2}$$

The axial energy released of E Joul/cm is easily obtainable from the slope of the data plot.

Shock data corresponding to the wires 22, 24, 26, 27, 29, 32 and 34 SWG have been fitted to the Lin equation by plotting R^2 versus t and selected the best straight line graphically. A typical example of the data plots used in this study are shown in Figures 3.28, 3.29 and 3.30. It can be seen that the early part of the graphs show a slow rise in velocity, and indicates that as the wire explodes 3 to 4 μ sec. elapses while energy is being fed into the explosion to reach its maximum, indicating that the blast-wave behaviour accords with blast-wave theory after this initial period.

The slopes m (cm^2/sec) and the output energy Joul/cm for all copper wires exploded at the energies of 280, 402 and 547 Joul/cm are presented in Table 3.1.

It should be noted that in the published paper by Jones and Galletts in Table 1, the units of the slope given as $m = \text{cm}^2/\text{sec}$ are in error and should read $\text{cm}^2/\mu \text{ sec}$.

3.9 EFFICIENCY OF THE EXPLODING WIRE.

That there should be a particular wire diameter giving the highest velocity blast-waves is explained by considering the energy transfer process from the capacitor. For 30 KV the stored energy is 5.6 KJ with the discharge reaching its peak after $\sim 5 \mu \text{ sec}$. The 34 SWG wire requires only $\sim 400 \text{ J}$ to vaporise (Hultgren (1963)). This means that vaporisation and blast-wave formation are so rapid that only a small part of the stored energy is used, i.e. the wire is not matched efficiently to the discharge system. The best match is provided by the 24 SWG wire for which 2.2 KJ are needed for

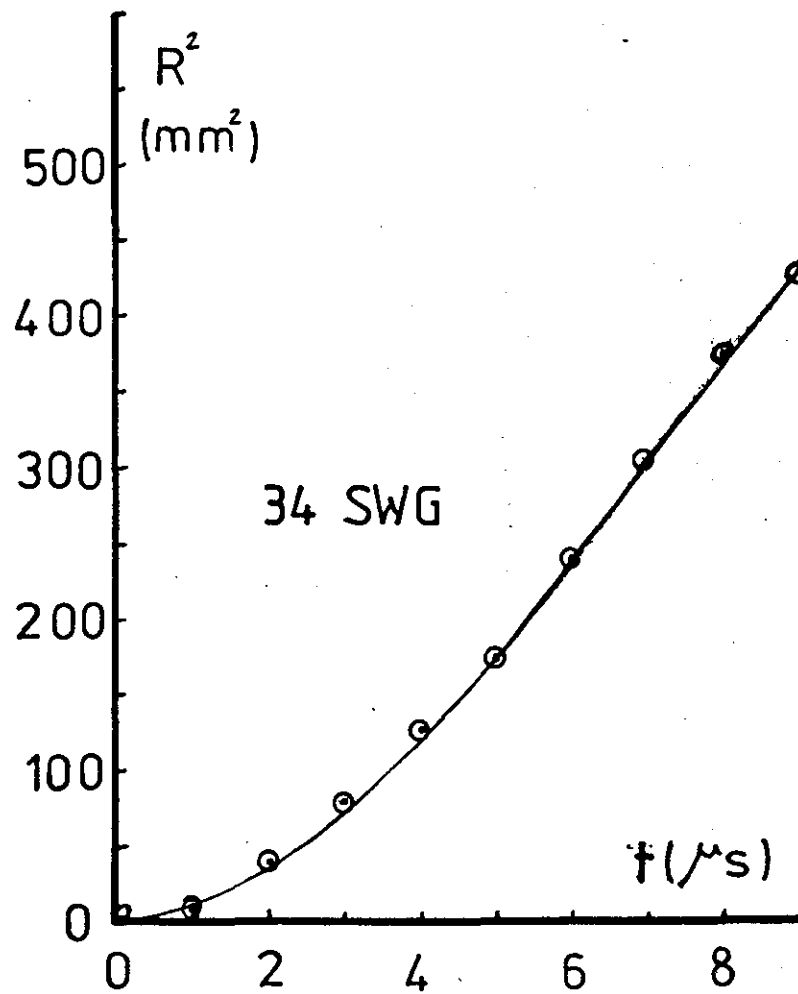
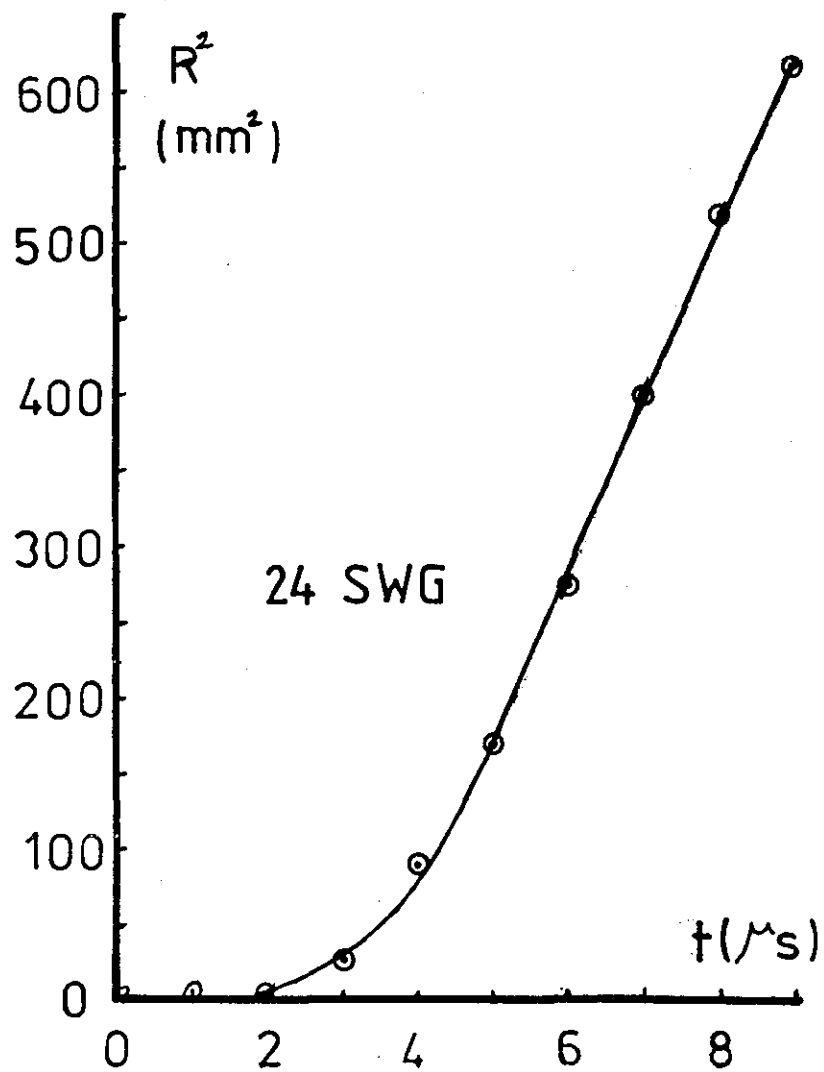


FIG. 3.28 R^2 as a function of time t for 24 & 34 SWG at 30 KV.

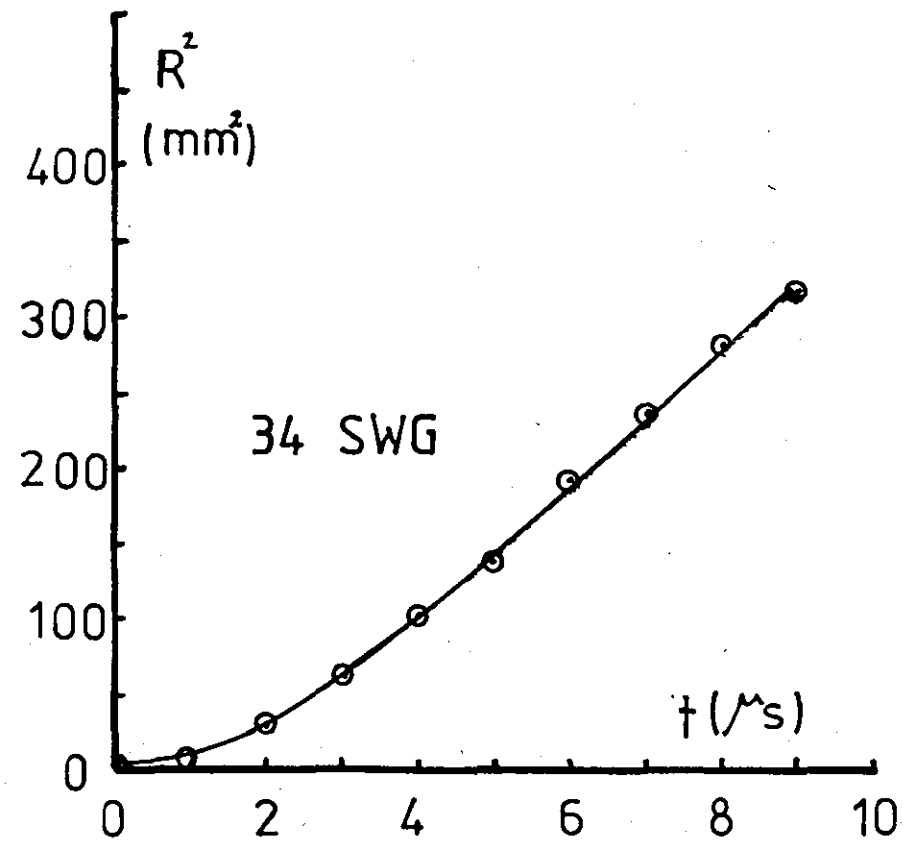
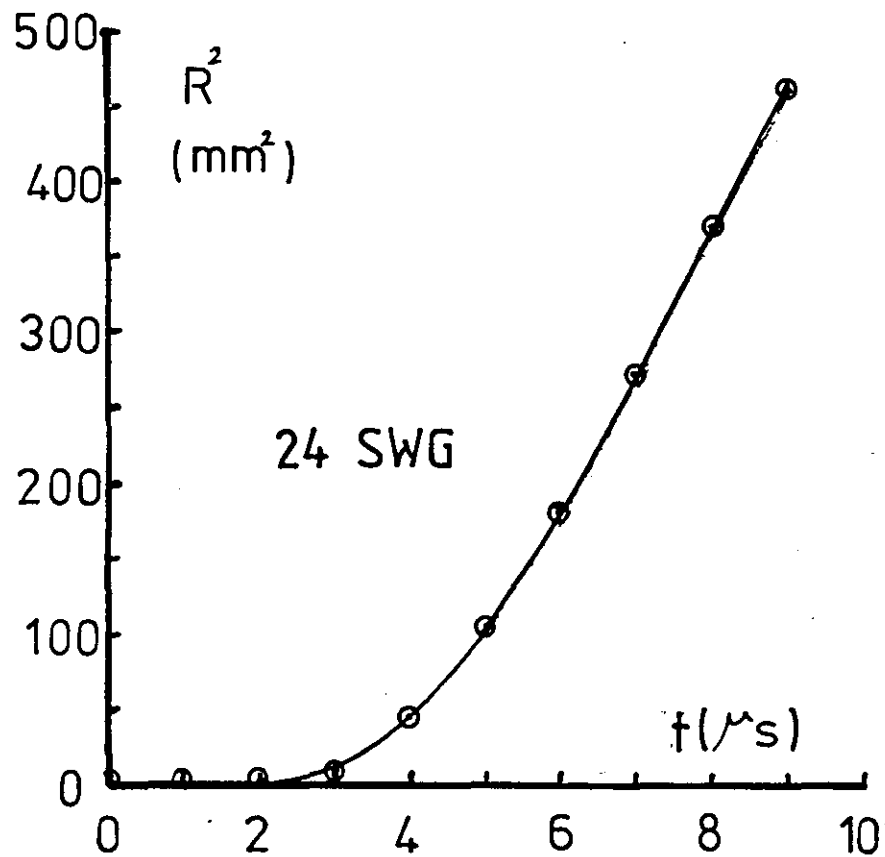


FIG. 3.29 R^2 as a function of time t for 24 & 34 SWG at 25 KV.

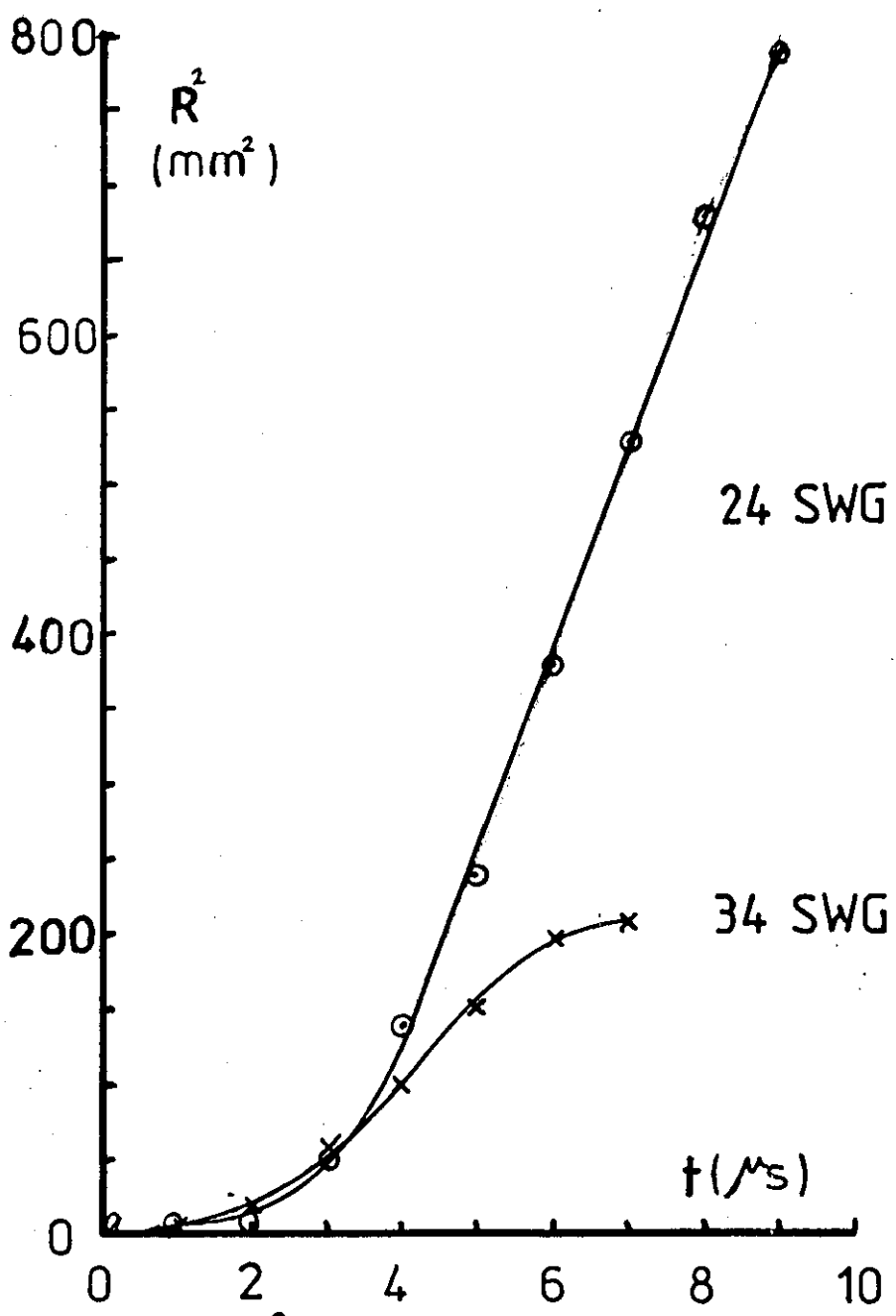


FIG. 3.30 R^2 as a function of time t for 24 & 34 SWG at 35 KV.

vaporisation; blast-wave formation occurs later in the discharge process nearer the peak of the energy input. This wire gives the highest velocities measured. For wires of greater diameter, more of the input energy is used for vaporisation (e.g. for 22 SWG. 3 KJ are required) leaving less to energise the blast-wave. With the maximum stored energy of 5.6 KJ the maximum diameter wire that can be vaporised is 19 SWG, even with perfectly efficient energy transfer.

One outstanding feature of the blast-wave is their high degree of reproducibility, an important factor when they are used for impact loading. For each wire diameter tested, several experiments were performed, the results differing by no more than the basic measurement error of about 2%. The only irregular results were for diameters of 20 SWG, or more, where the input energy was only just sufficient for vaporisation to occur. In these cases there was either no explosion at all, or one delayed so much that no explosion was seen in the 14 μ sec. of observation time.

A measure of the explosion efficiency, defined as the ratio of the blast-wave energy to the input energy from the capacitor, can be found from the theory of strong blast-waves (Sakurai, (1965)) as described in Section 3.8. From the graphs of R^2 versus time, blast-wave theory gives the output energy of blast-wave where the input energy per unit length calculated as $(\frac{1}{2} CV^2)$ and is given by 280 J/cm, 402 J/cm and 547 J/cm at 25 KV, 30 KV and 35 KV respectively. Table (3.1) shows the figures for energy output for various wire sizes.

A graph of the efficiency as a function of wire sizes exploded

at 30 KV is given in Figure 3.31. As indicated, the efficiency increases from about 10% for the thinnest wire to a maximum of over 40% for 24 SWG, and then decreases for larger wire diameters. These values are in reasonable accord with Jones and Gallet (1962), although in the present study the ambient pressures are somewhat higher to enable higher blast-wave pressures to be achieved.

The output energy values derived from the tests show that for the wire producing the stronger shock waves, about half of the input electrical energy reappears as energy of the flow behind the shock. The other half can be accounted for as heat lost in the residual circuit resistance, in heating the metal wire through its transition points to a temperature of several thousand degrees, also through heat conduction and radiation.

3.10 PRESSURE DETERMINATION.

The pressure generated at the inside wall of the cylindrical specimen is that due to the reflected shock wave. The peak pressure may be determined from Blast Wave Theory. Figures 3.24, 3.25 and 3.26 enables the Mach Number at any particular cylinder radius to be determined. Then by assuming air to be an ideal gas of constant $\gamma = 1.4$, the reflected shock pressure can be obtained in terms of Mach Number from standard shock wave theory as described by Gaydon and Hurl (1963). However at the extremely high temperatures associated with the reflected-shock at high Mach Number (e.g. for Mach 4 the reflected shock temperature is ~ 2000 k rising to ~ 10000 k at Mach 12) air does not behave as an ideal gas. Figure 3.32 gives theoretical curves of reflected shock pressure as a function of Mach Number of the incident shock for air an an "Ideal"

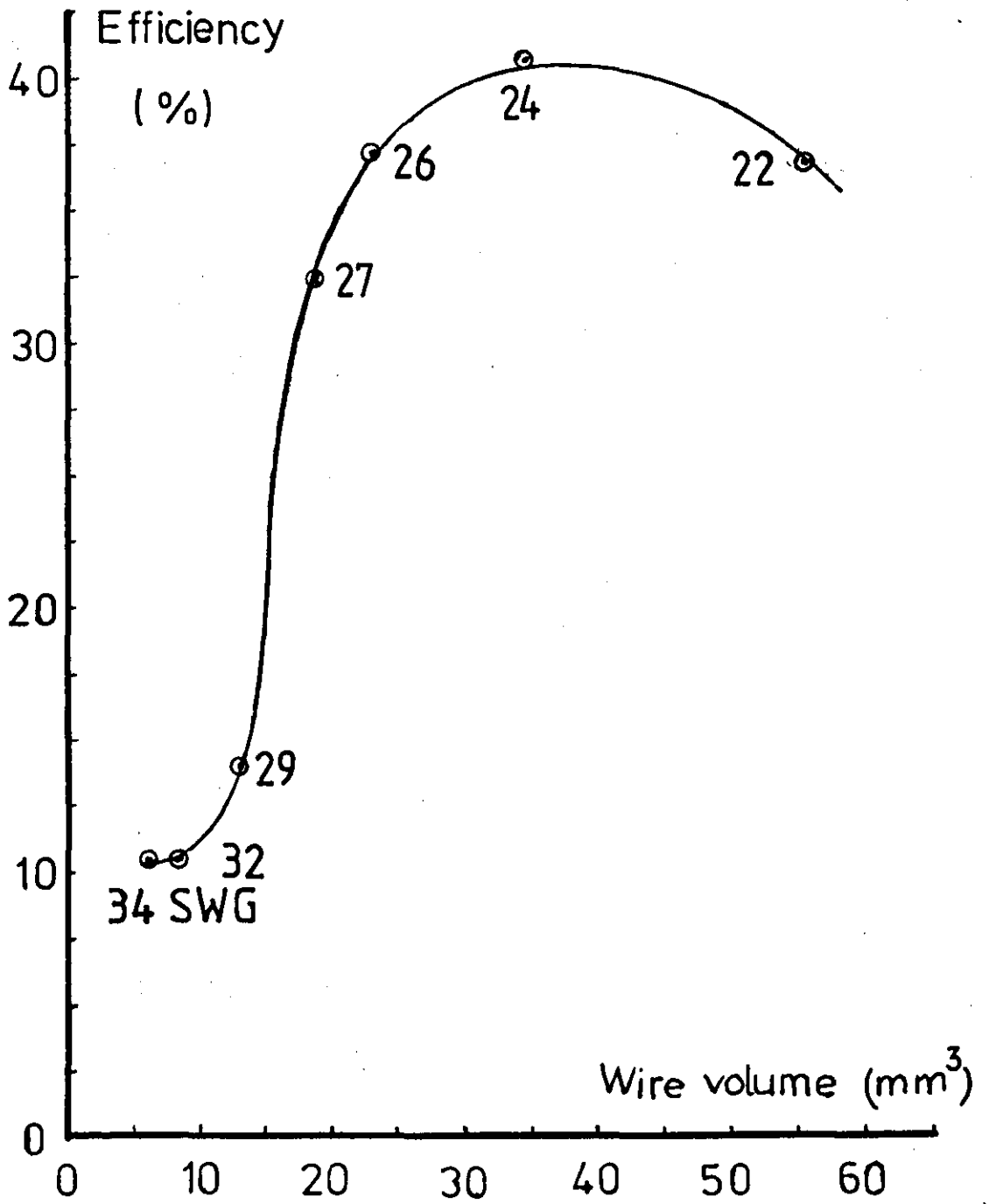


FIG.3.31 Explosion efficiency in terms of wire volume for 30 KV discharge.

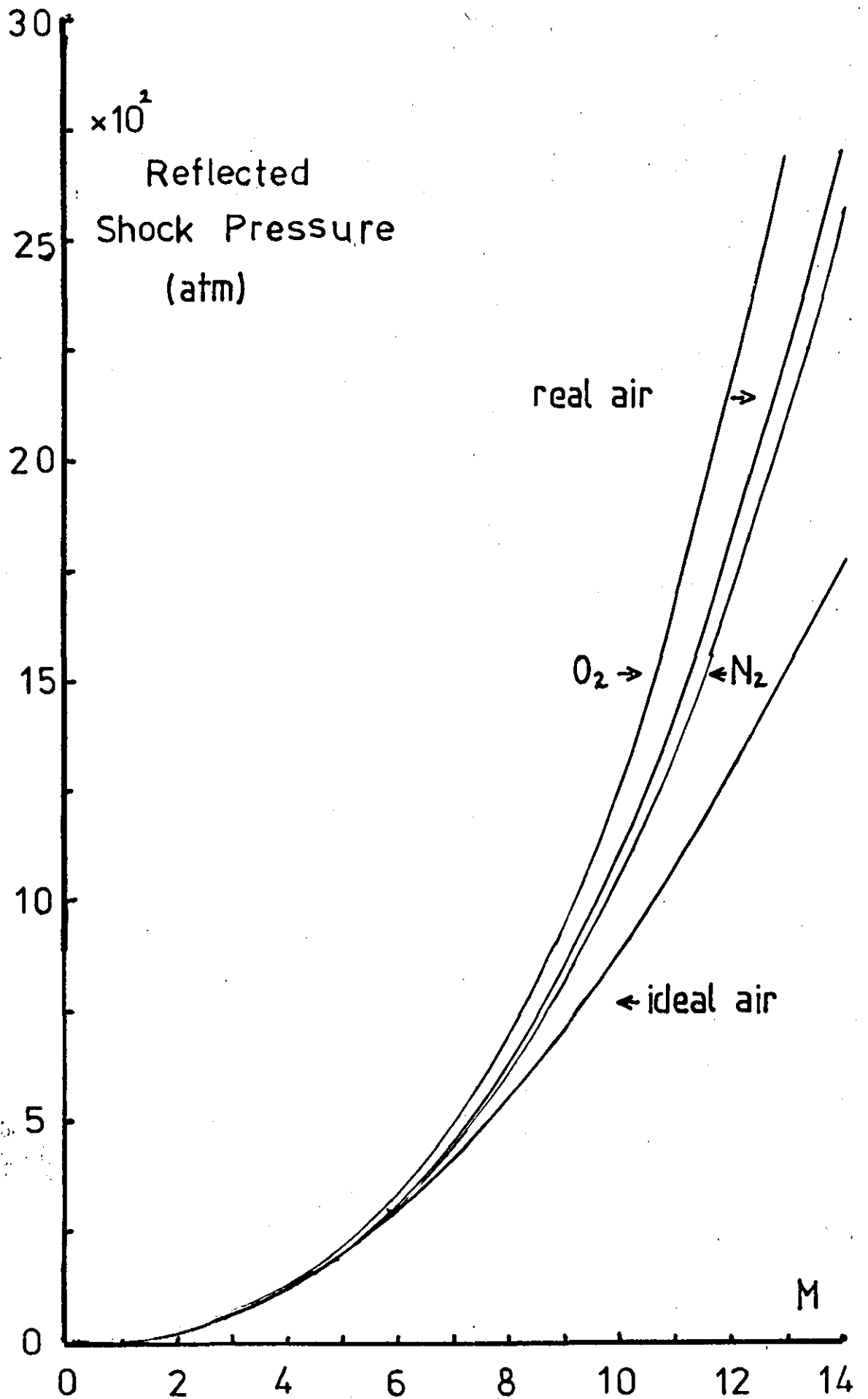


FIG.3.32 Reflected shock-front pressure against Mach number M .

gas, and as a "real" gas taking into account changes in γ caused by vibration and dissociation (Law and Bristow (1969)). These "real" shock pressures are considerably higher than the "ideal" at high Mach Numbers.

3.11 CONCLUSIONS.

The technique of high-speed schlieren photography has proved eminently suitable for showing that the blast-waves generated by exploding copper wires are both radially and axially symmetric for the wire sizes and capacitor voltages used.

Of all the wires tested, the 24 SWG size gave the highest blast-wave velocities attained of up to 4.5 km S^{-1} (Mach 13.0) for a 30 KV discharge. From the measured variation of Mach Number with radial distance, the peak pressures in blast-waves reflected by cylindrical surfaces at various radii have been determined.

The exploding-wire technique has thus been shown to produce symmetrical blast-waves of sufficiently high pressures to satisfy the requirements of impact loading of cylindrical specimens.

TABLE 3.1

| Input Energy J/cm | Wire Diameter | | Slope 10^4 $\text{cm}^2/\text{Sec.}$ | Output Energy J/cm | Efficiency % | Mach Number |
|----------------------|---------------|-----|--|-----------------------|-----------------|----------------|
| | mm | SWG | | | | |
| 280 | 0.234 | 34 | 45 | 24.0 | 8.6 | 7.5 |
| | 0.274 | 32 | 48 | 27.3 | 9.7 | 7.3 |
| | 0.345 | 29 | 63 | 47.1 | 17.0 | 9.3 |
| | 0.417 | 27 | 83 | 81.7 | 29.3 | 10.6 |
| | 0.457 | 26 | 85 | 85.6 | 30.7 | 11 |
| | 0.559 | 24 | 95 | 107.0 | 38.4 | 10.7 |
| 402 | 0.234 | 34 | 60 | 42.7 | 10.6 | 9.9 |
| | 0.274 | 32 | 60 | 42.7 | 10.6 | 9 |
| | 0.345 | 29 | 69 | 56.4 | 14.0 | 10.5 |
| | 0.417 | 27 | 105 | 130.8 | 32.5 | 11 |
| | 0.457 | 26 | 112.5 | 150.1 | 37.3 | 11.3 |
| | 0.559 | 24 | 117.5 | 163.7 | 40.7 | 12.7 |
| | 0.711 | 22 | 112 | 148.0 | 36.8 | 11.2 |
| 547 | 0.234 | 34 | 48 | 27.3 | 5.0 | 10.7 |
| | 0.274 | 32 | 58 | 39.9 | 7.3 | 10.9 |
| | 0.345 | 29 | 72 | 61.5 | 11.3 | 11.3 |
| | 0.417 | 27 | 120 | 170.8 | 31.3 | 12.7 |
| | 0.457 | 26 | 130 | 200.4 | 36.6 | 12.7 |
| | 0.559 | 24 | 154 | 281.3 | 51.4 | 13 |

CHAPTER 4

MEASUREMENT OF THE PRESSURE-TIME PROFILE

4.1 INTRODUCTION.

The loading conditions at the inner surface of a cylindrical specimen are very important since the pressure time history on the inner surface is a necessary input parameter to any theoretical study associated with this experimental technique. Unfortunately, the inner boundary condition controlled by the exploding wire is very complex being subjected to the time dependent flow properties of the air copper vapour mixture created by the exploding wire. Furthermore, the electro-magnetic noise generated by the sudden release of the stored electrical energy creates problems when using any direct measurement technique. The present method uses the Hopkinson pressure bar gauge.

4.2 THE HOPKINSON PRESSURE BAR.

The first experiments concerning compressive wave propagation were those conducted by Hopkinson (1914). The accurate measurement of stresses which are subject to rapid time variations is a matter of some difficulty. Hopkinson's experiments consisted in applying the unknown pressure, produced by either explosion or drop weight or some other rapid loading mechanism, to one end of a long cylindrical steel bar. The bar was attached to a short extension bar (the time-piece) of the same diameter and material as the pressure bar. The joint between the two bars was formed by 'wringing' the shorter piece onto the ground and lapped end face of the pressure bar.

On impact, a longitudinal pressure pulse travelled along the pressure bar, passed unchanged through the joint, and on reaching

the free end of the time-piece was reflected as a pulse of tension and travelled back towards the joint. At some stage the net stress at the joint became tensile, so that the time-piece was detached from the pressure bar. The time-piece flew off from the pressure bar, trapping a certain amount of momentum, corresponding to a portion of the pulse which was twice the length of the time-piece. The velocity of the time-piece was measured by means of a ballistic pendulum. Using time-pieces of different lengths, it was possible to partially reconstruct the pressure versus time profile of the initial impact, caused by the detonation of various explosives.

This method was subject to certain limitations (Davies (1956b)) since it was not possible to determine the exact relation between pressure and time. There were also doubts about the distortion and uniformity of the pulse, and the joint was thought to introduce an unknown variation. Modern experiments while using the same principle, employ more sophisticated electronic measuring techniques, Davies (1948) devised a pressure bar in which a continuous record was produced of the longitudinal displacement at the free end of the bar. This displacement was measured by using the bar as the earthed conductor of a parallel-plate condenser. The isolated conductor consisted of a metal plate held in a frame attached close to the free end. When the pressure pulse reached the free end of the bar, the small movement of the earthed side of the condenser caused a change in the capacity of the condenser, and this change was measured on an oscilloscope as a changing potential difference; a photographic record was then taken of the signal. Displacement versus time records were obtained in this way, and they demonstrated

the existence of the so-called Pochhammer-Chree oscillations at the end of the pulse, and showed the effects of dispersion in increasing the pulse length. Davies also used cylindrical condensers, in which an isolated metal tube was held with its axis parallel to the axis of the bar. Measurements of the radial and longitudinal displacement of the bar surface were possible, although these units were only useful for measurements with long pulses.

More recent techniques involve (i) resistance strain gauges mounted on the surface of the pressure bar, (ii) thin quartz crystals discs sandwiched between two bars so that direct measurements of the strain-time profile may be obtained. Since the pressure bar remains elastic, the relationships for longitudinal elastic stress waves can be used to reconstruct the applied stress loading.

The Hopkinson split bar test technique has been widely used to determine the dynamic stress-strain-strain rate behaviour of a material under one-dimensional stress conditions. Karnes and Ripperger (1966) and Chalupnik and Ripperger (1966) have used quartz crystal transducers to sense specimen stress, their work involved the use of strain gauges attached to a metal sample. Such a method is not suitable for plastic and other nonmetal test specimens because of the possibility of reinforcement of the plastic by the gauge and the difficulty of obtaining good adhesion between the gauge and specimen. Moreover, a nonconductive sample cannot be used to serve as an electrode for the quartz crystal. Walsley, Hoge and Cast (1969) used piezoelectric X-cut quartz pressure transducers in addition to strain gauges in the split bar method in order to develop a technique to obtain modulus and stress-strain-strain rate data for solids.

The diameters of the pressure bar, the crystal transducer and the test specimen they used in their experiment were 12.7 mm. The thickness of crystals, 0.51 mm and 1.27 mm, were used. The ends of the crystal transducers had vapour deposited gold surfaces to insure that the generated charge was gathered over the whole electrode area. Aluminium foils of 0.02 mm thickness were also cemented to the other end of the crystal. Shunting capacitors placed across the crystal acted as voltage dividers to reduce the generated voltage to desired values. Jones (1967) used a pressure bar gauge in plasma physics to measure a very low pressure. The diameter of the bar is 2.9 mm and its overall length is 21.0 cm. A PZT-4 polarized Ferroelectric disc of 3 mm diameter and 0.5 mm thickness is cemented into the bar 12.3 cm from the measuring end. The magnitude of the pressure measured inside a discharge tube is 60 mtorr.

There are a number of ways of detecting the stress pulse propagating in the bar but undoubtedly the most satisfactory is that reported by Edwards (1958), who used a duralumin rod system with quartz crystal transducers.

4.3 THE PRESSURE BAR GAUGE SYSTEM.

When the pressure changes are rapid, like those encountered in gaseous detonation, exploding wires and blast waves, the presence of gauge vibrations usually makes it difficult to obtain the true pressure variations in the waves; the problem may be complicated further if high frequency pressure oscillations occur in the wave being measured. For this reason and the presence of electro-

magnetic noise from the explosion, a good deal of attention has been devoted by using many kinds of bars such as steel, duralumin, quartz and Pyrex pressure bars. A detailed theoretical treatment of the propagation of stress pulses in cylindrical bars is given by Davies (1948), who has also devised and investigated several methods of recording the stress variations.

In order to measure the average stress over the cross-section of the bar, the method employs an X-cut circular quartz disc of the same diameter. If the quartz disc is backed by a second similar bar, then a stress pulse travelling in the first bar will be transmitted through the quartz into the second bar. Furthermore, no reflexion of the stress pulses will occur at the quartz-bar interface provided the acoustic impedance, ρc_0 (where ρ is the density of the material of the bar, $c_0 = \sqrt{E/\rho}$, and E is Young's modulus) of the bar is matched to that appropriate to the thickness vibrations in the quartz disc. The measured value of ρc_0 for steel, duralumin and Pyrex bars used in the present work and the accepted value for X-cut quartz vibrating in a thickness mode are labeled in Table 4.1.

TABLE 4.1 The Acoustic Impedance ρc_0 .

| Steel | Duralumin | Pyrex | Quartz |
|-------|-----------|-------|---|
| 4.1 | 1.42 | 1.15 | $1.44 \times 10^6 \text{ gm.cm}^{-2} \cdot \text{S}^{-1}$ |

Thus provided that good mechanical contact is obtained between the quartz disc and the bar surfaces then the composite bar thus formed will behave as a continuous one as far as longitudinal pulses are concerned. Sufficiently good mechanical contact is achieved by

careful grinding and lapping of the bar faces and cementing with an Araldite or CN.

A diagram of the pressure bar and its housing is shown in Figure 4.1. The material of the bar is Steel, Duralumin, Quartz or Pyrex and has a circular cross-section of diameter $\frac{1}{4}$ or $\frac{1}{8}$ inch. The X-cut quartz disc which is cemented to the bar faces is of the same diameter as the bar; the disc thicknesses generally used are one or half millimeter. The first section of the composite bar called the "Loading bar", the second section as "Transmitting bar". The length of the "Loading bar" was chosen to be 15 to 30 cm to give a delay time of about 30-60 micro-seconds by which time most of the electrical noise generated will have died away; this illustrates an advantage of a Hopkinson bar in providing a suitable delay time to avoid the noise, whereas the length of the "Transmitting bar" is determined by the duration over which it is desired to record.

The composite bar ~~was~~ rested on V-Blocks made of polyethylene rigidly fixed in an Aluminium housing channel, this gave freedom to the bar to slide avoiding breaking the cemented bond. The "Loading bar" is earthed whilst the "Transmitting bar" forms the insulated electrode. The charge developed by the crystal produces a voltage across the insulated electrode and this is fed into a 556 Tetrax oscilloscope by a coaxial line. The capacitance of the composite bar and the coaxial line were measured before each experiment. It was found to be between 270 and 280 pF.

The head of the pressure bar can be pushed through a hole drilled in the wall of the cylinder in order to measure the pressure inside

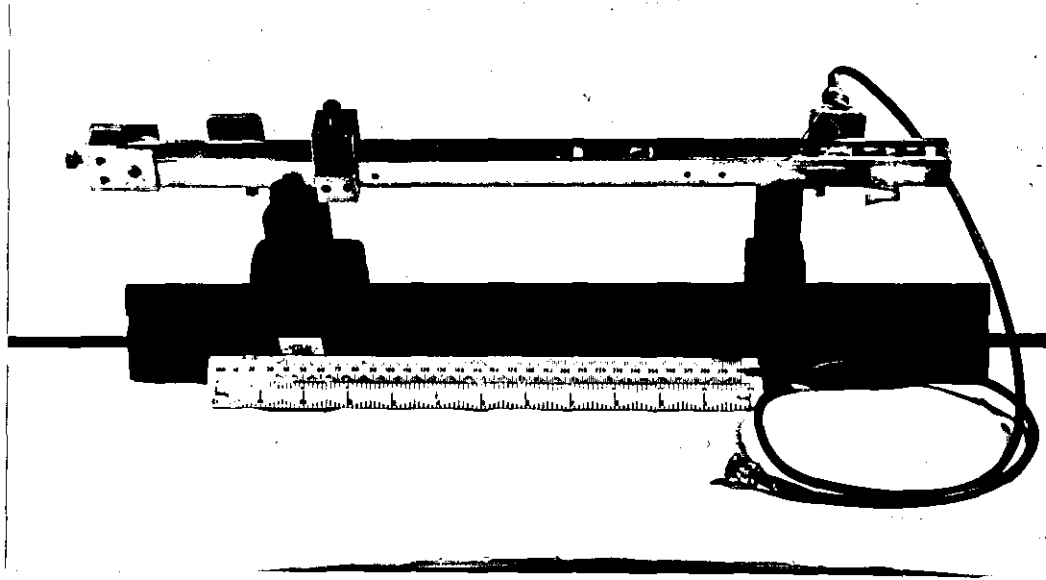


FIG.4.1 PRESSURE BAR GAUGE & HOUSING

the wall of the cylinder. Thus in the present work the seating must satisfy the following requirements:

- (i) it must provide a good vacuum seal between the bar and the cylinder,
- (ii) the bar must be mechanically insulated from the explosion inside the cylinder wall to prevent transmission of stress pulses propagating in the latter from reaching the momentum bar,
- (iii) it is essential that the thrust exerted by the seating on the lateral surface of the bar be kept as small as possible in order to permit free radial movement of the surface, and
- (iv) the pressure bar must be kept horizontal.

In order to stress the importance of condition (ii) a sheet of melinex was fixed inside the cylinder wall to cut down the electrical pick-up. The use of Pyrex bar instead of steel or duralumin, was also considered for this work.

4.4 CALIBRATION OF THE PRESSURE BAR.

Calibration of the crystal pressure transducer was achieved by both experimental and theoretical methods. In the former the voltage recorded on an oscilloscope from an impacted crystal transducer was compared with the pressure calculated from ^{the} shock wave. The relationship of pressure with the output voltage obtained by Percival (1967) is as follows:

$$P = \frac{VC_T}{KA} \quad 4.1$$

where P is the pressure in the quartz crystal in atmospheres, V is the voltage in volts, and C_T is the total capacitance being charged in farads, A is the crystal area (which equals the bar cross-

section area) in square centimeters, and K the appropriate piezo-electric strain constant equal to 2.31×10^{-11} c.cm⁻²/atm.

Percival (1967) used in his work the value for K appropriate to one-dimensional strain experiments.

This calibration was confirmed by placing the pressure bar gauge in contact with the struck bar of a Split Hopkinson pressure bar rig which used $\frac{1}{2}$ inch diameter steel bars. The pressure in the Split Hopkinson pressure bar system was produced by a gas-gun in which the velocity of the impacting projectile could be measured accurately enabling the peak pressure in the stress pulse to be calculated. It was shown that the measured pressure (approximately 2000 atm) from the pressure bar gauge agreed with this calculated value — Verifying that the piezo-electric strain constant value applies to the very high pressures produced in the work with exploding wires.

4.5 PRESSURE MEASUREMENTS.

The experiment^d set-up is illustrated schematically in Figure 4.2, a copper wire of 0.559 mm diameter exploded inside a cylinder of inner radius range between 8 to 13 mm. The pressure produced from the explosion is applied to the incident pressure bar of diameter 0.635 cm. The length of the steel pressure bar was chosen between 10 and 30 cm.

A typical oscillogram obtained by the steel pressure bar is shown in Figure 4.3. In the beginning of the pressure signal an oscillation can be seen which due to the pick-up from the explosion and this oscillation decreases slightly by inserting a sheet of

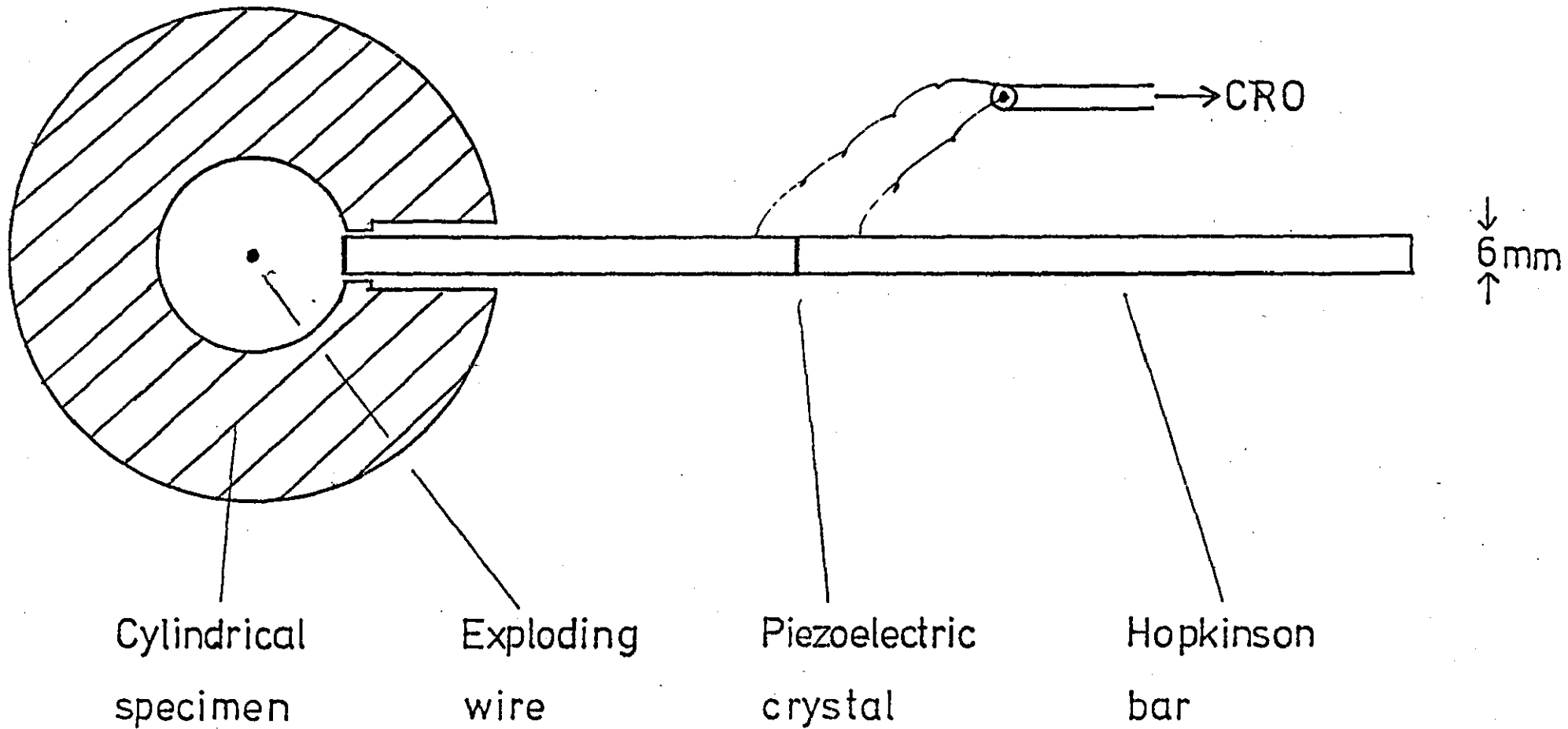
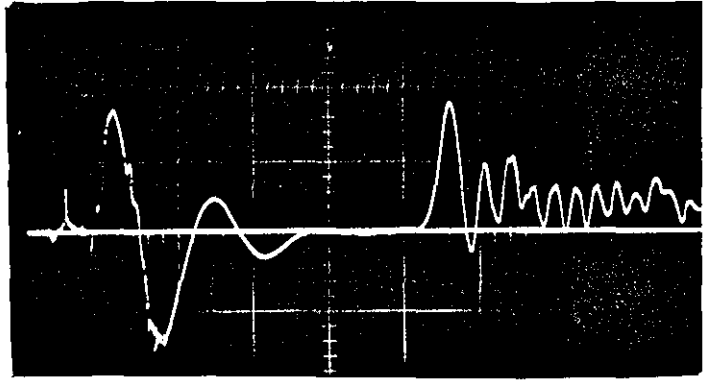


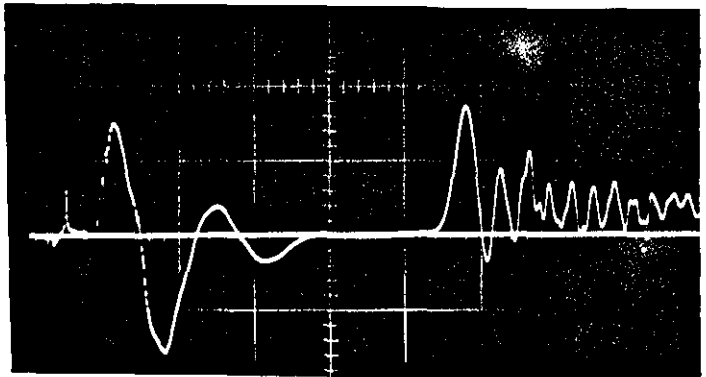
FIG.4.2 HOPKINSON BAR PRESSURE GAUGE

Bar length

23 cm



24 cm



26 cm
(without melinex)

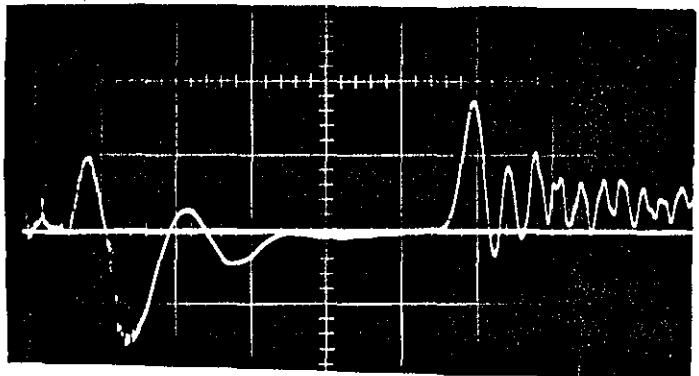


FIG. 4.3 PRESSURE-TIME FOR STEEL BAR

$Y = 10 \text{ V/cm}$ $X = 10 \mu\text{s/cm}$

$R_i = 12 \text{ mm}$ $C_T = 280 \text{ pF}$

$P = 650 \text{ atm}$

melinex attached to the inside wall of the cylinder. The periods of the noise oscillations is about 40-50 microseconds before the arrival of the pressure pulse; this^{is} cut down to 30-35 microseconds after inserting the melinex sheet.

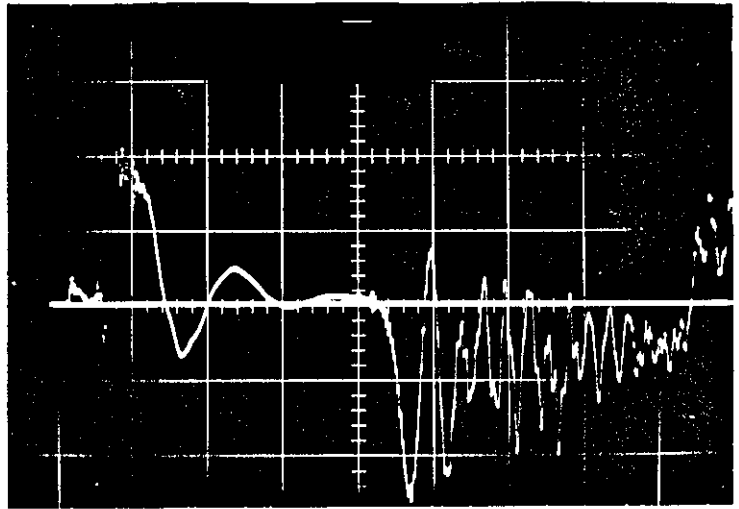
To separate the pressure pulse from the noise, the loading bar length chosen was 20-30 cm and that increased the rise-time to 4 microseconds and gave a low pressure profile. The relation between the rise-time and the length of the loading bar is mentioned in Section 4.6.

Following the initial rise of the pressure pulse, there occurred oscillations of decreasing period. These oscillations arise from the dispersion of the stress pulse as it travels along the pressure bar and are not due to any vibrations. A detailed analysis of the various modes of vibration in cylindrical bars is described by Davies (1948) and Curtis (1954) and has shown that when shock waves are used to initiate stress waves in a bar both the first and second longitudinal mode vibrations are excited. Oscillations due to dispersion appearing in the recorded pulse can therefore, be identified and distinguished from oscillations which may occur in the wave being measured, provided that their frequencies are not too close to the bar frequencies.

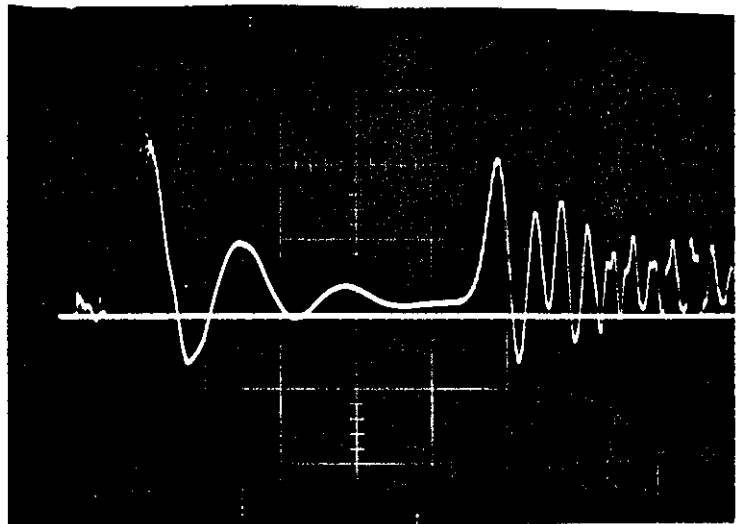
To minimize the size of the pick-up noise a Duralumin pressure bar was used. As shown in Figure 4.4 the pick-up is still there and it is impossible to use short bars. Then it was decided to use a glass (Pyrex) bar.

The technique of sandwiching the crystal is by using CN adhesive to cement a thin Aluminium foil on both faces of the crystal. One

Bar length
20 cm
 $R_i = 8.5$ mm
 $P = 840$ atm



25 cm
 $R_i = 12$ mm
 $P = 660$ atm
(without melinex)



25 cm
 $R_i = 12$ mm
 $P = 660$ atm

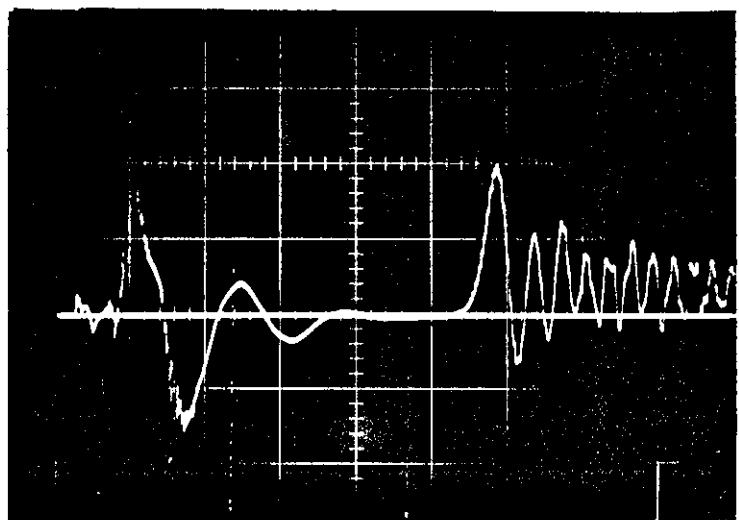


FIG. 4.4 PRESSURE-TIME FOR DURALUMIN BAR.
 $Y = 10$ V/cm. $X = 10$ μ s/cm. $C_T = 240$ pF.

side live and the other side earthed, fed to BNC plug to the oscilloscope.

The results were very good and the pick-up noise was reduced to a minimum of 12-15 microseconds. With this technique the pressure measured from the explosion was satisfactory compared with the predicted pressure as shown in Figures 4.5 and 4.6.

Table 4.2 shows the comparison of the pressure measured and predicted also the rise time of the pressure profile.

The measured reflected-shock pressure at several radii, and hence known Mach numbers are plotted on Figures 4.7, 4.8 and 4.9, showing good agreement with the real air graph and also shows that the blast-wave has the characteristically sharp pressure jump of a shock front followed by a rapid decay.

4.6 THE RISE TIME OF THE OUTPUT SIGNAL FROM THE PRESSURE BAR.

The high frequency response of a pressure bar in terms of a uniform pressure having a step function time dependence. The risetime of the output signal is intimately connected with the high frequency response of the bar.

Theoretical treatments of the problem of the shock loading of a bar have been given by Curtis et al. (1958) and by Rosenfeld and Miklowitz (1965).

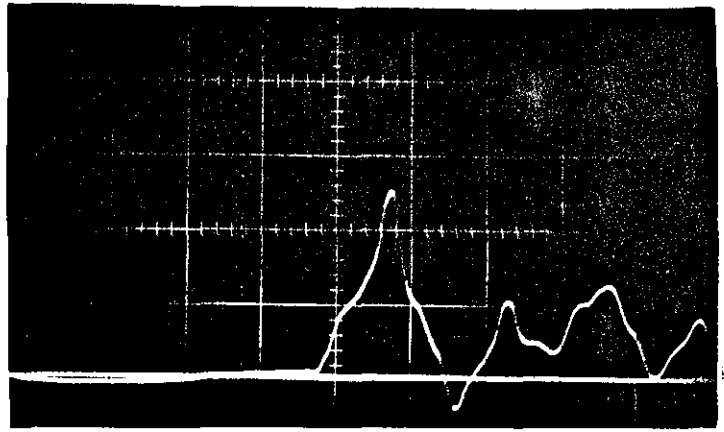
Jones (1966) defined the risetime τ_1 to be the time taken for the signal to increase from 10% to 90% of its maximum value. He predicts that for long pressure bars the risetime varies as $(Z_o)^{1/3}$ as in equation (2),

$$\tau_1 = 2.28 (v)^{2/3} \left(\frac{Z_o}{a} \right)^{1/3} \left(\frac{a}{C_o} \right) \quad 4.2$$

TABLE 4.2

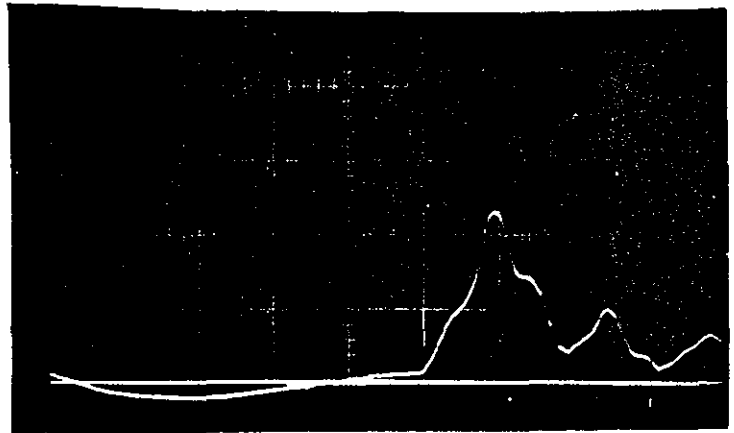
| Cylinder Inner Radius R_i (mm) | Loading Bar Length (cm) | Rise- Time (μ sec) | Calculated Pressure (atm) | Measured Pressure (atm) |
|---|----------------------------------|-------------------------------|---------------------------------|-------------------------------|
| 6.5 | 7.9 | 1.75 | 2256 | 2100 |
| 8.5 | 6.6 | 1.55 | 1800 | 2000 |
| 10.0 | 6.1 | 1.48 | 1650 | 1800 |
| 10.5 | 4.5 | 1.35 | 1550 | 1650 |
| 10.5 | 6.5 | 1.53 | 1550 | 1700 |
| 10.5 | 7.8 | 1.62 | 1550 | 1400 |
| 11.0 | 5.2 | 1.40 | 1375 | 1400 |
| 11.0 | 9.7 | 1.71 | 1375 | 1530 |
| 11.5 | 8.2 | 1.6 | 1340 | 1400 |
| 12.0 | 6.9 | 1.6 | 1300 | 1400 |
| 13.0 | 5.0 | 1.36 | 1250 | 1075 |
| 13.0 | 3.7 | 1.25 | 1250 | 1300 |

Bar length
6.6 cm
 $R_i = 8.5$ mm
 $P = 2000$ atm



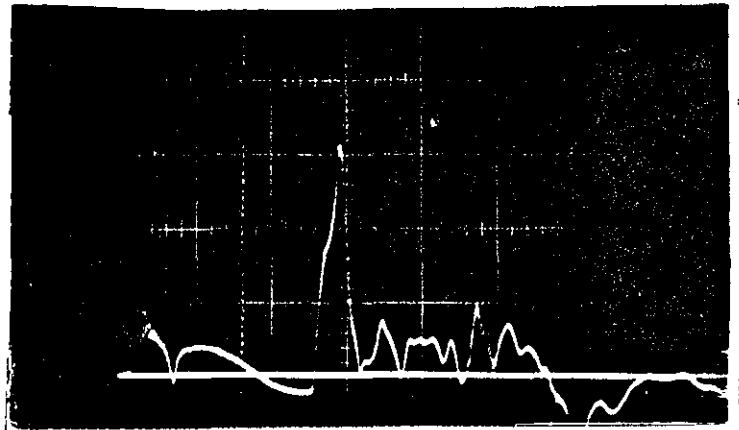
20 V/cm 2 μ s/cm

6.5 cm
 $R_i = 10.5$ mm
 $P = 1700$ atm



20 V/cm 2 μ s/cm

3.7 cm
 $R_i = 13.0$ mm
 $P = 1300$ atm

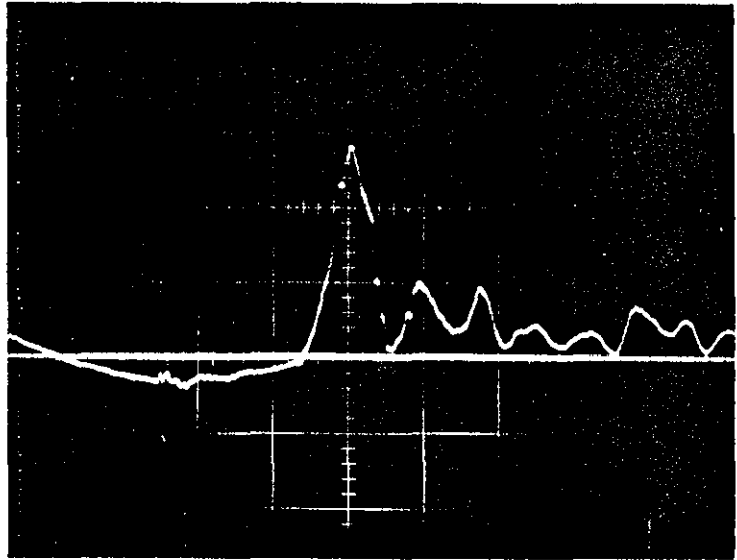


10 V/cm 5 μ s/cm

FIG. 4 5 PRESSURE-TIME FOR PYREX BAR.

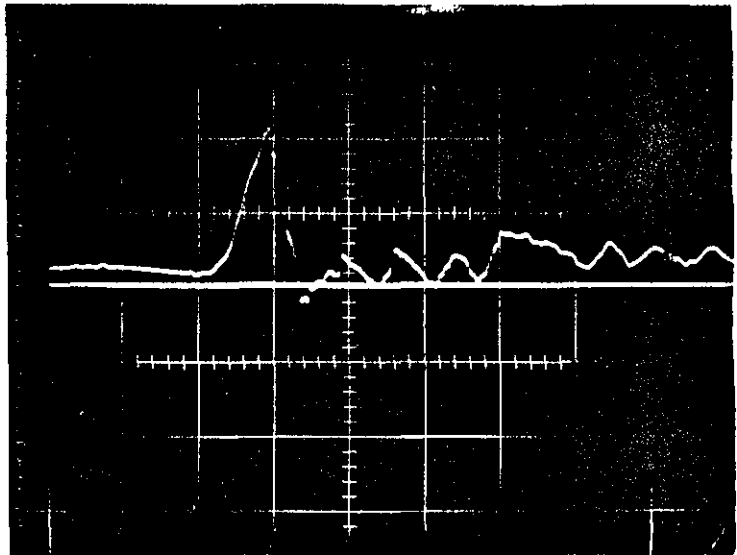
$C_T = 280$ pF

Bar length
5.0 cm
 $R_i = 6.5$ mm
 $P = 2100$ atm



$8 \mu\text{s}$ Time delay

8.6 cm
 $R_i = 10.0$ mm
 $P = 1650$ atm



$17 \mu\text{s}$ Time delay

FIG. 4.6 PRESSURE-TIME FOR PYREX BAR.

Crystal diameter = $\frac{1}{8}$ inch.

$Y = 5$ V/cm $X = 2 \mu\text{s/cm}$ $C = 275$ pF

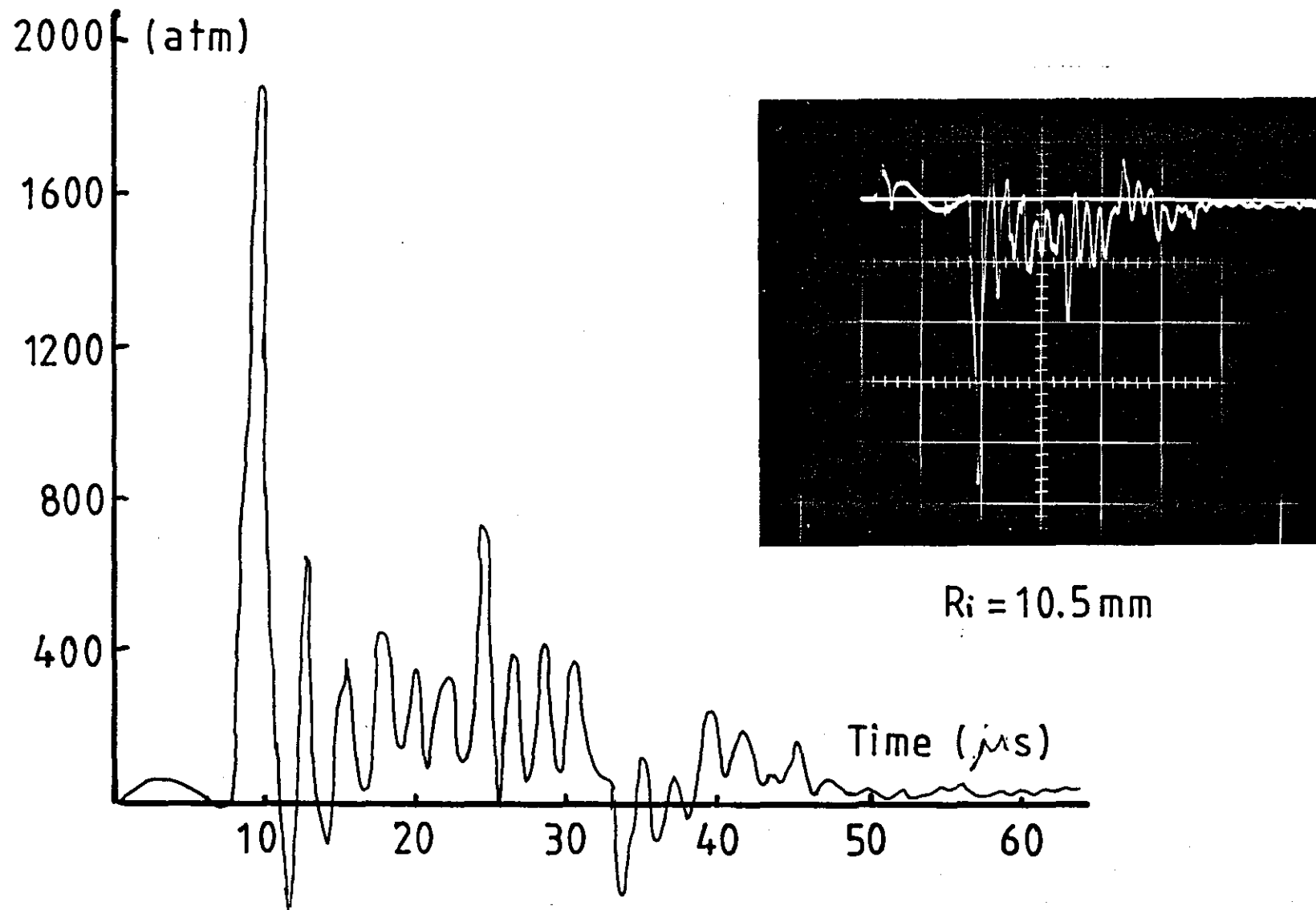


FIG.4.7 PRESSURE-TIME PROFILE FROM 6.1 cm PYREX BAR.

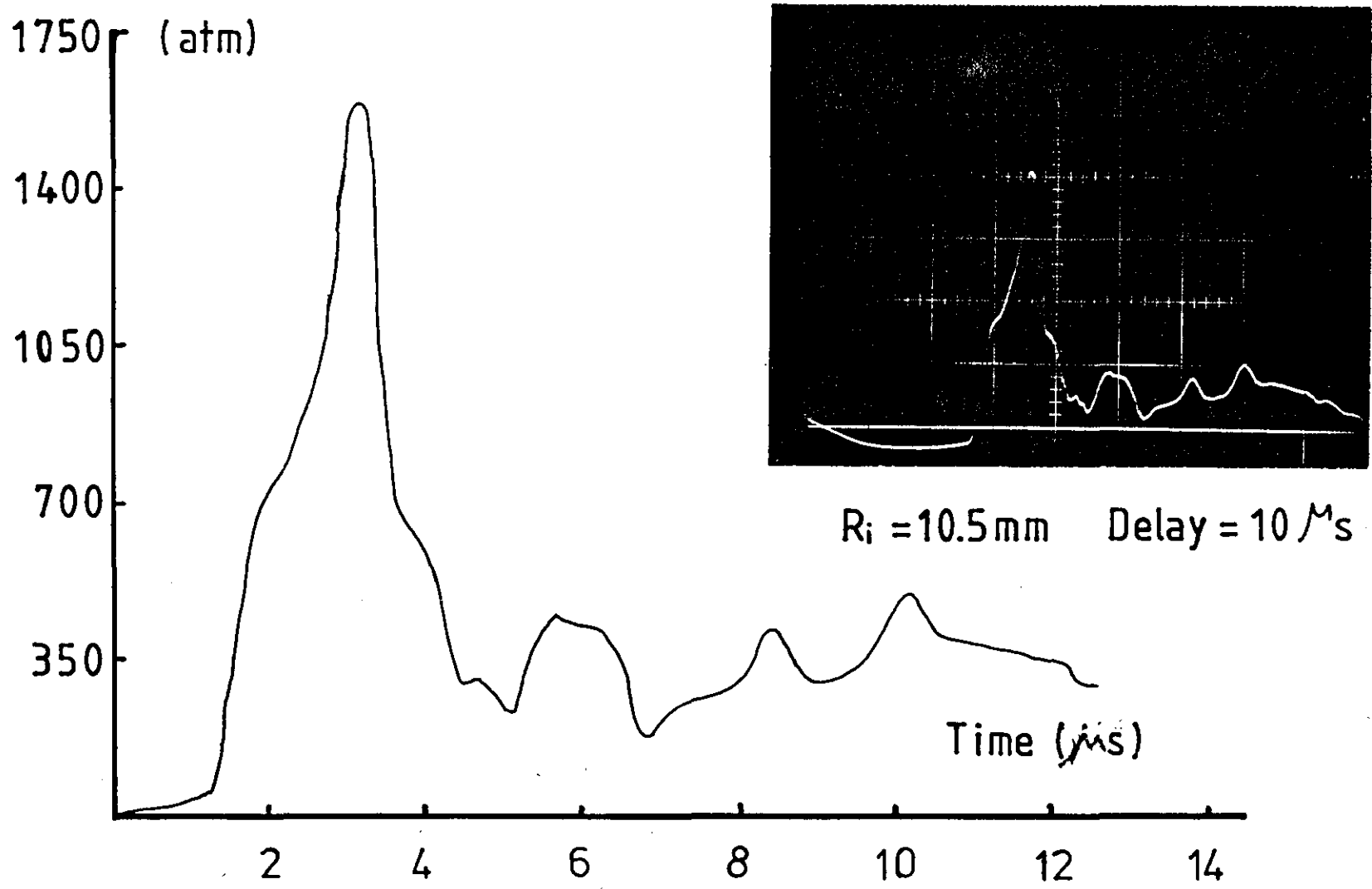


FIG.4.8 PRESSURE-TIME PROFILE FROM 4.5 cm PYREX BAR.

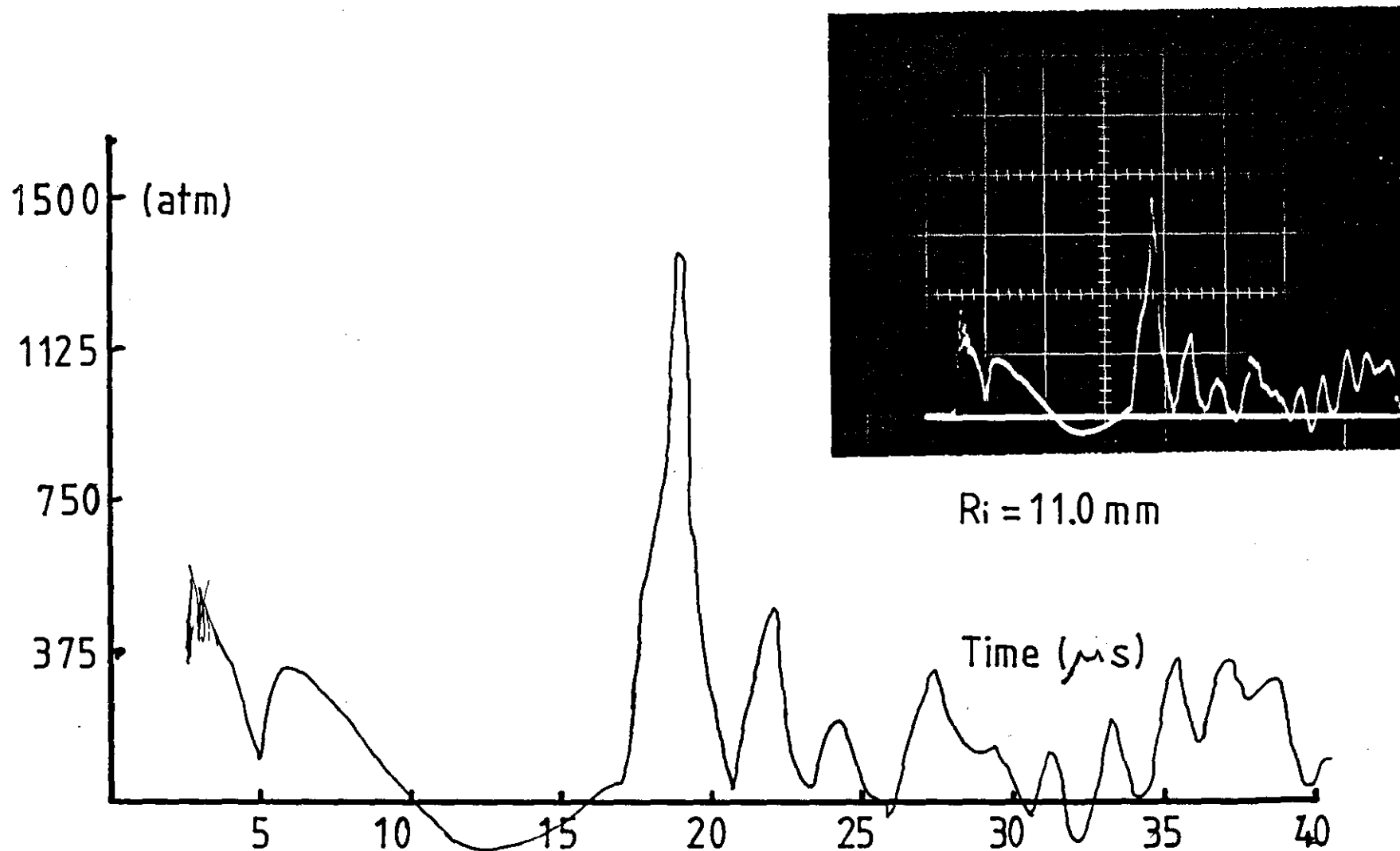


FIG. 4.9 PRESSURE-TIME PROFILE FROM 5.2 cm PYREX BAR.

where Z_0 is the distance along the bar from the stressed end to the point of observation in cm, τ_1 the risetime in microseconds, ν is the Poisson's ratio for the bar material, (a) is the radius of the bar in cm and C_0 is the bar velocity ($=\sqrt{\frac{E}{\rho}}$ where E is Young's modulus and ρ is the density of the bar material). Jones showed in his report that for a pressure bar of given dimensions, the risetime is faster if materials are used which have small values of Poisson's ratio but large values of bar velocity.

The results of the experiment together with the appropriate theoretical dependence are shown in Figure 4.10, for pyrex bars of diameter $\frac{1}{4}$ and $\frac{1}{8}$ inch the result shows excellent agreement with the theory, this is due to the good cemented bond of the crystal and the bars, and also shows a sharp jump of the reflected pressure.

Butler (1970) states that using a sleeve of Brittle Foodstuff (Macaroni) round the wire could reduce the risetime of the pressure pulse depending on the inner radius of the cylinder. This technique can be used to obtain a high reflected pressure pulse of low risetime. A 'loading bar' of length 6 cm was inserted inside a cylinder of inner radius 10.5 mm, and the pressure signal obtained is shown in Figure 4.11. It shows that the risetime of the pulse is twice that obtained by exploding a bare wire inside a cylinder of the same inner radius. The pressure measured is about two thirds that of the expected pressure. It was therefore decided not to proceed with this technique.

4.7 CONCLUSION.

The peak pressures in blast-waves reflected by cylindrical

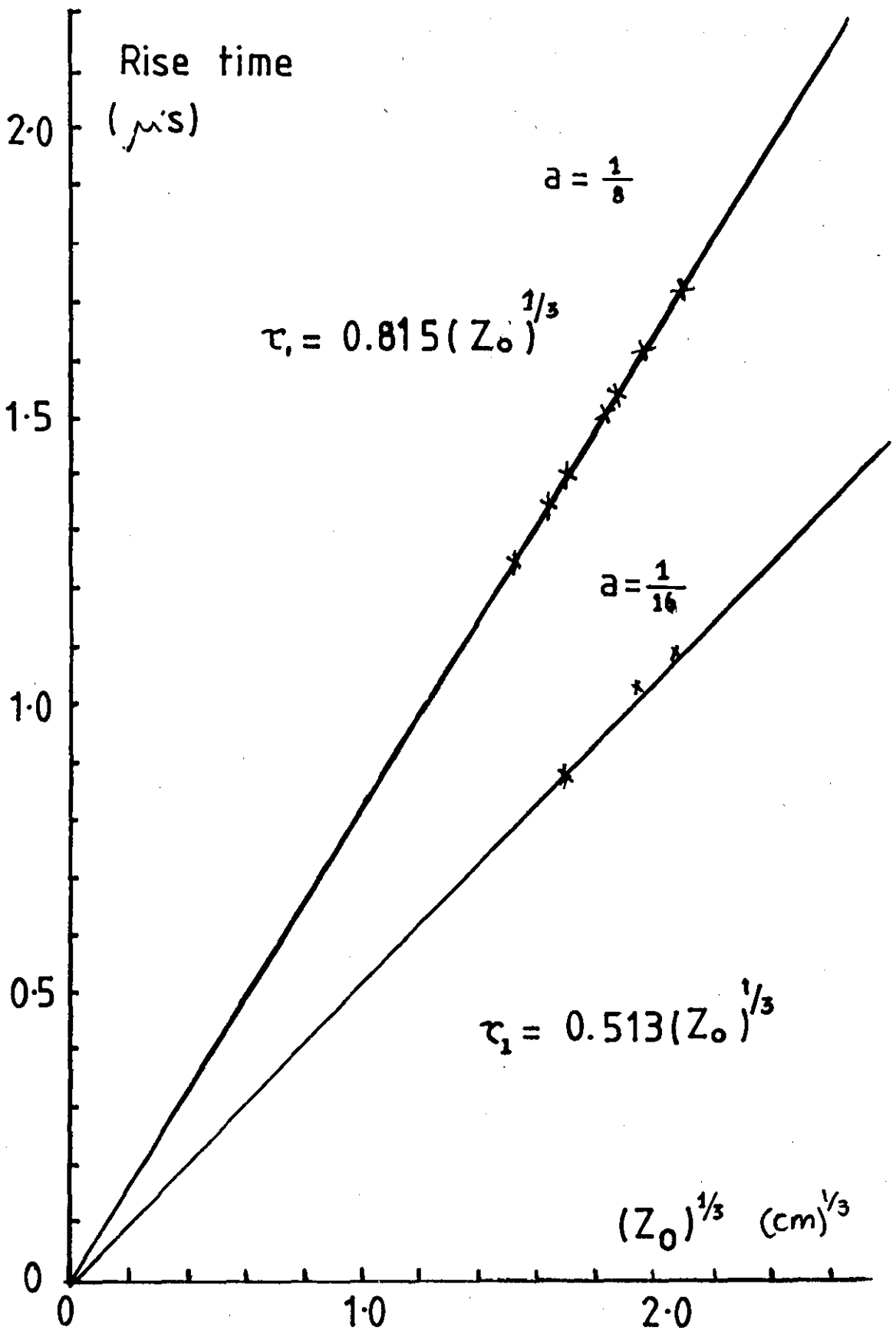


FIG.4.10 Observed and predicted rise time of pressure pulse against $(Z_0)^{1/3}$.

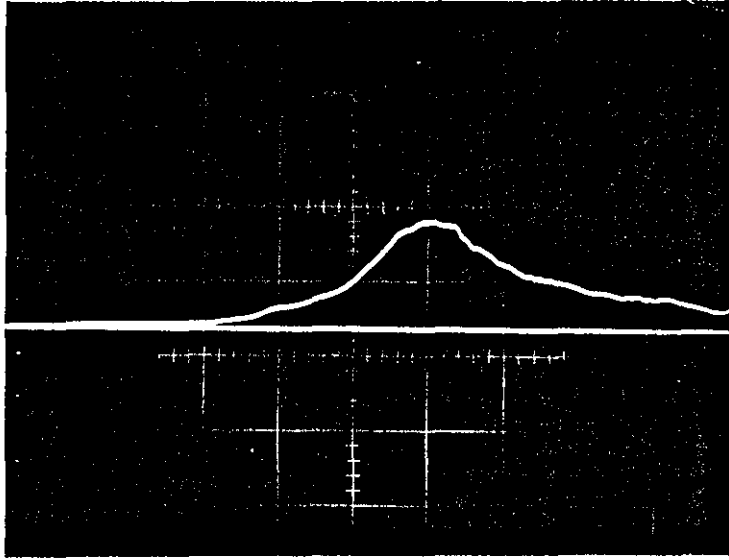


FIG. 4.11 PRESSURE-TIME FOR PYREX BAR.
Bar length = 6.0 cm $R_i = 10.5$ mm
 $Y = 20$ V/cm $X = 2$ μ s/cm.

surfaces at various radii have been determined (as described in Chapter 3). For the 24 SWG wire at 30 KV, peak pressure of up to 2000 atmospheres are predicted. These pressures have been confirmed using a piezo-electric pressure bar gauge. The measured risetime of the peak pressure using $\frac{1}{4}$ and $\frac{1}{8}$ inch diameter bars, compares well with the prediction.

The pressure-time history found from the experimental results will be used as a time dependent boundary condition in a theoretical treatment concerned with the calculation of the response of cylindrical specimens.

CHAPTER 5

THEORETICAL TREATMENT

5.1 INTRODUCTION.

When investigating the properties of materials at high rates of loading, one uses the pressure-time history at the inner surface of the cylinder as an input function to determine the outer surface displacement according to the type of theory used. The detailed work of Ensminger (1966) has shown that the deformations produced by the exploding wire are cylindrically symmetrical and, at least in the early stages, occur only in the radial direction. This can be described as a condition of plane strain. For a given material the magnitude of the pressure pulse will determine whether the deformation will be elastic or plastic in nature.

This chapter first presents part of the theory associated with the propagation of elastic cylindrical waves. In the second part of this chapter, the computer program which was used for numerical calculation has been modified so that the outer surface displacement is calculated for various input pressure pulse profile in particular to attempt to determine the surface displacement for a profile of the form determined experimentally by Hopkinson pressure bar gauge described earlier.

5.2 ANALYSIS OF WAVE PROPAGATION IN CYLINDRICAL COORDINATES.

The mathematical theory of the propagation of stress waves in solids has been presented by many authors, in particular Love (1927), and Kolsky (1953). The nature of the present problem dictates the use of cylindrical coordinates and the notation used here is that of Von Kármán (1910). Coordinates are r, θ, z shown in Figure 5.1 and the following symbols are used:

- u_r, u_θ, u_z = particle displacements in directions r, θ, z
- $\sigma_r, \sigma_\theta, \sigma_z$ = components of stress in directions r, θ, z
- $\epsilon_r, \epsilon_\theta, \epsilon_z$ = components of strain in directions r, θ, z
- E = Young's modulus
- r = radial position
- ν = Poisson's ratio
- t = time
- ρ = density

The complete equations become considerably simplified by the following assumptions:

Arising from symmetry, $\frac{\partial(-)}{\partial\theta} = 0$ and $u_\theta = 0$.

From the condition of plane strain, $\epsilon_z = 0$.

Application of the conservation of momentum leads to the equation:

$$\frac{\partial\sigma_r}{\partial r} + \frac{(\sigma_r - \sigma_\theta)}{r} = \rho \frac{\partial^2 u_r}{\partial t^2} \quad 5.1$$

Hook's law relationships between stresses and strains in cylindrical coordinates are:

$$(1 - \nu^2)\sigma_r - \nu(1 + \nu)\sigma_\theta = E\epsilon_r \quad 5.2$$

$$(1 - \nu^2)\sigma_\theta - \nu(1 + \nu)\sigma_r = E\epsilon_\theta \quad 5.3$$

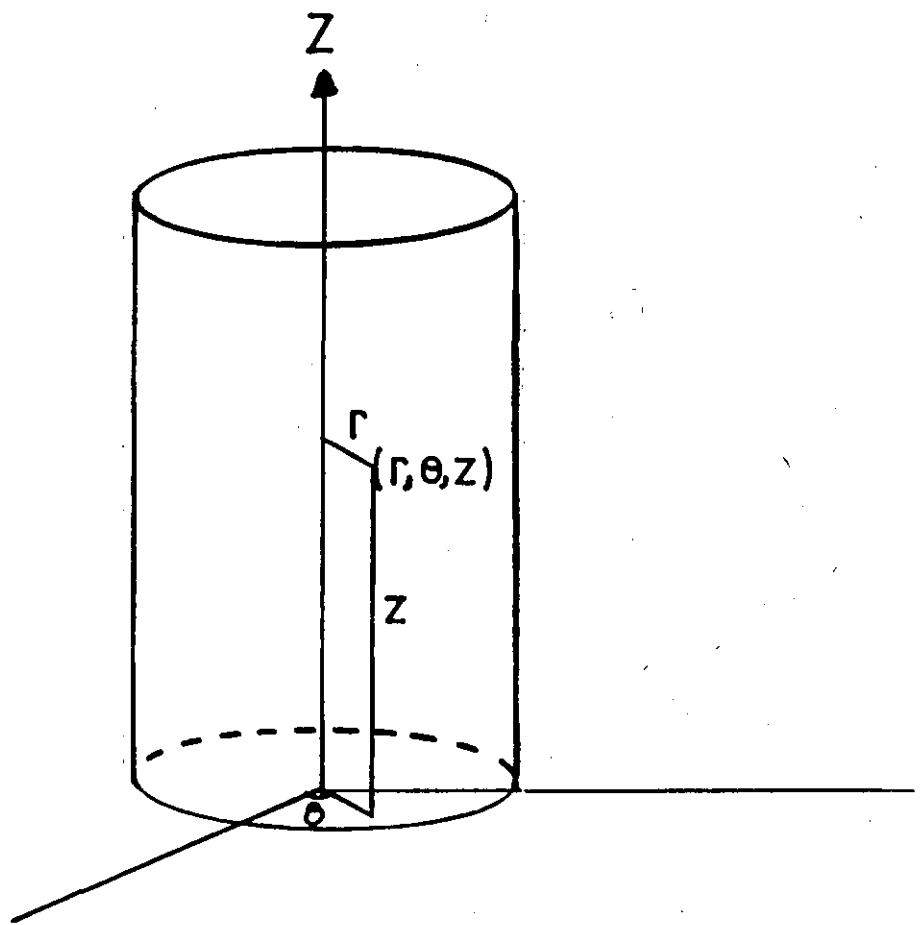


FIG. 5.1 CYLINDRICAL CO-ORDINATES

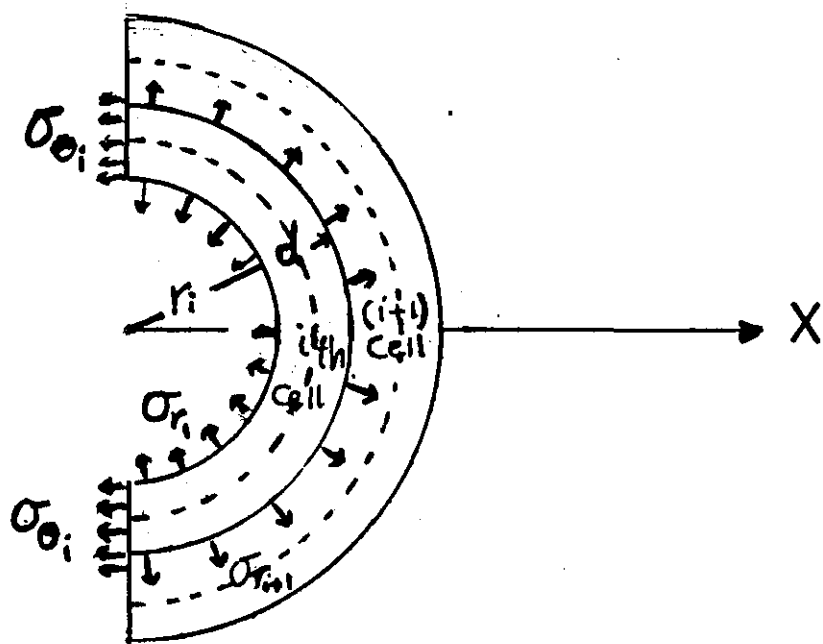


FIG. 5.2 SEMI-CYLINDRICAL ELEMENT

Strains ϵ_r and ϵ_θ are defined by:

$$\epsilon_r = \frac{\partial u_r}{\partial r}, \quad \epsilon_\theta = \frac{u_r}{r} \quad 5.4$$

Elimination of ϵ_θ between 5.2 and 5.3, combined with 5.4 leads to the equation:

$$\frac{\partial^2 u_r}{\partial r^2} + \frac{1}{r} \cdot \frac{\partial u_r}{\partial r} - \frac{u_r}{r^2} = \frac{1}{c_e^2} \cdot \frac{\partial^2 u_r}{\partial t^2} \quad 5.5$$

where

$$c_e^2 = \frac{E}{\rho} \cdot \frac{(1 - \nu)}{(1 + \nu)(1 - 2\nu)}$$

c_e is the elastic dilational wave velocity for the unbounded medium.

Equation 5.5 is a second-order partial differential equation relating the radial particle displacement u_r at radius r with time for an unbounded medium, and is hyperbolic in form. Its application to a finite cylinder of inner radius a , and outer radius b , requires the imposition of the following boundary conditions:

$$\text{At } t = 0, \quad u_r = 0, \quad \sigma_r = 0.$$

$$\text{At } t = t, \quad \sigma_{r=a} = -P(t), \quad \sigma_{r=b} = 0.$$

5.3 NUMERICAL SOLUTION.

A number of workers, e.g. Kromm (1948), Goldsmith and Allen (1955), Hopkins (1960), Chou and Koenig (1966), Mehta and Davids (1966), Mok (1968), Garg (1968), Chadwick and Morland (1969), and Morland (1969) have presented solutions to problems involving spherical and cylindrical wave propagation. Although some solutions have been obtained analytically, it has been found that more satisfactory treatments result from the use of numerical techniques. In particular, analytical approaches are severely limited in the treatment of mixed

elastic and plastic deformations because of the complexity of the mathematics.

The numerical solution of equation 5.5 above has involved the use of finite difference methods (e.g. Mok, (1968)) and the method of characteristics (e.g. Chou and Koenig, (1966)). An alternative treatment, referred to as a 'discontinuous-step method', has been presented by Mehta and Davids (1964, 1966) and used by Butler (1970) has been adopted in the present work.

5.4 THE DISCONTINUOUS STEP ANALYSIS.

This method of analysis is described in detail in Mehta (1966), Mehta and Davids (1964, 1966) and Butler (1970). Basically it is similar to finite difference methods and has been for the solution of a variety of problems (Mehta and Davids, (1966)) including spherical and cylindrical elasto-plastic wave propagation. In the 'discontinuous-step' procedure the differential equation resulting from the combination of momentum and Hooke's law equations and the strain relationships is not derived. Instead the body under consideration is divided into a finite number of elements or cells and the separate equations representing the physical laws are applied to each cell in turn at prescribed time intervals. Because the sequence of calculations is conveniently performed by means of a digital computer, the method has been termed (Mehta, (1966)) a 'computer analysis'.

5.4.1 Application to Cylindrical Wave Propagation.

Mehta and Davids (1966) have presented the method in a unified

form for cylindrical and spherical elastic and elastic-plastic waves. The following is a brief summary of their analysis for propagation of elastic waves in cylinders.

The cylinder, is of inner radius a , and outer radius b , divided into a finite number i_m of semi-cylindrical elements as in Figure 5.2 (semi-cylindrical elements are used because of symmetry).

If c_e is the elastic wave velocity, and dt an arbitrary time interval between applications of the equations, then cell width dr is given by

$$dr = c_e dt \quad . \quad (1)$$

Relation (1) is generally referred to as the 'characteristic' assumption. It can be shown to be equivalent to energy conservation and insures stability of the calculations.

In this case c_e , the dilational wave velocity, is given by

$$c_e = \left[\frac{E}{\rho} \cdot \frac{(1 - \nu)}{(1 + \nu)(1 - 2\nu)} \right]^{1/2} \quad (2)$$

The inner surface area A_i and the mass m_i of the i^{th} cell are given by

$$A_i = \pi r_i \ell \quad (3)$$

$$m_i = \frac{\pi \rho \ell}{2} \cdot \left(r_{i+1}^2 - r_i^2 \right) \quad (4)$$

where ℓ is the length of the cylinder.

The process begins by noting the state of the system of cells at a given time t . If the radial velocities of two adjacent cells i and $i+1$ are V_i and V_{i+1} , an average radial strain increment of amount $d\epsilon_r$ is generated during the time interval dt , given by

$$d\epsilon_r = (V_{i+1} - V_i) \frac{dt}{dr} \quad (5)$$

This applies for all cells $i = 1, 2, 3, \dots, i_m$ where dr is the distance between the cells i and $i+1$ given by (1).

Since the element may already be previously strained by an amount $\epsilon_{r(i+1)}$, the strain level must be increased by $d\epsilon$ from (5), giving a strain $\epsilon'_{r(i+1)}$ after time dt :

$$\epsilon'_{r(i+1)} = \epsilon_{r(i+1)} + d\epsilon_{r(i)} \quad (6)$$

or, in a form more suitable for computer use

$$\epsilon_{r(i+1)} \leftarrow \epsilon_{r(i+1)} + d\epsilon_{r(i)} \quad (7)$$

(N.B. The subscript $i+1$ is used in order that $\epsilon_{r(1)}$ is never computed).

The increment of tangential strain $d\epsilon_\theta$ is written as

$$d\epsilon_{\theta(i)} = V_i dt/r_i \quad (8)$$

and the corresponding cumulation equation is

$$\epsilon_{\theta(i)} \leftarrow \epsilon_{\theta(i)} + d\epsilon_{\theta(i)} \quad (9)$$

From the constitutive equations 5.2 and 5.3 of Section 5.2, the following relations can be derived for radial and tangential stresses, σ_r and σ_θ .

$$\sigma_{r(i+1)} = \frac{E}{(1+\nu)(1-2\nu)} \left[(1-\nu)\epsilon_{r(i+1)} + \nu\epsilon_{\theta(i)} \right] \quad (10)$$

$$\sigma_{\theta(i)} = \frac{E}{(1+\nu)(1-2\nu)} \left[(1-\nu)\epsilon_{\theta(i)} + \nu\epsilon_{r(i+1)} \right] \quad (11)$$

The impulse-momentum balance for the elements of the body applied in the direction of X (Figure 5.2) results in the following

equation (see Mehta and Davids, (1966)):

$$dV_i = \left[\left[\sigma_{r(i+1)} A_{(i+1)} - \sigma_{r(i)} A_i \right] + \sigma_{\theta(i)} \left(A_{(i)} - A_{(i+1)} \right) \right] dt / m_i \quad (12)$$

where dV_i is the increment in velocity of cell i in time dt .

The cumulation equation for V is:

$$V_i \leftarrow V_i + dV_i \quad (13)$$

Finally, the increment in radial displacement of an element $du_{r(i)}$ over a time dt is given by

$$du_{r(i)} = V_i dt \quad (14)$$

leading to the relation

$$u_{r(i)} \leftarrow u_{r(i)} + du_{r(i)} \quad (15)$$

The parameters described by these equations are calculated for each element, $i = 1$ to $i = i_m$, over a number K_m of time intervals. The ordering of the calculations is critical and a summary of the sequence is given below.

5.4.2 Summary of Discontinuous-Step Analysis.

1. Input data: $a, b, \ell, \rho, E, \nu, dt, K_m$
2. Define the following:

$$c_e = \left[\frac{E}{\rho} \cdot \frac{(1-\nu)}{(1+\nu)(1-2\nu)} \right]^{1/2}$$

$$E_1 = E / (1+\nu)(1-2\nu)$$

$$dr = c_e \cdot dt$$

$$i_m = (b-a) / dr$$

$$r_{i+1} = r_i + dr$$

$$A_i = \pi r_i \ell$$

$$m_i = \frac{\pi \rho \ell}{2} \left[r_{(i+1)}^2 - r_i^2 \right].$$

3. Input pressure functions for inner and outer cylinder surfaces.

$p(t)$ and $q(t)$.

4. Propagation procedure:

(a) Define radial strain: $d\epsilon_{r(i)} = (V_{i+1} - V_i)dt/dr$.

(b) Cumulate radial strain $\epsilon_{r(i+1)} = \epsilon_{r(i+1)} + d\epsilon_{r(i)}$.

(c) Radial stress-strain law:

$$\sigma_{r(i+1)} = E_1 \left[(1-\nu)\epsilon_{r(i+1)} + \nu\epsilon_{\theta(i)} \right]$$

(d) Tangential stress-strain law:

$$\sigma_{\theta(i)} = E_1 \left[(1-\nu)\epsilon_{\theta(i)} + \nu\epsilon_{r(i+1)} \right]$$

(e) Boundary correction for $\sigma_{\theta(i)}$ when $i = i_m$.

(This arises because the term $\epsilon_{r(i+1)}$ is meaningless for $i = i_m$).

$$\sigma_{\theta(i_m)} = \left[E\epsilon_{\theta(i_m)} + \nu(1+\nu)\sigma_{r(i+1)} \right] / (1-\nu)(1+\nu)$$

(f) Boundary conditions:

$$\sigma_{r(1)} = -p(t) = -p$$

$$\sigma_{r(i_{m+1})} = -q(t) = 0.$$

- (g) Define tangential strain increment:

$$d\epsilon_{\theta(i)} = V_i dt/r_i .$$

- (h) Cumulate tangential strain:

$$\epsilon_{\theta(i)} = \epsilon_{\theta(i)} + d\epsilon_{\theta(i)} .$$

- (i) Impulse momentum law:

$$dV_i = \left[\left[\sigma_{r(i+1)} A_{(i+1)} - \sigma_{r(i)} A_{(i)} \right] + \sigma_{\theta(i)} \left[A_i - A_{(i+1)} \right] \right] dt/m_i$$

- (j) Cumulate velocity:

$$V_i = V_i + dV_i .$$

- (k) Define radial displacement increment:

$$du_{r(i)} = V_i dt .$$

- (l) Cumulate radial displacement:

$$u_{r(i)} = u_{r(i)} + du_{r(i)} .$$

- (m) Repeat (a) to (l) for $i = 1$ to $i = i_m$.

5. Increment time:

$$t = t + dt .$$

Repeat steps 3 to 5 for specified number of times km.

As emphasised by the originators of the method, it will be seen that no specific operation or expression is included to distinguish between forward moving and reflected waves. The boundary conditions themselves are sufficient to generate the reflected wave.

As mentioned in the discussions of Butler, M.Sc. thesis 1970,

that the accuracy of the method depends on the choice of cell width, the finer the cell width the more accurate are the results.

5.5 RESULTS AND DISCUSSIONS.

The validity of the discontinuous-step analysis originated by Mehta and Davids (1966) has been well tested by Butler (1970). His analysis consists of:

(a) Comparison with the results presented by Mehta and Davids. He obtained similar curves using the same parameters as those of Mehta. The outer surface displacement-time variation was given for cylinders of various b/a ratios subject to a step internal pressure $p(t) = p_0$.

(b) Comparison with the results obtained by Ensminger (1965), Butler (1970) made a number of computer runs using Ensminger's input data. (The input pressure pulse to the inner surface of the cylinder was that measured by Ensminger, obtained from a piezo-elastic crystal probe). He obtained a reasonable agreement with the discontinuous step analysis and the method of characteristics used by Ensminger.

5.5.1 Variation of Exponential Decay Pressure Pulses.

The experimentally determined pressure-time profile at a radial distance of 10.0 mm from a 24 SWG at discharge voltage 30 KV (Figure 5.3) shows that the blast-wave has the characteristically sharp pressure jump of a shock-front followed by a rapid decay, the whole lasting about 5 μ sec. The trace was smoothed to various

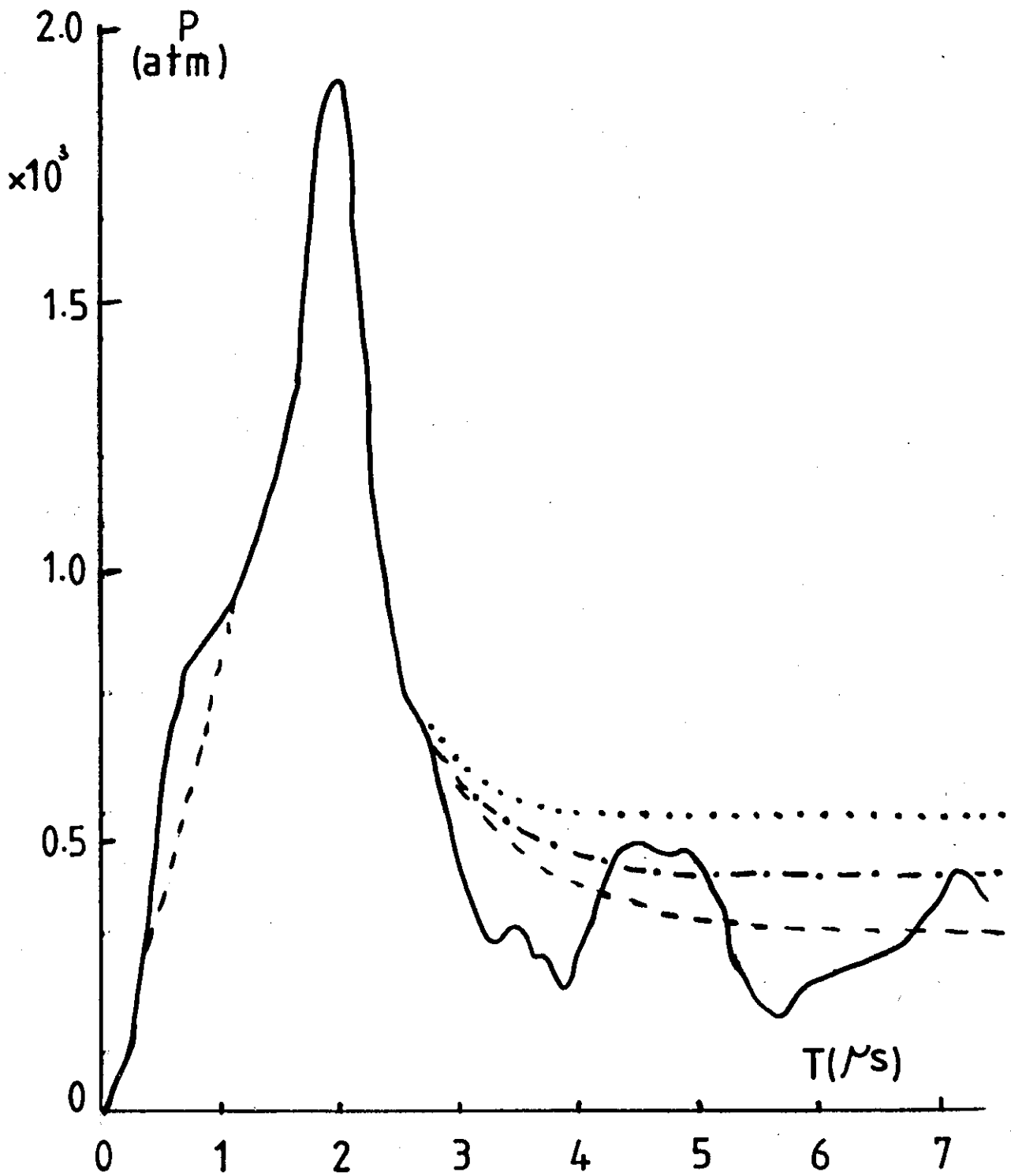


FIG.5.3 PRESSURE-TIME PROFILE FROM A PIEZO-ELECTRIC PRESSURE-BAR GAUGE

exponential decays for the last 3 μ sec. This trace was smoothed to a pressure value of 3.3×10^7 N/m², 4.4×10^7 N/m² and 5.5×10^7 V/m² respectively. This profile was used in the computer calculations and the results are presented in Figure 5.4 and are for a cylinder of inner radius $a = 10.0$ mm, outer radius $b = 27.5$ mm, length $\ell = 11.5$ cm, density $\rho = 1160$ kgm/m³ of material having physical characteristics of Young modulus $E = 36 \times 10^8$ N/m² and Poisson's ratio $\nu = 0.35$. These physical characteristics are very close to Nylatron characteristics.

The displacement of the outer cylinder surface begins when the outward moving blast-wave first reaches it. The stress wave is reflected and travels inwards superimposing itself on the outward wave and after subsequent reflection at the inner cylinder surface reaches the outer surface again. Discontinuities appear on the displacement curves corresponding to these times of reflections. The shapes of ~~each~~^{the} curves are basically similar, the displacements decreasing almost proportionately with the pressure. It also shows that the reflection (discontinuity) times are independent of the magnitude of the pressure, and in addition there is a progressive rounding-off of the discontinuity regions with decreasing pressure pulse. Further, the faster the pressure decay the greater is the tendency for the displacement to fall-off before the first reflection of the wave. The dilatational wave velocity c_e measured from the curves is $\sim 2.2 \times 10^5$ cm/sec. for Nylatron cylinder.

Due to the fact that the crystal used to obtain the pressure-time profile had a finite rise time, it is suggested by Ensminger

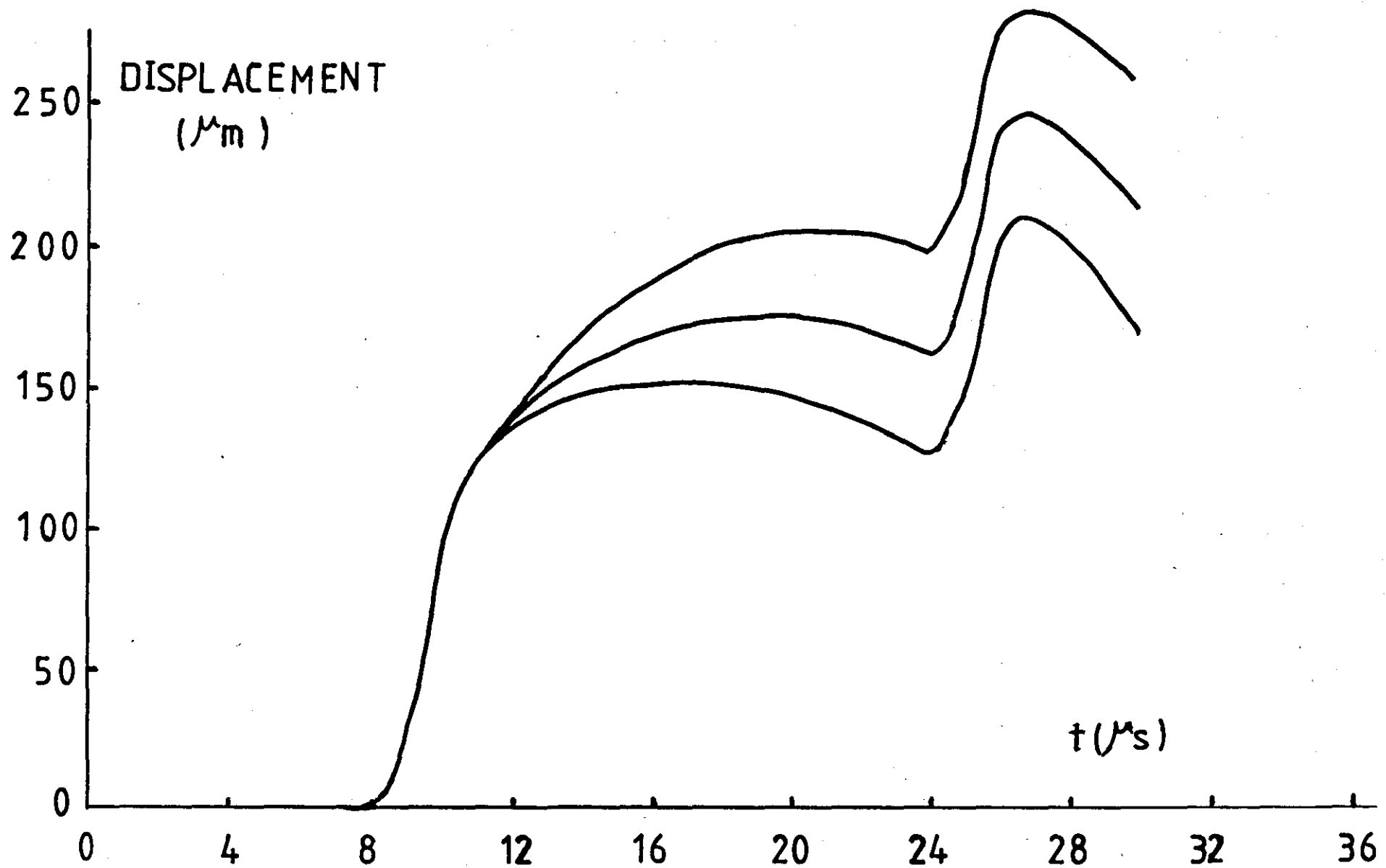


FIG. 5.4 VARIATION OF OUTER SURFACE DISPLACEMENT WITH TIME

and Fyfe (1966) that the zero and finite rise-time be used as a bound on the pressure-time boundary. Figure 5.5 shows the result using the same pressure profile with the zero rise time. The wave reflection (discontinuities) in the curve are sharp and clearly defined, and the rise time of the displacement is faster than in Figure 5.4. The magnitude of the peak displacement is slightly smaller but the elastic wave velocity c_e measured $\sim 2.2 \times 10^5$ cm/sec. Table 5.1 shows the peak displacement obtained from Figures 5.4 and 5.5.

TABLE 5.1.

| | Displacement (μ m) | | Pressure decay N/m^2 |
|-----|-------------------------|-----------------|---------------------------|
| | From Figure 5.4 | From Figure 5.5 | |
| (1) | 210 | 180 | 3.3×10^7 |
| (2) | 260 | 230 | 4.4×10^7 |
| (3) | 290 | 260 | 5.5×10^7 |

5.6 CONCLUSIONS.

Part of the theory of elastic wave propagation has been presented in cylindrical coordinates. The discontinuous-step method originated by Mehta and Davids has been described and applied to the case of elastic waves propagating radially in hollow cylinders.

The pressure-time profile measured from Hopkinson pressure bar gauge was used to determine the displacement-time variation of the outer surface of a hypothetical material having the elastic properties of Nylatron.

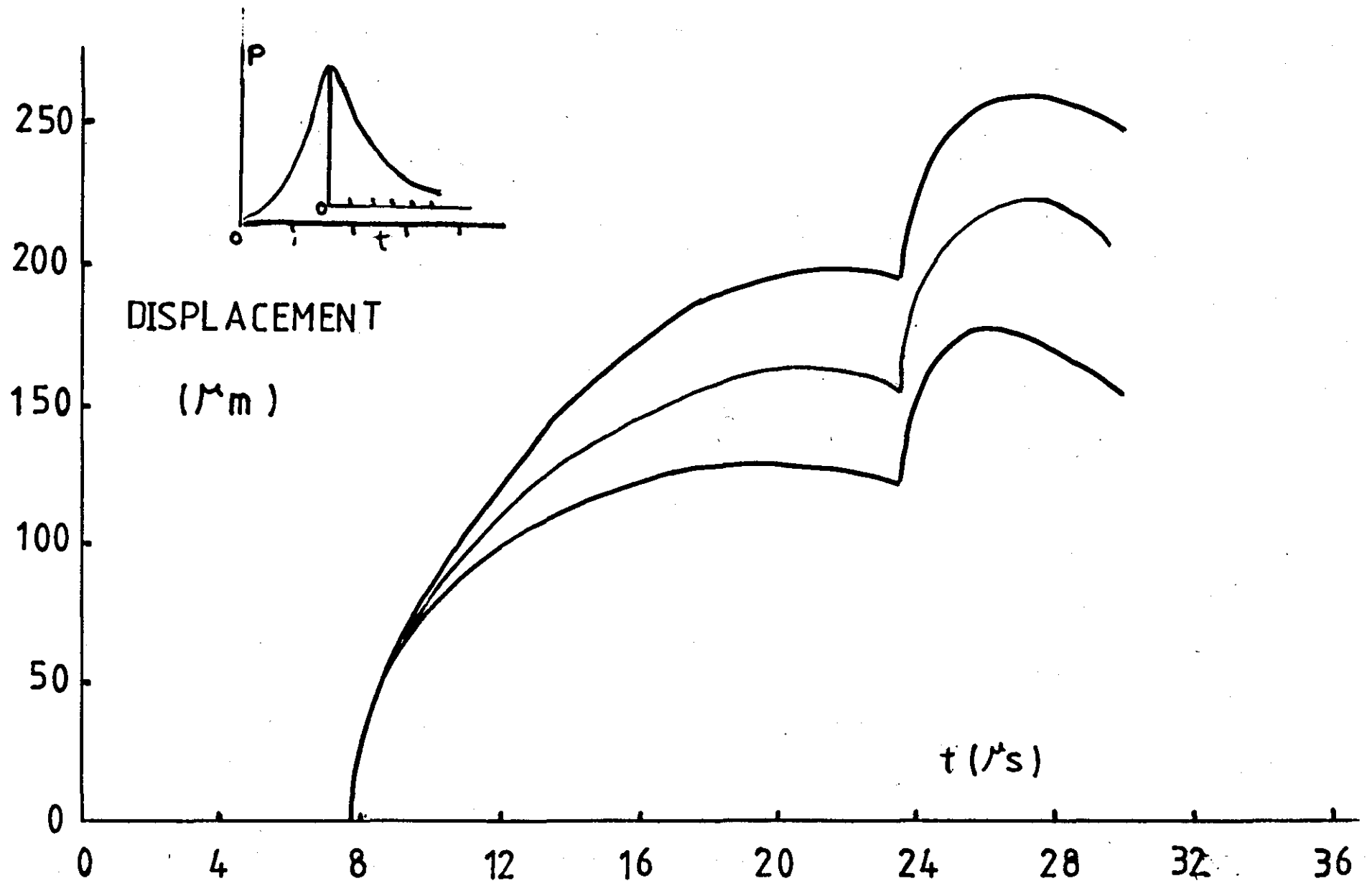


FIG. 5.5 VARIATION OF OUTER SURFACE DISPLACEMENT WITH TIME

CHAPTER 6

DISPLACEMENT MEASUREMENTS

6.1 THE DISPLACEMENT MEASUREMENT SYSTEM.

In order to obtain experimental measurements of the free surface of the cylinder for given loading pressures on the inner surface, an optical system was used. Although, similar to that used by Fyfe (1968) it differed in certain respects. Figure 6.1 shows a schematic diagram of the arrangement of the system. A thin copper wire (24 SWG 0.559 mm) is placed along the axis of a cylinder of variable internal diameter and thicknesses. When the capacitor is discharged through the wire it vaporizes almost instantaneously as mentioned in Chapter 3. This produces in the surrounding air a supersonic pulse having a shock-front across which there is an abrupt increase in pressure followed by a smooth pressure decrease, i.e. a blast-wave. When this blast-wave strikes the inside wall of the cylinder, it generates on reflection a high amplitude cylindrical stress-wave in the cylinder. A narrow beam from a gas laser is partially cut off by the cylinder's outer surface (near the middle) and a fixed knife-edge shutter before reaching a photo-detector. The outer surface movement varies the beam width and hence the photo-detector signal, enabling the displacement-time variation to be determined, and the results displayed on an oscilloscope.

From this displacement and the pressure-time loading profile on the inner surface, the mechanical modulus of the cylinder can be computed from a theoretical analysis (as in Chapter 5) which assumes that the cylinder is subjected to plane strain.

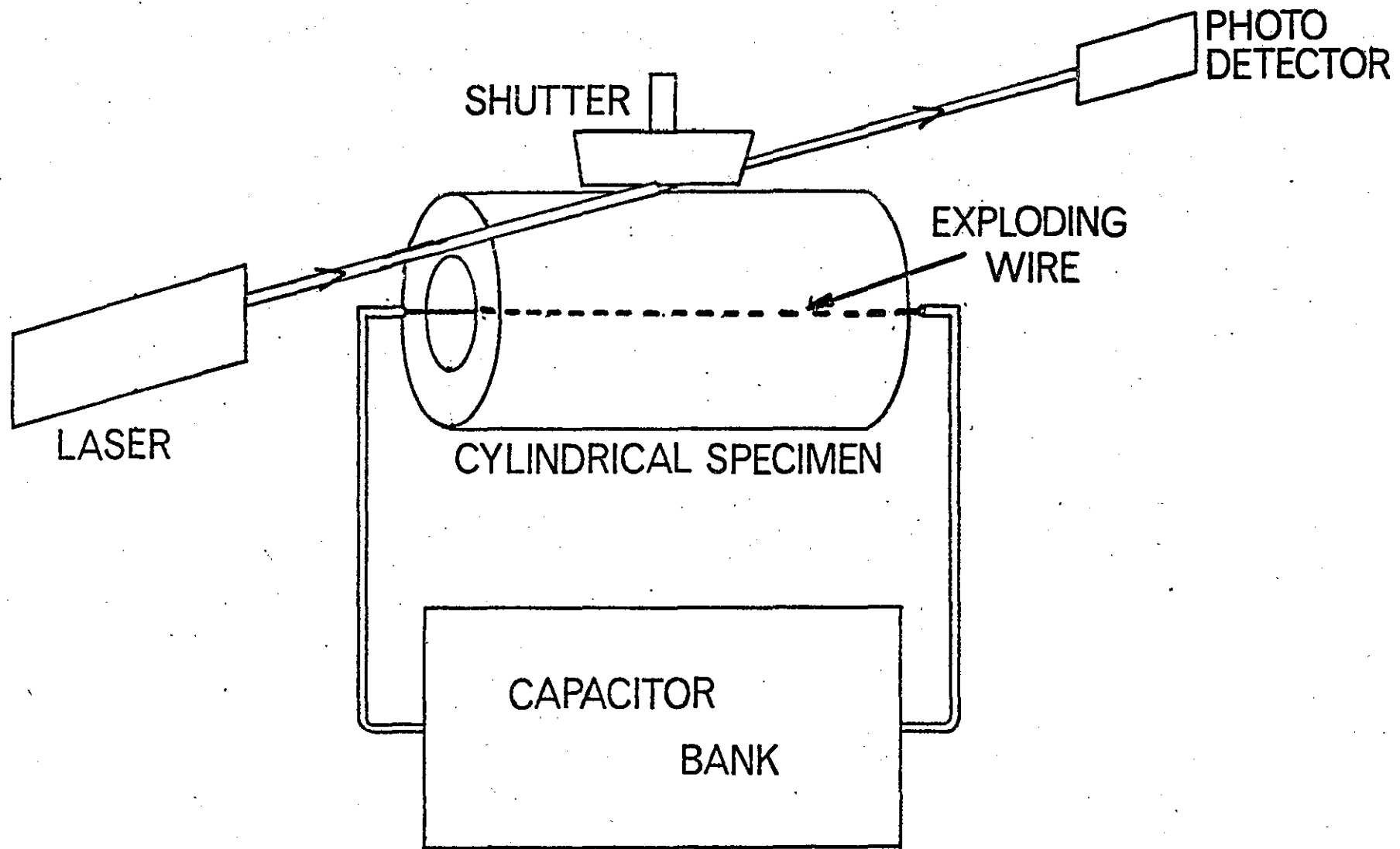


FIG. 6.1 BASIC SYSTEM FOR IMPACT TESTING OF CYLINDRICAL SPECIMEN

6.1.1 The Calibration Units.

Figures 6.2 and 6.3 show the rig in relation to the optical system. Positioned above the rig is the micrometer calibration arrangement. This unit is detachable from the main rig and is shown in detail in Figure 6.4. It consists of a fixed knife-edge shutter (A) lying near the specimen surface at the end of a circular shaft (B). The collar at (C) provides a piston fit for the shaft which is restrained from rotation by a screw inside cross-piece (D). A micrometer (F) reading to 1/500 th of a millimetre is supported above this. Spring (E) provides an upward force on the shaft sufficient to maintain contact between the end of the shaft of the micrometer and a ball bearing sunk into the upper end of (B). With this system it is possible to vary the slit formed by the top of the specimen and the knife-edge shutter very accurately. Specimens of diameter 20 to 50 mm and lengths 50 mm to 140 mm can be accommodated in this apparatus.

6.1.2 The Optical System.

The system developed to measure the displacement-time history of the specimen requires:

- (i) Relative simplicity.
- (ii) Facility to measure a fairly large range of displacement, with a sensitivity to resolve to ± 250 micrometer.
- (iii) An adequate response time.
- (iv) A linear relationship between slit width and photomultiplier output signal with an accurate means of calibration.

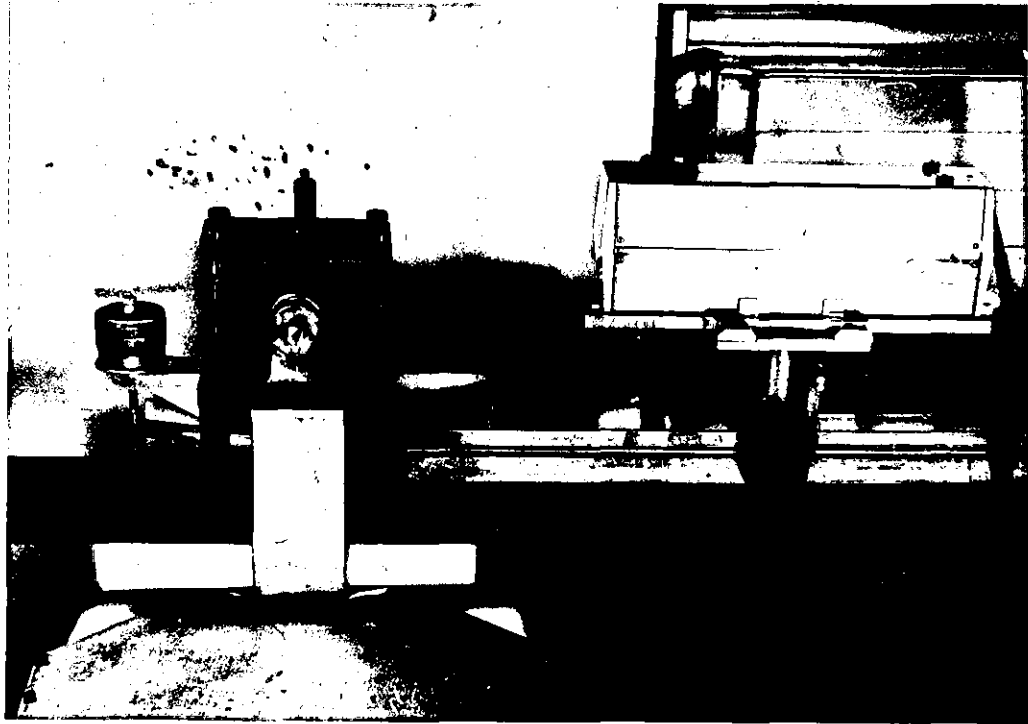


FIG. 6.2 OPTICAL SYSTEM RELATING TO THE RIG

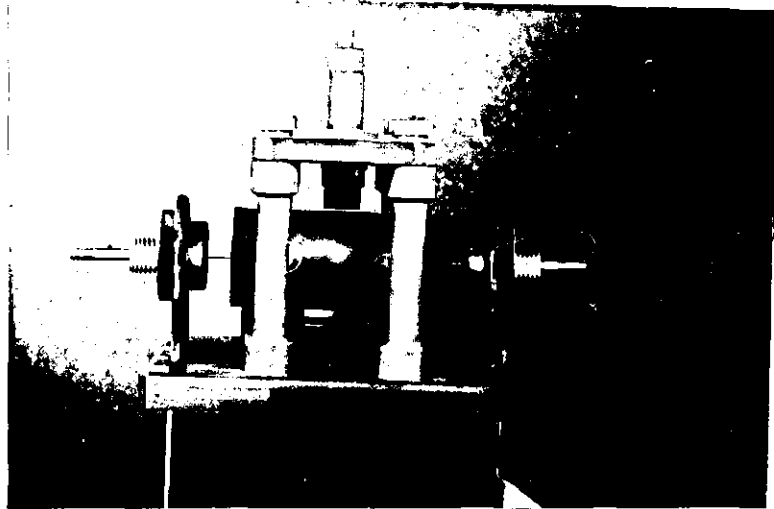


FIG.6.3 OPTICAL RIG

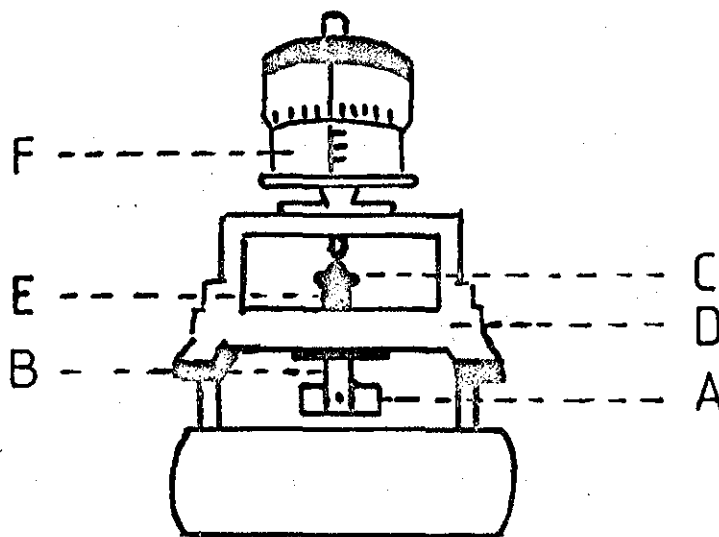


FIG. 6.4 THE CALIBRATION ARRANGEMENT

The requirement in obtaining a linear relationship between a slit width and photomultiplier signal is a constant area of illumination of the photocathode regardless of slit width, laser light source would facilitate this. The amount of the laser light passing the specimen is limited by the knife-edge shutter which is controlled by the micrometer. After passing the specimen the light is contained in a long tube ($\sim 15\text{m}$) which lies close to the specimen. At the other end of the tube lies the photomultiplier, in this arrangement extraneous light is kept from reaching the photomultiplier. Before reaching the detector the light can be chopped to give an A.C. signal by means of a rotating chopper disc situated between the laser and the specimen.

6.1.3 The Light Detector.

The intense parallel beam of light was produced by a He - Ne laser (Spectral Physics 134, output 2 milli-watts). The photo detector and amplifier used are a commercial instrument Lite-Mike and a photodiode. The photodiode acts as a current generator where current depends linearly on the intensity of the received light.

The schematic diagram of Lite-Mike is shown in Figure 6.5.

To test the sensitivity of Lite-Mike and the photodiode, a light source from the Argon arc applied to both of them, it was

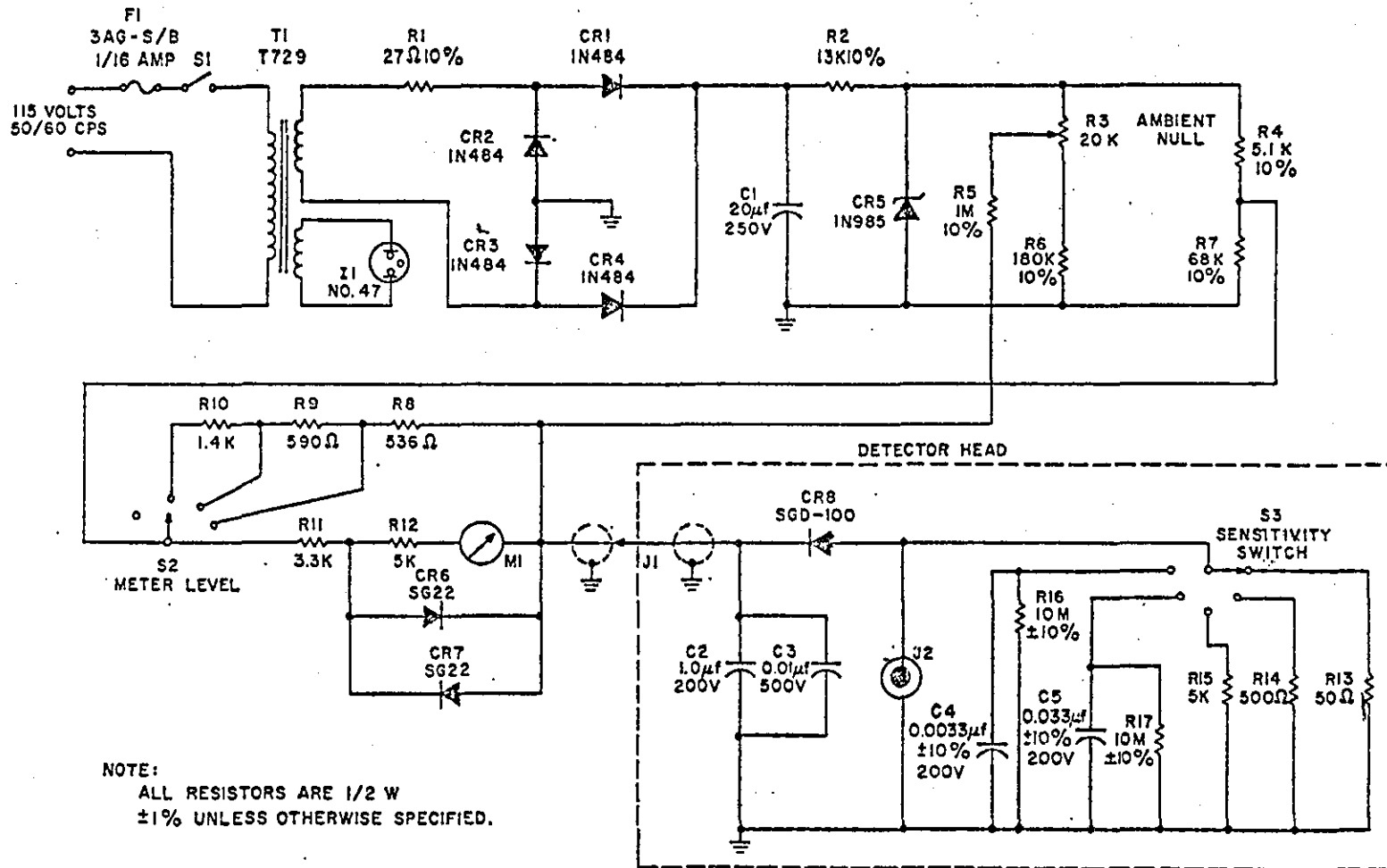


FIG. 6.5 LITE - MIKE CIRCUIT DIAGRAM.

found that Lite-Mike rise-time is shorter than the rise-time obtained from photodiodes as shown in Figure 6.6. Although a photodiode has a lower sensitivity than a photomultiplier, it does have certain advantages:

(i) Even though its sensitivity is less, it does have a better spectral response at red wavelengths.

(ii) It seems to be less susceptible to electro-magnetic radiation pick-up and can be operated from a D.C. supply with minor modification.

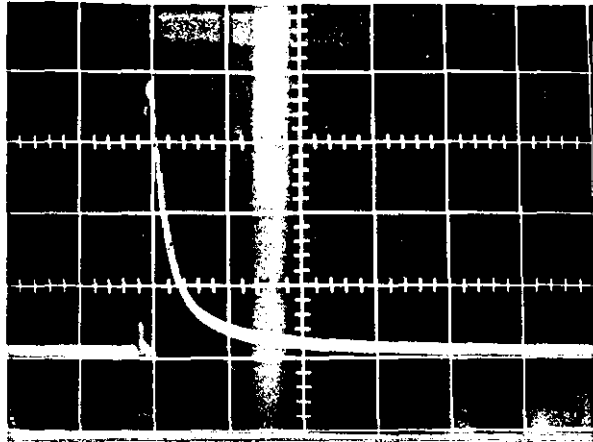
(iii) It is easier to use and calibrate.

For these reasons it was decided to use the photodiode and since a fairly intense source was used, it was thought that the lack of sensitivity would not be a problem. Another factor of importance in the choice of detector was the response time, for it was too long. The kinks in the displacement records that corresponded to reflections at the cylinder boundaries would be missed. The response of a photomultiplier is faster, but the predicted response of the diode at maximum gain was of the order of 150 nsec. which should be sufficiently fast for accurate measurements.

The main advantage of the optical system was the ability to place the electronic detection apparatus as far from the exploding wire rig as possible, thereby reducing noise interference to a minimum. For the explosion of a wire and the corresponding large current pulse are large sources of electro-magnetic radiation.

The problem of light pick-up by using Nylon cylinders in the experimental tests was high because the nylon was not completely

(a)
0.1 V/cm



(b)
0.05 V/cm

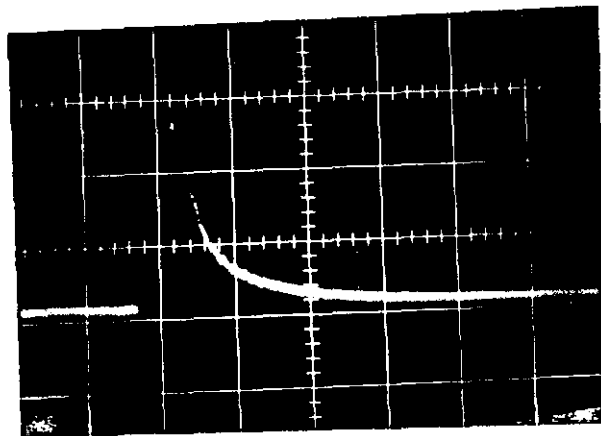


FIG.6.6 RESPONSE OF LITE-MIKE (a) AND PHOTO-
DIODE (b) TO LIGHT SOURCE
Sweep: 2 μ s/cm

opaque to the light from the explosion. It was found necessary to spray the specimens completely with matt-black, and it was generally found necessary to use two coats of paint.

6.2 THE RECORDING SYSTEM CALIBRATION.

In order to determine the amount of displacement of the cylinder's surface, it is necessary to calibrate the detection system by allowing the knife-edge to intersect the laser beam. Precise control of this movement is accomplished using the micrometer. The knife-edge is aligned vertically parallel to the edge of the specimen in prescribed increments. The intensity of the beam will thus decrease. By measuring the change of the voltage on the scope and the micrometer movement, a voltage - displacement calibration curve is obtained. The calibration curve is shown in Figure 6.7. The important effects associated with the linearity of the curves were observed during calibrations are:

(i) When the optics were such that the area of illumination of the photocathode was not constant during the variation of slit width. The calibration curve of the output voltage on the scope against slit width was not linear and was of the form shown in Figure 6.8. The nature of the curvature indicates that as the slit width increased, the sensitivity of the photomultiplier increased with increase in area of illumination of the photocathode. It was necessary thereafter to ensure a constant area of illumination.

(ii) With the correct optics for constant area of illumination non-linear regions were obtained on the calibration curves at low

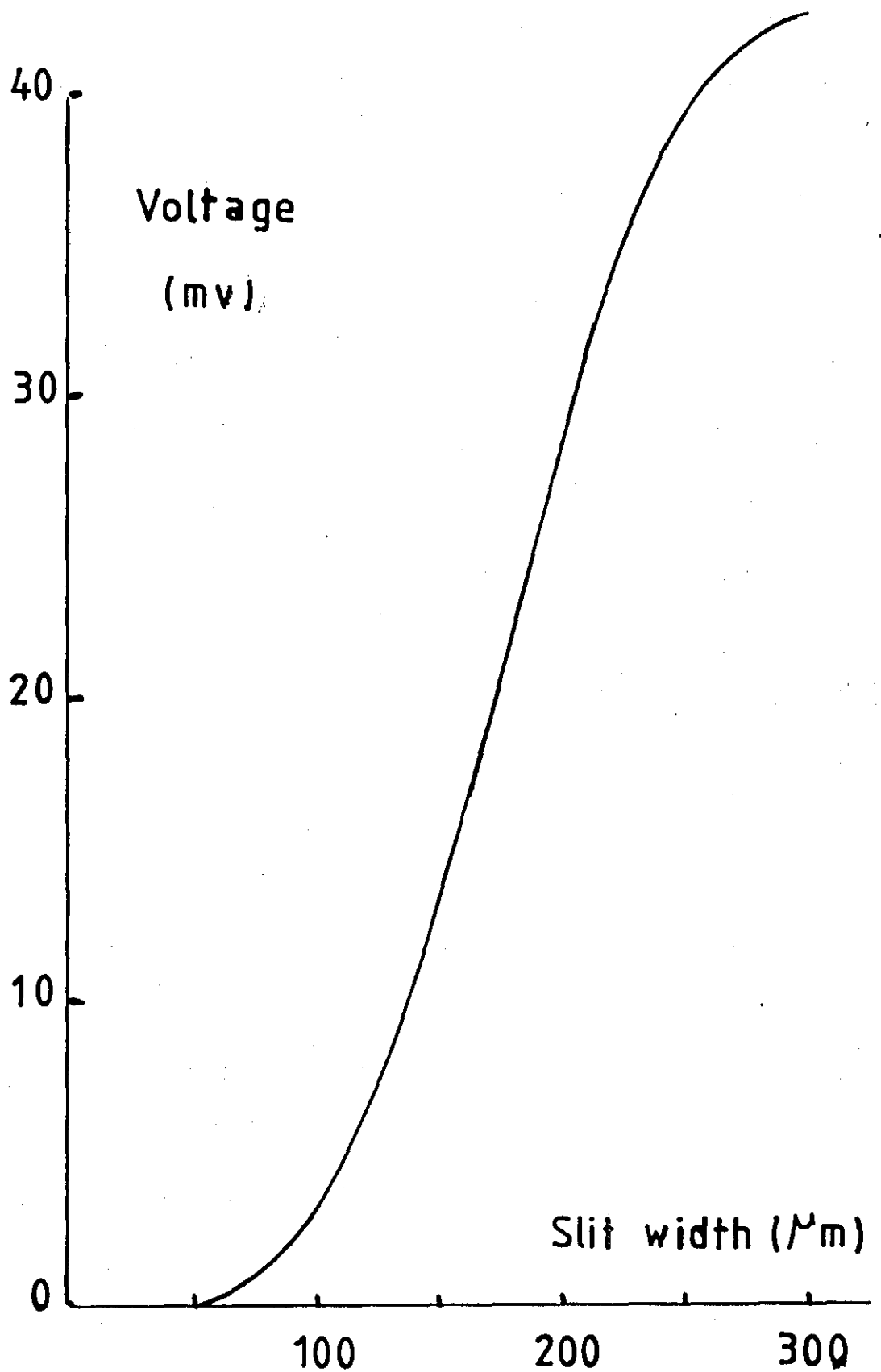


FIG. 6.7 CALIBRATION CURVE

and high slit widths as in Figure 6.7. The curvature at high light levels indicates that the sensitivity of the photomultiplier response decreased progressively towards a state of saturation. In this condition the maximum anode current was reached corresponding to peak emission from the photocathode.

(iii) By avoiding saturation of the photodiode, a filter was placed in front of the photocathode to cut down the light intensity.

(iv) At low slit widths the non-linearity of the calibration curve, which is not so marked as at high light levels, was probably due to a combination of diffraction effects and irregularities of the slit surface. Diffraction patterns were obtained on a screen placed close to the specimen but became indistinct further away.

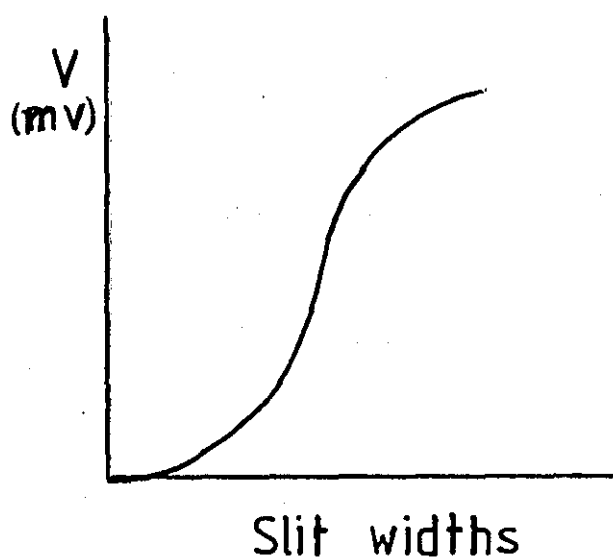


Figure 6.8 Non-Linear Calibration Curve.

6.3 THE PEAK DISPLACEMENT MEASUREMENTS.

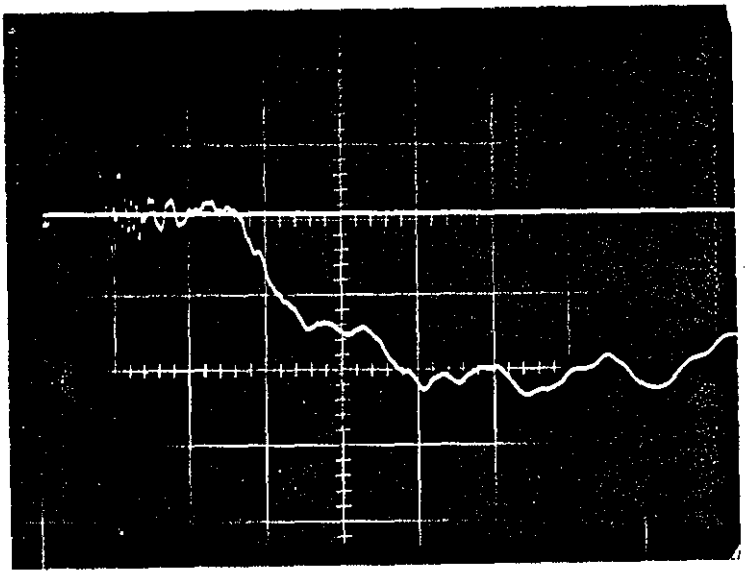
It was found that discharge energies of about 2.5 kilo-joules, corresponding to initial charging voltages of around 20 KV were required to produce a deformation in Nylatron (Polypenco) cylinders capable of measurement with the present maximum sensitivity. With the photodiode positioned as far as 15 m from the exploding area, pick-up levels became intolerable at charging voltages 25 KV, 30 KV and 35 KV. Some preliminary tests indicated that the energy required to give a significant deformation corresponded to a charging voltage of 20 KV.

A series of tests were performed using Nylatron and Nylon specimens of various dimensions. With the charging voltage constant at 20 KV and using a 24 SWG copper and phospho-bronze wire, each specimen was subjected to deformation. Some of the tests were intended to observe the reproducibility and the wave velocity of stress waves and the displacement history. Under these conditions the nature of the resulting pressure pulse on the specimen inner surface is markedly changed (see Chapters 4 and 5). A typical displacement trace starts with an initial zero displacement which then rises to a maximum with subsequent fall off to zero.

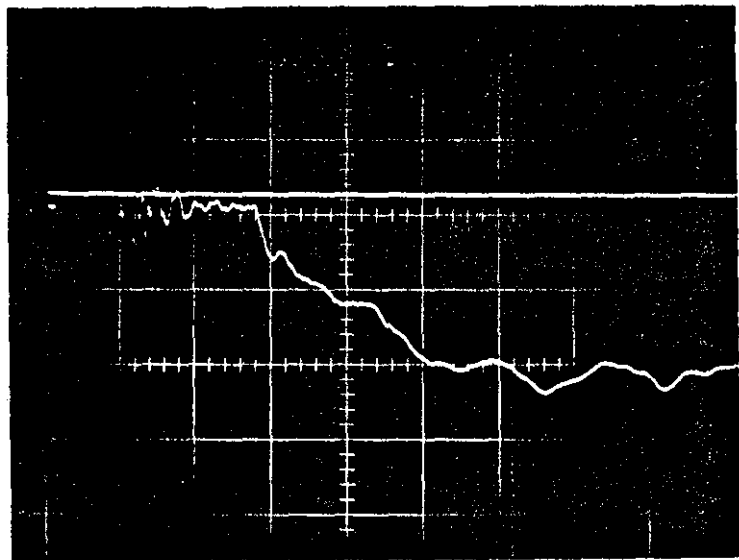
Figure 6.9 shows three traces of the displacement as the cylinder clamped (a) loosely, (b) tightly and (c) lightly, it can be seen from the oscillograms, that no significant changes in the shape and peak displacement with the clamping conditions.

Further tests were made concerning the centring of the exploding wire inside the cylinder. Figure 6.10 shows two displacement-time records of the wire (a) in the centre and

(a)



(b)



(c)

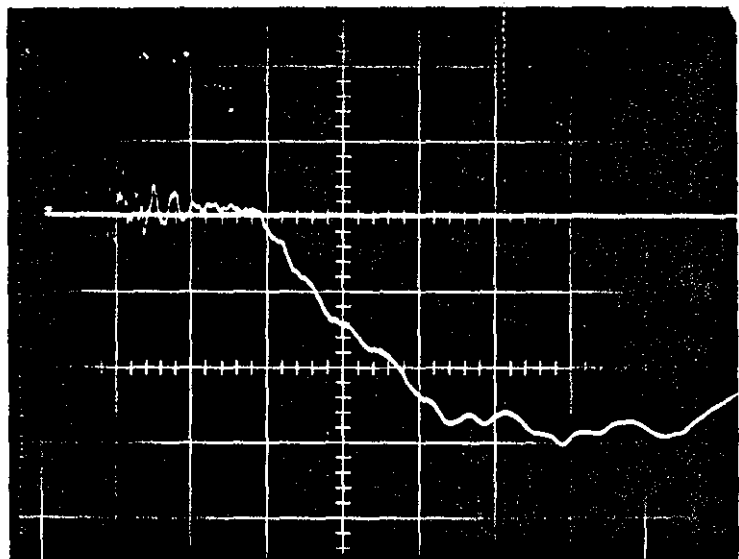
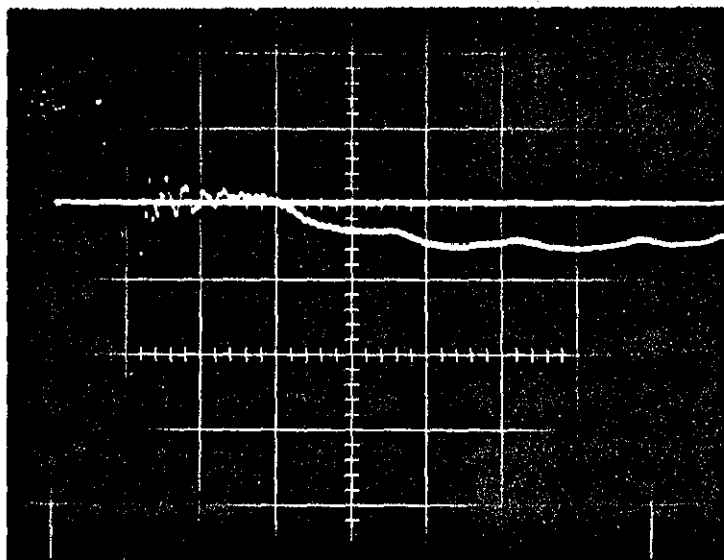


FIG. 6.9 EFFECT OF CLAMPING THE CYLINDER

(a)



(b)

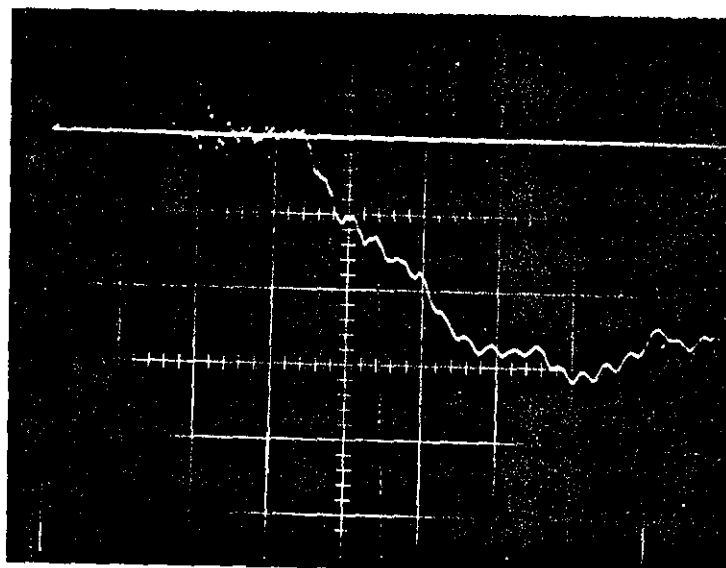


FIG.6.10 CENTERING OF THE WIRE

(b) off centre near the top surface of the cylinder. The displacement trace of (a) shows discontinuities corresponding to reflections of the stress pulse at the outer surface of the specimen. Often these discontinuities are distinct as in (b) they are not so well resolved. Also characteristic of the trace is the presence of a low noise ripple arising from the mode of operation of the photodiode, and a pick-up signal from the wire explosion in the earlier part of the traces.

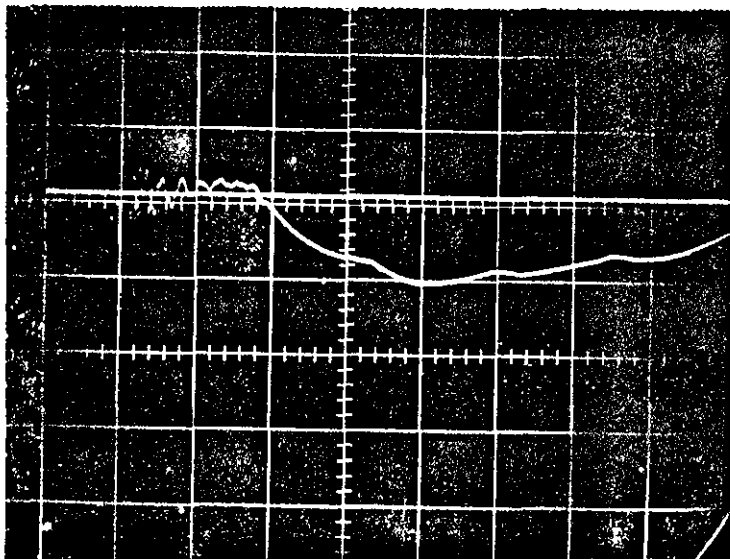
The time period over which the displacement traces have any meaning is limited by the inward propagation of disturbances from the ends of the specimen. Assuming these propagate with the longitudinal wave velocity 2.7×10^5 cm/sec. for a cylinder length of 14 cms, this time is approximately 54 μ sec. Since most of the displacements are confined to a period of 30-40 μ sec. after the explosion this presents no problem. So the position of the exploding wire is very important to reduce the noise ripples.

From the traces it is possible to measure the velocity of the pulse through the specimen. These measurements are given in Section 6.4.

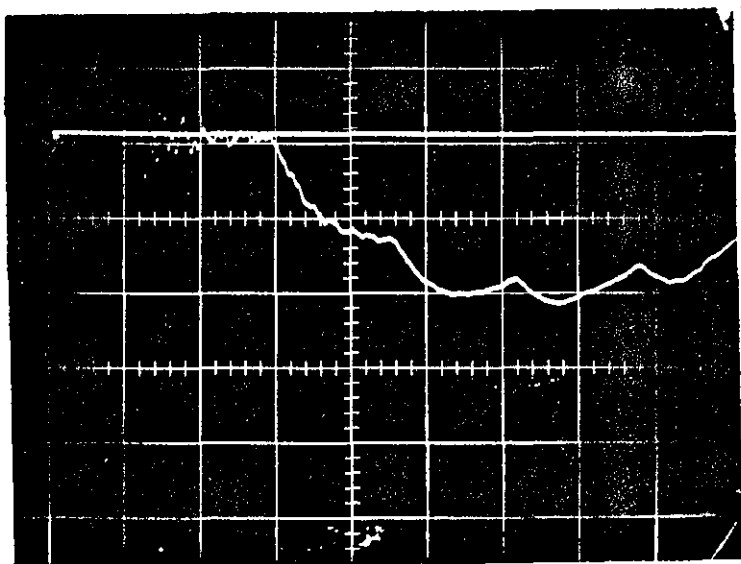
6.3.1 Reproducibility.

Figure 6.11 shows an oscillogram obtained for Nylatron cylinder of inner radius 15 mm and outer radius of 25,5 mm, gives the corresponding derived displacement-time diagrams. It is seen that the general form of the traces shows a very reasonable reproducibility, especially with regard to the peak displacements. Close examination of the traces reveals that the timing of the

(a)
 $X = 5 \mu\text{s} / \text{cm}$
 $Y = 10 \text{ mV} / \text{cm}$



(b)
 $X = 5 \mu\text{s} / \text{cm}$
 $Y = 5 \text{ mV} / \text{cm}$



(c)
 $X = 5 \mu\text{s} / \text{cm}$
 $Y = 5 \text{ mV} / \text{cm}$

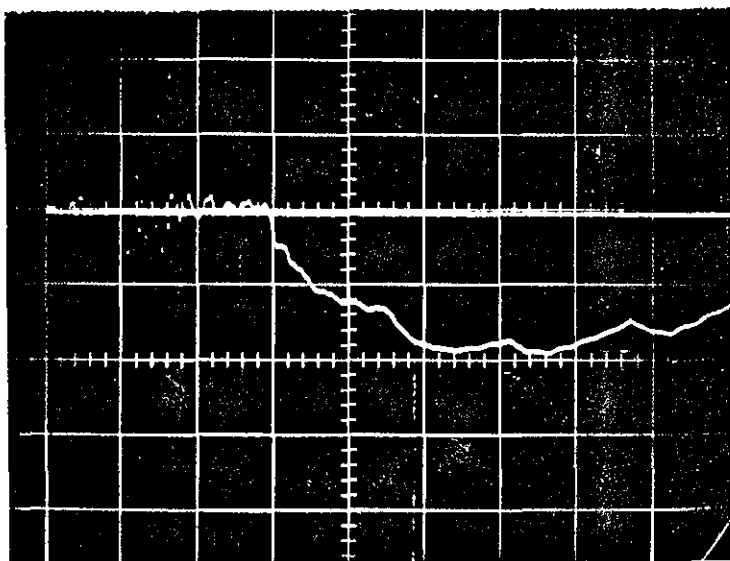


FIG. 6.11 DISPLACEMENT OSCILLOGRAMS

displacement and of the discontinuities always correspond.

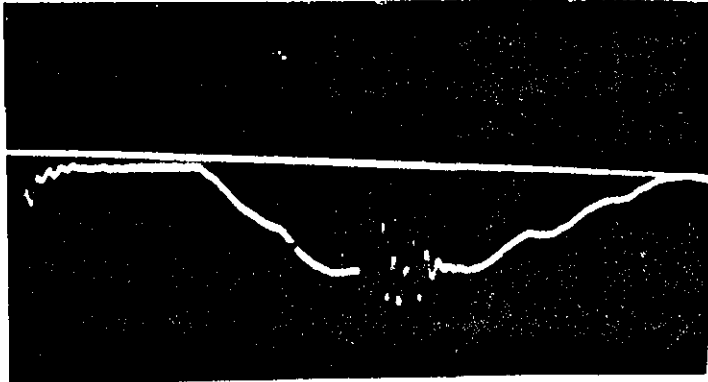
In further tests a phospho-bronze wire of 24 SWG was used for the explosion inside Nylatron specimens of inner radius 1.6 and 1.1 cm, and outer radius of 2.6 cm. Unlike the copper wire, the phospho-bronze wire test shown in Figure 6.12 produced a tiny pick-up which has occurred in previous tests, it is likely that this pick-up arose from a combination of variations in the experimental conditions between tests and factors relating to the properties of the material. Possible changes in experimental conditions between tests may arise from a variation in the following:

- (i) contact resistance between wire and clamps,
- (ii) structure and diameter of the wire along its length,
- (iii) alignment of the wire inside the specimen,
- (iv) intensity of light from the laser. Care was taken at all times to ensure as far as possible that experimental conditions were constant.

6.3.2 Peak Displacement.

The loading pressure on the inner surface of the specimen is independent of the material itself, but in a function of the surroundings of the wire, i.e. the inner radius of the specimen, as mentioned earlier that the possible discharge energy to avoid the pick-up, is 2.5 kilo-Joules corresponding to voltage of 20 KV, where the pressure measurement were obtained at higher input energies of 5.6 kilo-joules. An important parameter affecting a cylinder's response to a particular pressure pulse is the ratio

(a)



(b)

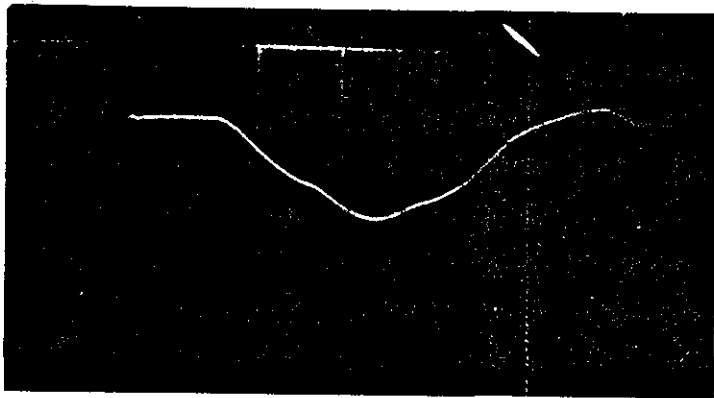


FIG.6.12 DISPLACEMENT-TIME RECORD FROM
EXPLODING 24 SWG PHOSPHO-BRONZE
WIRE INSIDE NYLATRON CYLINDER

Sweep: $10\mu\text{s}/\text{cm}$

of the outer radius to the inner radius.

Table 6.1 summarises the results of the investigation with regard to the peak displacements. As expected from the theoretical treatment in the previous chapter, it is seen that for a given pressure pulse the displacement decreases with increasing wall thickness of the specimen. However, because the specimens were subjected to different pressure pulses, the results indicate that the wall thickness has a greater effect on the magnitude of the peak displacement. Figure 6.13 shows displacement-time records for Nylatron cylinder of inner radius 10.5 mm and outer radius of 23.5 mm. The displacement measured is higher compared with the previous tests and the velocity is about 2.9×10^5 cm/sec., it is quite possible that some type of work hardening effect is operative. This will tend to increase the dynamic modulus of the material, which means an increase in the velocity. The frequency of the cylinder measured from the records is about 2×10^4 /sec⁻¹.

The nature of the displacement-time record:

(i) It can be seen that the initial part of the record has a very distinctive pattern consisting generally of two or three discontinuities separated by about 9 μ s.

(ii) After the first three discontinuities it can be seen that the trace becomes wavy and the sharpness of the discontinuities is considerably reduced.

(iii) In addition the mean displacement has a longer time period of about 45 μ s.

The early sharp discontinuities clearly indicate that the stress pulse suffers consecutively distinct reflections from the outer and inner surfaces of the cylinder, so that a wave velocity can be derived from this early stage of the displacement record.

The effect of the dispersion of the stress pulse has resulted in the progressive smoothing out of the pulse to produce the wave-like short-term displacement in the later stages. The longer term period of the trace seems to indicate the oscillation of the whole cylinder.

6.4 WAVE VELOCITY MEASUREMENTS.

It is possible from the displacement records to calculate the wave velocity of radial stress wave through the specimen. This can be done in two ways.

6.4.1 Wave Velocity Measurements from Discontinuities.

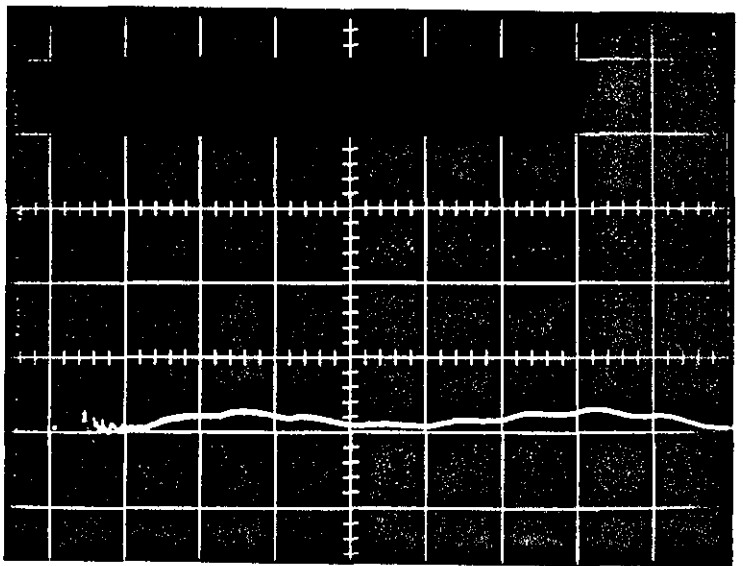
As described in Chapter 5, the outer surface of the cylinder begins to move when the stress wave first reaches it. The pulse is then reflected and propagates inwards until it is reflected back from the inner surface, on reaching the outer surface, it

(a)

$$X = 10 \mu\text{s}/\text{cm}$$

$$Y = 20 \text{ mV}/\text{cm}$$

$$300 \mu\text{m} = 20 \text{ mV}$$

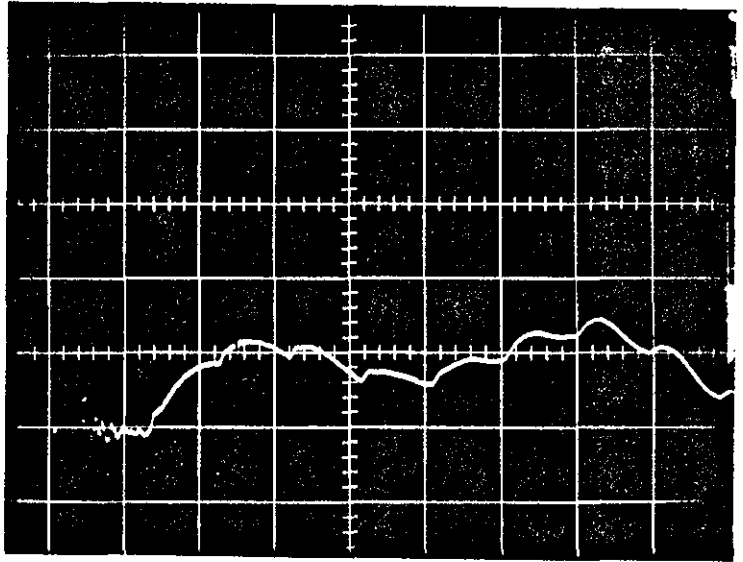


(b)

$$X = 10 \mu\text{s}/\text{cm}$$

$$Y = 10 \text{ mV}/\text{cm}$$

$$300 \mu\text{m} = 40 \text{ mV}$$



(c)

$$X = 10 \mu\text{s}/\text{cm}$$

$$Y = 5 \text{ mV}/\text{cm}$$

$$300 \mu\text{m} = 22 \text{ mV}$$

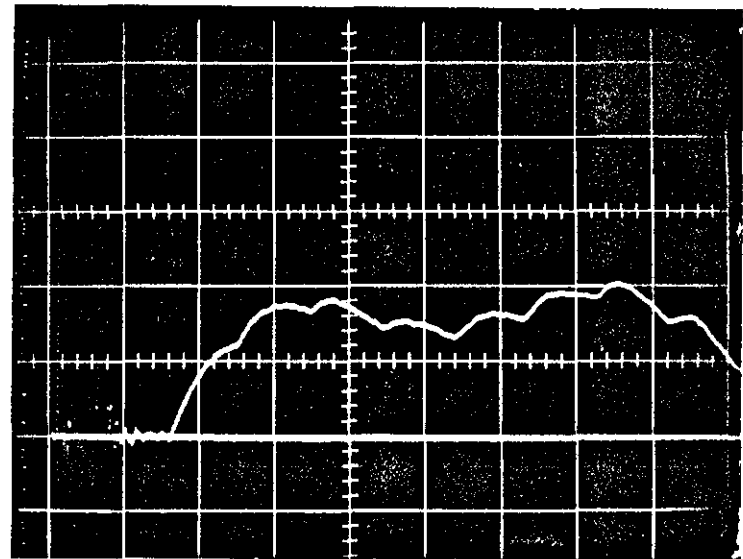


FIG. 6.13 DISPLACEMENT-TIME RECORDS

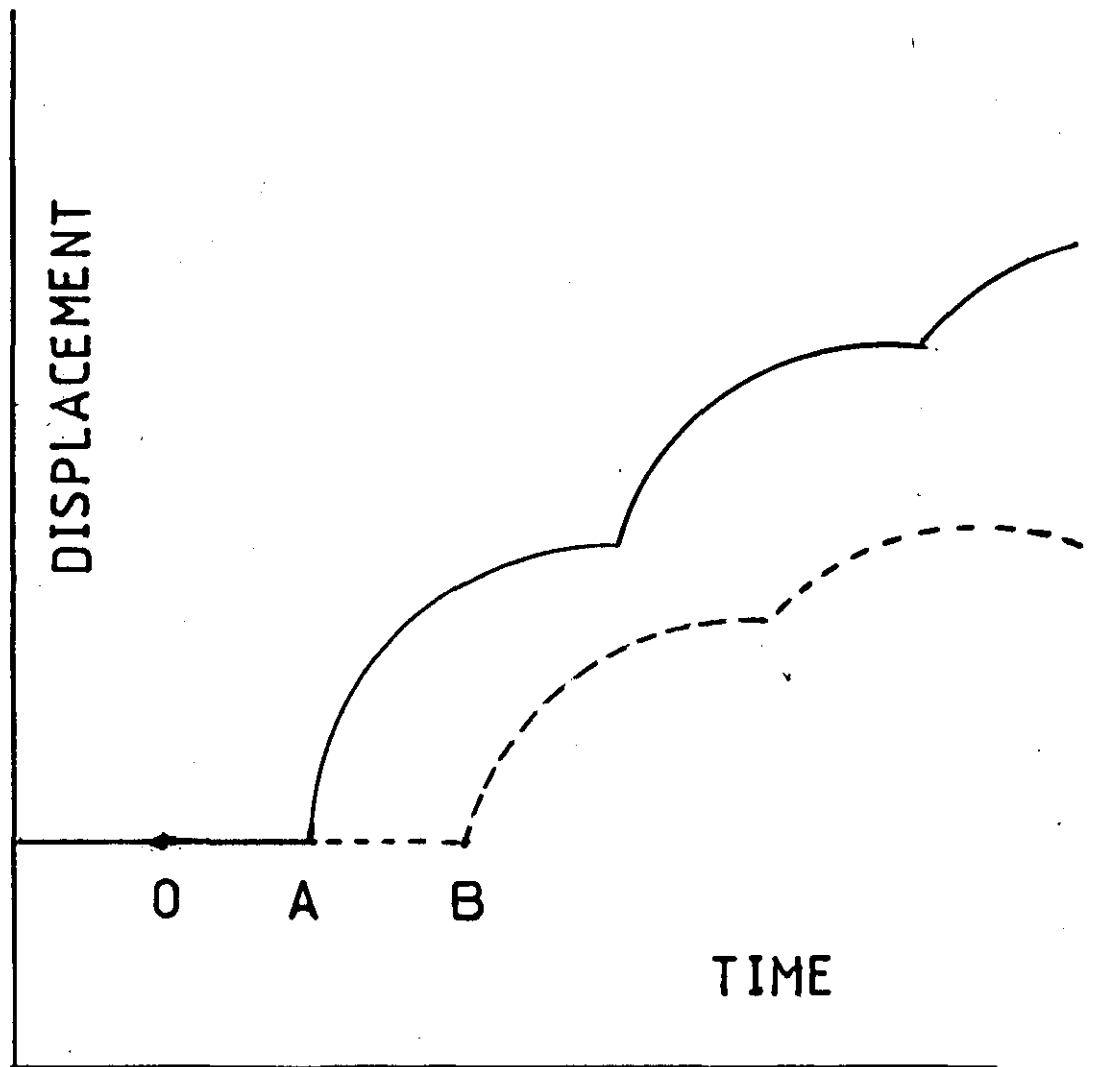


FIG. 6.14 BASIS FOR ESTIMATING VELOCITIES

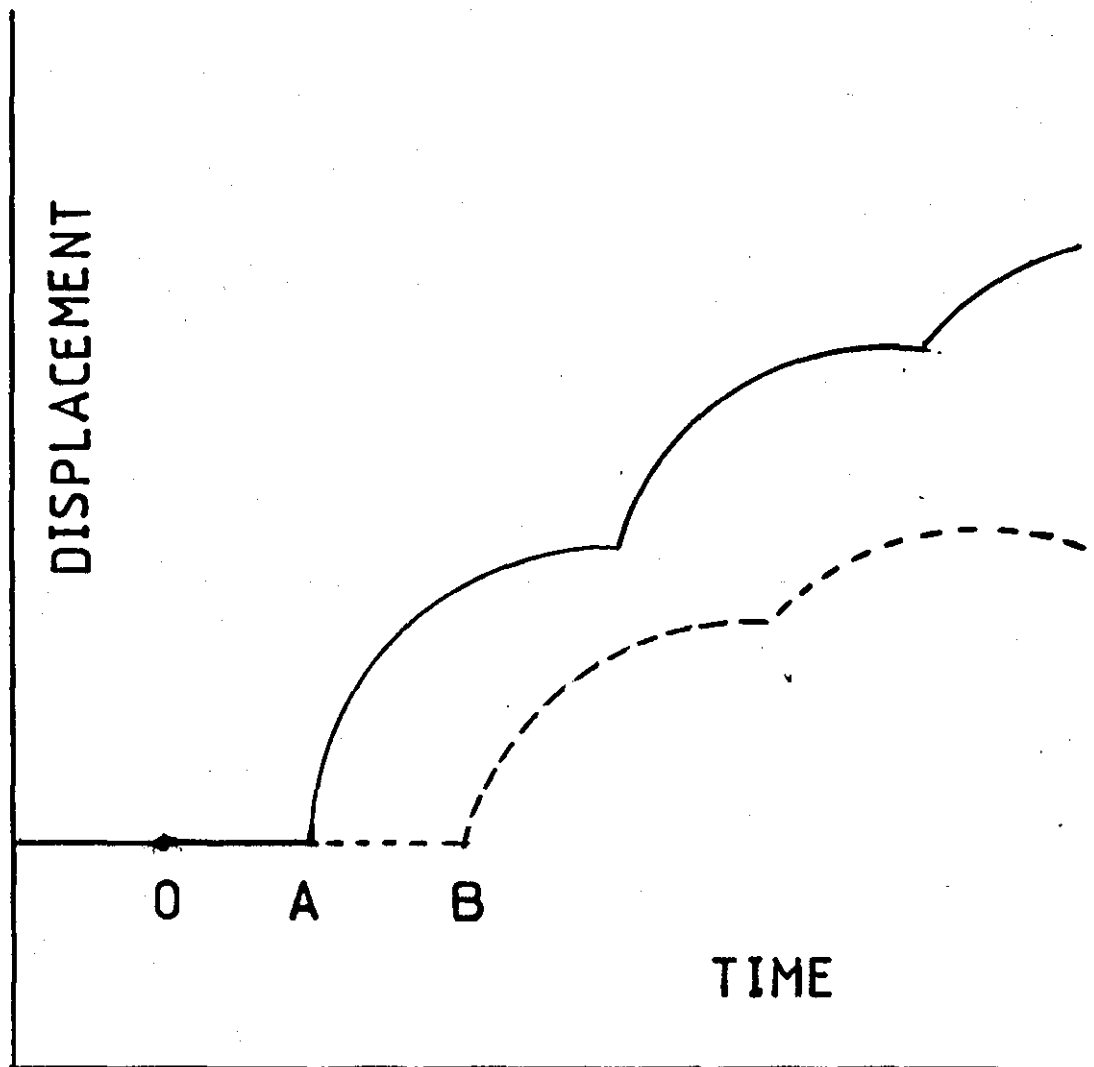


FIG. 6.14 BASIS FOR ESTIMATING VELOCITIES

will produce a discontinuity in the slope of the displacement record. Further reflections from the outer surface will produce more discontinuities until the pulse is completely attenuated. The time between two discontinuities represents a movement of the stress pulse over twice the wall thickness of the cylinder, hence by measuring the time taken the velocity can be calculated.

The displacement traces in Figures 6.11, 6.12, and 6.13 showed discontinuities quite distinct and very clear. The measurements of the velocity are presented in Table 6.1.

6.4.2 Wave Velocity Measurements using Differences in Transit Times.

This method of measuring the velocity is based on the difference in transit times of the pulse through two specimens of equal inner radius but different outer radius. Referring to Figure 6.14 typical displacement-time variations for two specimens of equal inner radius, assuming that the point O is the time origin of the shock wave from the exploding wire for both specimens, the times OA and OB represent the times for the wave to travel outwards in air (as a blast wave) to the inner surface of the specimens together with the time of transit of the stress pulse in the specimen to the outer surface. The difference between these times, AB, is a measure of the time taken for the pulse to travel the extra distance through the larger specimen. From this an estimate of the velocity of the pulse in the material can be obtained. For this purpose the point O need not be the time of origin of the explosion, but a point representing a common occurrence for the two tests.

The comparison of the velocity of wave obtained from experiments and the values from theory is discussed in the Conclusions.

TABLE 6.1.

| Figure Number | Inner Radius (a) (mm) | Outer Radius (b) (mm) | Wall Thickness (b-a) mm | Ratio b/a | Peak Displacement μ m | Wave Velocity cm/sec |
|---------------|-----------------------|-----------------------|-------------------------|-----------|---------------------------|----------------------|
| 6.11(a) | 15 | 25.5 | 10.5 | 1.7 | 75 | 2.7×10^5 |
| 6.11(b) | 15 | 25.5 | 10.5 | 1.7 | 80 | 2.7×10^5 |
| 6.11(c) | 15 | 25.5 | 10.5 | 1.7 | 70 | 2.7×10^5 |
| 6.12(a) | 16 | 26.0 | 10.0 | 1.6 | 41 | 2.66×10^5 |
| 6.12(b) | 11 | 26.0 | 15.0 | 2.36 | 30 | 2.66×10^5 |
| 6.13(a) | 10.5 | 23.5 | 13.0 | 2.24 | 90 | 2.88×10^5 |
| 6.13(b) | 10.5 | 23.5 | 13.0 | 2.24 | 100 | 2.88×10^5 |
| 6.13(c) | 10.5 | 23.5 | 13.0 | 2.24 | 122 | 2.88×10^5 |

6.5 CONCLUSION.

As mentioned in Chapter 1, the dynamic behaviour of viscoelastic materials such as rubber and plastic is radically different from that of metal which respond in a way that is, in comparison, almost perfectly elastic. Viscoelastic materials are characterised by their highly dispersive nature, i.e. their elastic-properties vary strongly with frequency. Consequently the results of experiments involving the propagation of pulses in those materials are very difficult to interpret satisfactorily. For example, the stress pulse produced by the wire explosion, contains a wide range of Fourier components which, on account of dispersion, travel with different velocities through the media. Further, that the attenuation of these components by internal friction processes increases with frequency (Kolsky, (1953)), means that the net result is a change in shape of the pulse as it travels through the specimen. This effect has been well illustrated by Kolsky (1956), and Davies and Hunter (1963) in their studies of the propagation of stress pulses along rods of various polymers. Using rods of sufficient length so that dispersion effects due to lateral inertia was negligible (i.e. any dispersion was attributed to properties of the material), Kolsky obtained displacement-time records for the ends of the rod specimens which showed varying degrees of distortion of the pulse. His records showed a number of steps in the displacement corresponding to reflections of the pulse at the end of the rod, and the distortion appeared as a rounding-off of these steps. This rounding-off was more severe for later reflections and more pronounced the greater

the internal friction coefficient of the material. In particular, for polythene having the highest coefficient of internal friction, the pulse rapidly lengthened after only a few reflections and the motion of the end of the rod became almost continuous.

The Nylon and Nylatron GS used in the present investigation are ~~X~~ high polymers and would be expected to behave in a manner similar to that described above for polythene, the nature of the displacement records for some cylinders seems to point to marked dispersion effects, in others the steps corresponding to pulse reflections are very sharp.

The measurements of wave velocities presented in Table 6.1 are the average velocity of reflections through the specimen. It is interesting to note the consistency of the pulse velocity as constant for all tests made. The average value of the wave velocity obtained in this investigation is 2.65×10^5 cm/sec. for Nylon and 2.7×10^5 cm/sec. for Nylatron. This represents an approximation to the limiting dilational wave velocity, c_e for Nylon (Hunter (1960)), Kaye and Laby a value of 2.62×10^5 cm/sec. and Davies and Hunter (1963) obtained a value of 1.6×10^5 cm/sec. for the longitudinal wave velocity of propagation in Nylon (Polycaprolactam) derived from their measurements of dynamic modulus and density ($c = (E/\rho)^{1/2}$). If the value of Poisson's ratio given in Davies and Hunter (1963) is 0.37, then the corresponding dilatational wave velocity c_e is 2.2×10^5 cm/sec. (calculated using equation 5.5 in Chapter 5).

$$c_e = \left[\frac{E_D (1 - \nu)}{\rho (1 + \nu)(1 - 2\nu)} \right]^{1/2}$$

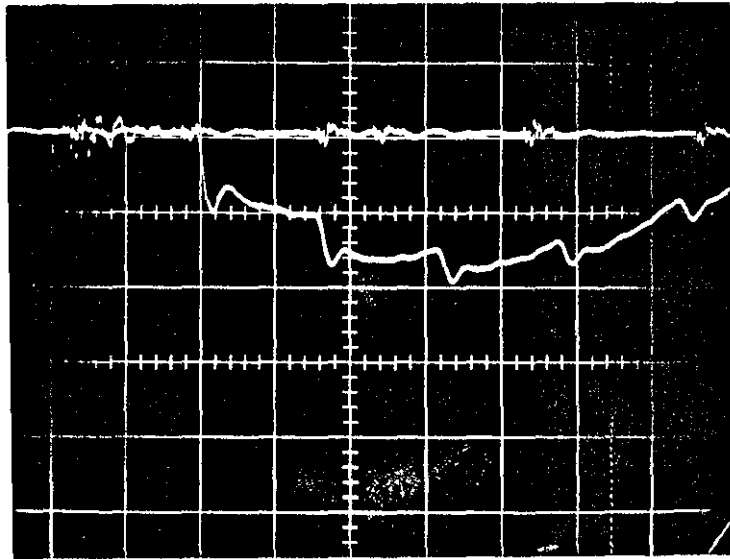
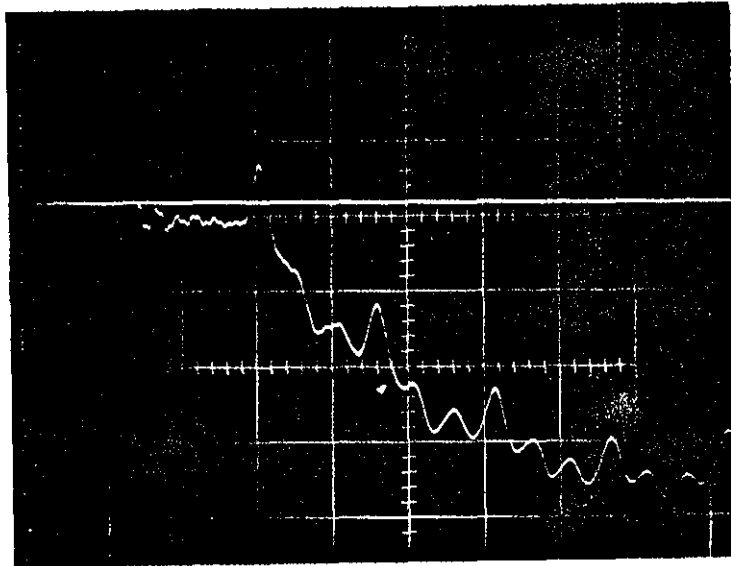
The calculation of dilatational wave velocity c_e for Nylatron GS is found to be 2.4×10^5 cm/sec. (Poisson's ratio for Nylatron is 0.35). Although care must be exercised when comparing values of velocities obtained under conditions where the strain rates differ, it is seen that the present investigation has yielded results which compare well with those of others and with the theory.

While a value of the wave velocity may be derived from the displacement measurement which has been made, it is clear that there is dispersion present, so that each frequency component of the pulse will have its own velocity so that it is necessary to exercise caution in specifying a wave velocity for the material if one assumes for this purpose that the material behaves elastically, then it would be possible in view of the consistency of the wave velocity measurement to specify a reasonable exact value of the materials modulus. However as has been stated, materials such as nylon behave visco-elastically and a proper analysis of the exploding wire test should be mirrored in the specification of a visco-elastic constitutive relationship for these materials.

It is found difficult to compare the values of peak displacement measured from the experiment with values calculated in Chapter 5, because the tests were made under different conditions of loading for the reasons mentioned earlier.

Figure 6.15 is the displacement-time records for nylon, shows the ripples occurred in place of the discontinuities, some of the ripples are negative and others are positive. These tests were made under the same conditions as the previous tests. The rise-

time and the periods of the ripples are $1 \mu \text{ sec.}$ and $2 \mu \text{ sec.}$ respectively. It could be associated with the pressure pulse obtained in Chapter 4. There is no explanation for these ripples at the present time.



$Y=10 \text{ mV cm}$
 $X=5 \text{ }^{\mu}\text{s cm}$

FIG. 6.15

CHAPTER 7

CONCLUSIONS AND RECOMMENDATIONS

7.1 CONCLUSIONS.

To study the mechanical properties of ~~the~~ materials under dynamic loading, an exploding wire system has been set-up to produce a cylindrical shock wave resulting from the explosion inside a cylindrical specimen. High-speed schlieren photography was used to study the explosion. This technique has proved eminently suitable for showing that the blast-waves generated by exploding wires are radially and axially symmetric. The wire was photographed before and during the explosion.

Voltages of 25, 30 and 35 kv have been discharged through copper wires of sizes 22, 24, 26, 27, 29, 32 and 34 SWG each of length 14 cm. Of all the wires tested, the 24 SWG copper wire gave the highest blast-wave velocities attained of up to 4500 m/sec. for a 30 kv discharge. It was found that the efficiency of the explosion increases from about 10% for the thinnest wires to a maximum of 51.4% for 24 SWG and then decreases for larger wire diameters. These values are in reasonable accord with the values obtained by Jones and Gallet (1962) for the explosion in air.

The exploding wire technique has thus been shown to produce symmetrical blast-waves of sufficiently high pressures to satisfy the requirements of impact loading of cylindrical specimens. To verify the shock pressure and to determine the full pressure profile of the reflected blast-wave, measurements were made using Pyrex pressure bar gauge. Peak pressures of up to 2000 atmospheres were obtained and are in good agreement with the calculated values from blast-waves theory. The small differences between the calculated and measured peak pressures were due to the accuracy

of positioning the pressure bar at the exact inner radius of the cylinder. By placing the bar \mp 2 mm from the inner surface of the cylinder, changed the pressure by a factor of \mp 8%.

The rise-time of the pressure signal is intimately connected with the high frequency response of the pressure bar. The measurements of the rise-time of the pressure signals obtained for different lengths and diameters are in good agreement with the theoretical values presented by Jones (1966).

The pressure-time profile of 24 SWG copper wire for 30 kv discharge was used as a time dependent boundary condition in the theoretical treatment concerned with the calculations of a cylindrical specimen response.

The discontinuous-step analysis method for elastic material originated by Mehta and Davids (1966) was used because of difficulties in specific visco-elastic behaviour in a computer programme. The displacement-time variations of the outer surface of a hypothetical material having the elastic properties of Nylatron were determined. The elastic dilatational wave velocity measured from the discontinuities was found to be 2.2×10^5 cm/sec. To verify these values an experiment was performed by discharging high voltages through copper wires inside Nylatron cylinders, to obtain displacement-time records from the movement of the outer surface of the cylinder. Because of the pick-up noise interference, the measurements were made at a possible discharge energy of 2.5 kilo - Joules corresponding to a voltage of 20 kv. The general form of the displacement shows a very good reproducibility and the average value of the dilatational wave velocity through

Nylon and Nylatron calculated are 2.65×10^5 and 2.7×10^5 cm/sec. respectively and these values compared well with values obtained from the theory even though these tests were made under different conditions. The strain-rate measured is of the order of 10^4 /sec.

The investigation of the aspects of the experiment which are described above have shown that the exploding wire method with cylindrical geometry for the specimen shows a good deal of promise as a method for determining the dynamic mechanical behaviour of materials. Early experiments with an exploding wire method using an aluminium cylinder showed a very large amount of pick-up and it was found impossible to reduce this so that reasonable displacement record could be obtained. The main work described in this thesis involves the use of Nylon and Nylatron cylinders. Since with ^{an} insulating behaviour the amount of pick-up could be reduced to a level sufficient for measurement of the displacement.

While the discontinuous-step analysis here has been applied on the simplifying assumption that the material behaves elastically, the interpretation of the experimental results are necessarily incomplete. The positive identification of the constitutive behaviour of these materials must await the successful outcome of a computer ^{programme} based on discontinuous-step analysis which include amongst other parameters a strain-rate term and a yielded stress.

7.2 Recommendations for Future Work.

(i) Because of the difficulty of measuring the displacement-time of a cylindrical specimen at 25, 30 and 35 kv discharge, it

is desirable to measure the shock wave velocity at lower discharge energy in order to calculate (a) shock pressure, (b) use of the pressure in the theoretical treatment of visco-elastic material,

(ii) In order to measure a pressure pulse of very ^{short} rise-time, it is necessary to use smaller lengths of pressure-bars.

(iii) The present analysis of the method has been confined to the elastic case and clearly it is important to develop a discontinuous-step analysis method to cover the cases of plastic and visco-elastic wave propagations using the reflected pressure as an input boundary condition in the theoretical treatment of the material.

(iv) Further investigation is required to explain the presence of the spikes occurring in the displacement records, and why the magnitude of the spikes decrease with increasing time.

REFERENCES

REFERENCES

1. Alter, B.E. and Curtis, C.W. (1956) J.Appl. Phys., 27. 1079.
2. Arenz, R.J. (1964) J.Appl. Mech., 31. 17.
3. Arenz, R.J. (1965) J.Appl. Mech., 32. 303.
4. Becker, R. (1922) Z.Phys., 8. 321.
5. Bell, J.F. (1951) Johns Hopkins. Univ.Tech.Report No.!
6. (1966) J.Mech. Phys.Solids., 14. 309.
7. (1968) (Springer-Verlag, N.Y.).
8. Bennett, F.D. (1958) Fluids. Phys., 1. 347.
 (1958) " " ., 1. 515.
 (1962) " " ., 5. 102.
9. Berry, D.S. and Hunter, S.C. (1956) J.Mech. Phys.Solids., 4. 72.
10. Berry, D.S. (1958a) Phil.Mag., 25. 100.
11. (1958b) J.Mech. Phys.Solids., 6. 177.
12. Bland, D.R. (1958) Inst.Mech.Engrs.Conf. on High Rates and Strain.
13. Bleakney, W., Weimer, D and Fletcher, J. (1949) Rev.Sci.Instrum., 20. 807.
14. Bodner and Kolsky, H. (1958) Proc. 3rd U.S. Nat.Cong.Appl.Mech.
15. Butler, I.G. (1970) M.Sc. Thesis - Loughborough University.
16. Campbell and Doby. (1956) Proc.Roy.Soc.(A). 236. 24.
17. Chace, W. and Moore, H. (eds) (1959-1965) Exploding Wires 1,2,3,4 (Plenum Press N.Y.)
18. Chadwick, P. and Morland, L.W.(1969) J.Mech.Phys.Solids., 17. 419.
19. Chalupink, J.D. and Ripperger, E.A. (1966) Exp.Mech., 6. 547.
20. Charles, H. (1951) Bull.Soc.Roy.Sci.Liege. 20. 195.
 AMR. 4. (1951).Rev. 4392.

21. Chiddister and Malvern. (1963) Exp.Mech. 3. 81.
22. Chou, P.C. and Koenig, H. (1966) J.Appl.Mech. 313. 159.
23. Chree, C. (1889) Trans.Camb.Phil.Soc. 14. 250.
24. Conn, A.F. (1965) J.Mech.Phys.Solids. 20. 195.
25. Curtis, C.W. (1954) Amer.J,Appl.Phys. 25. 928.
26. Davies, R.M. (1948) Phil.Trans.Roy.Soc.A.240. 375.
27. (1956b) British J.Appl.Phys. 7. 203.
28. (1956a) Surveys in Mechanics. C.U.P. 64.
29. Davies, E.H. and Hunter S. (1963) J.Mech.Phys.Solids. 11. 155.
30. Dillon, D.W. (1967) J.Mech.Phys.Solids. 15. 241.
31. Dixon, H.B. (1903) Phil.Trans. A.200. 315.
32. Donnell, L.H. (1930) Trans. ASME. 52. 153.
33. Dunwoody, J. (1966) Int.J.Engog.Sci. 4. 277.
34. Duvall, G.E. (1962) Appl.Mech.Rev. 15. 849.
35. Duwez, P.E. and Clark, D.S. (1947) Proc.Amer.Soc.Test.Mat. 47. 502.
36. Earnshaw, S. (1860) Trans.Roy.Soc.(London). 150. 133.
37. Edwards, D.H. (1958) J.Sci.Instr. 35. 346.
38. Ensminger, R. (1965) Ph.D. Thesis. University of Washington.
39. Ensminger, R. and Fyfe, I. (1966) J.Mech.Phys.Solids. 14. 231.
40. Eubanks, R.A., Muster, D and Volterra, E. (1955) Appl.Mech.Rev. 3652.
41. Fox, G. and Curtis, C.W. (1958) J.Acoust.Soc.Am. 30. 559.
42. Fyfe, I.M. (1968) Mechanical Behaviour of Materials under Dynamic Loads (Springer-Verlag. N.Y.). 314.
43. Fyfe, I. and Ensminger, R. (1964) Exploding Wire. 3. 257. (eds. Chace & Moore, Plenum Press).
44. Fyfe, I. and Swift. (1969) Univ. Wash.Dept.Aeronautics and Astronautics Report 69. 3.

45. Garg, S.K. (1968) Z.Ang.Math. 19. 243.
46. Gaydon, A.G. and Hurlle, I.R. (1963) The Shock Tube in High Temperature Chemical Physics. Chapman and Hall London.
47. Glawz, R. and Lee, E.H. (1954) J.Appl.Phys. 25. 947.
48. Goldsmith, W. and Allen, W.A. (1955) J.Acoust.Soc.Amer. 27. No.1.
49. Graggs, J.W. (1961) Prog. in Sol.Mech. 11. 143. (eds. Sneddon & Hill) Amsterdam.
50. Green, W.A. (1960) Prog. in Sol.Mech. 1. 225. (eds. Sneddon & Hill) Amsterdam.
51. Hauser, Simmons and Dorn. (1961) A.I.M.E. Conference. 93. "Response of Metals to High Velocity Deformation".
52. Hertzberg, A. and Kantrowitz, A. (1950) J.Appl.Phys. 21. 874.
53. Hillier, K.W. (1949) Proc.Phys.Soc.London. B.62. 701.
54. (1960) Inter.Symp.on Stress Wave propag. in Materials (ed. N.Davids). 183.
55. (1961) Progress in Solid Mechanics. 2. 201
56. Hopkinson, B. (1914) Phil.Trans.Roy.Soc. A.213. 437.
57. Hopkins, H.G. (1960) Progr.Solid.Mech. (Eds. Sneddon and Hill). 1. 85.
58. (1961) Appl.Mech.Rev. 417.
59. Hugoniot, H. (1889) J.de Pecole Polytechnique. 58. 1.
60. Hultgren, R., Orr, R.L., Anderson, P.D. and Kelly, K.K. (1963) Selected Values of Thermodynamic Properties of Metals and Alloys. Wiley. N.Y.
61. Hunter, S.C. (1960) Progs.Sol.Mech. 1. 3. (eds. Sneddon and Hill).
62. (1967) "Mechanics and Chemistry of Solid Propellants". Proc. 4th Sym. on Naval.Struct.Mech. 257.
63. Jones, D.L. and Gallett, R.M. (1962) Exploding Wire. 1. 127. (Chace & Moore eds.) Plenum Press. New York.

64. Jones, I.R. (1966) Laboratoire De Recherches Sur La Physique Des Plasmas (LAUSANNE), 20.
65. Jones, I.R. (1967) Helvetica.Physica.Acta. 40. 325.
66. Karman, T., Von, Bohnenblust, H.F. and Hyers, D.H. (1942) "The Propagation of plastic waves in Tension Specimens of Finite Length." O.S.R.D. Rep. 946.
67. Karns, C.H. and Ripperger, E.A. (1966) J.Mech.Phys.Solids. 14. 75.
68. Knauss, W.G. (1968) J.Appl.Mech. 35. 449.
69. Kolsky, H. (1949) Proc.Physical.Soc. 62B. 676.
70. Kolsky, H. (1953) Stress Waves in Solids (Dover Publ).
71. (1956a) Phil.Mag. 1. 693.
72. (1956b) Proc. 2nd.Inst.Congr.Rheology. 77. (Butterworths).
73. (1958) Appl.Mech.Rev. 11. 465.
74. (1960) International Symposium on Stress Waves Propagation in Materials (ed. N. Davids). 59.
75. (1960) Naval Structural Mechanics Conference (eds. Godier and Hoff. Pergamon). 196
76. Kolsky, H. and Douch. (1962) J.Mech.Phys.Solids. 11. 195.
77. Kolsky, H. (1963) Stress Waves in Solids (Oxford).
78. (1967) Proc. 4th.Sym. on Naval Struct. Mech. 357.
79. Kraft, Sullivan and Tipper. (1954) Proc.Roy.Soc. A221. 114.
80. Kromm, A. (1948) Zeits.Ang.Mat.Mech. 28. 104.
81. Law, C.K. and Bristow, M. (1969) UTIA Technical Note No.148 Toronto.
82. Lee, E.H. and Kanter, I. (1953) J.Mech.Phys.Solids. 4. 72.
83. Lee, E.H. and Tupper, S.J. (1954) Appl.Mech. 21. 63.
84. Lee, E.H. (1955) "Deformation and flow of Solids". 129. Springer-Verlag. Berlin.
85. Lee, E.H. and Morrison, J.A. (1956) J.Polym.Sci. 19. 93.
86. Lifshitz, J.M. and Kolsky, H. (1965) J.Mech.Phys.Solids. 13. 361.

87. Lin, S.C. (1954) J.Appl.Phys. 25. 54.
88. Lindholm, U.S. (1964) J.Mech.Phys.Solids. 12. 317.
89. (1974) Phys.Inst. (Harding. eds.London).3.
90. Love, A.E. (1927) "The Mathematical Theory of Elasticity". 4th edn.-Dover Reprint
91. Malvern, L.E. (1951) Quart.Appl.Math. 8. 405.
92. (1965) Amer.Soc.Mech.Eng. 81.
"Behaviour of Materials under Dynamic Loading."
93. McNiven, H.D. and Mengi, Y. (1971) Int.J.Solids.Struct. 8. 979.
94. Mehta, P.K. and Davids, N. (1964) Final Rep.Ballistic.Res.Lab., Aberdeen. Prov.Gro. Maryland.USA. (No.3576RD).
95. (1966) A.I.A.A. Journal. 4. 112.
96. Michel, Levy, A. and Muraour, H. (1936) C.R.Acad.Sci.Paris. 202. 755.
97. (1937) C.R.Acad.Sci.Paris. 205. 1054.
98. (1938) C.R.Acad.Sci.Paris. 206. 1566.
99. Miklowitz, J. (1960) Appl.Mech.Rev. 13. 865.
100. Mok, C.H. (1968) J.Appl.Mech. 35. 372.
101. Morland, L.W. (1969) J.Mech.Phys.Solids. 17. 371.
102. Morrison, J.A. (1956) Quart.Appl.Maths. 14. 153.
103. Muller, W. (1937) Physik. 149. 397.
104. Norris, J.M. (1967) Exp,Mech. 7. 297.
105. Payman, W. (1931) Proc.Roy.Soc.(London) A 132. 200.
106. (1935) Proc.Roy.Soc.(London) A 148. 604.
107. (1937) Proc.Roy.Soc.(London) A 158. 348.
108. (1937) Proc.Roy.Soc.(London) A 163. 575.
109. Percival, C.M. (1967) Lawrence Radiation Laboratory, Livermore UCRL-50252.
110. Petschek, H., Rose, P., Glick, H., Kane, A. and Kantrowitz, A. (1955) J.Appl.Phys. 26. 83.

111. Pochhammer, L. (1876) J.Reine.Angew. Math. 81. 324.
112. Rakhmatulin, K.A. (1945) Appl.Math.Mech. 9. 1.
113. Rankine, W.J. (1870) Trans.Roy.Soc.(London). 160. 277.
114. Rarhmatulin, K. (1945) Prinkl.Mat.Mekh. 9. 91.
115. Rayleigh, J. (1910) Proc.Roy.Soc.(London). 84, 247:
116. Resler, E., Lin, S.C. and Kantrowitz, A. (1952) J.Appl.Phys. 23. 1390.
117. Riemann, B. (1876) Gesammelte Werke. 144.
118. Rosenfeld, R.L. and Miklowitz, J. (1965) J.Appl.Mech. 32. 290.
119. Sakurai, A. (1965) Acad.Press. (Holt. ed) New York. 1. 309.
120. Smith, L.G. (1945) Office of Scientific Research and Development Rept. No. 6271.
121. Sternglass, E.J. and Stuart, D.A. (1953) J.Appl.Mech. 20. 427.
122. Taylor, G.I. (1946) J.Inst.Civ.Eng. 26. 486.
123. Tennyson, Ewert and Niranjan. (1972) Exp.Mech. 12. 502.
124. Valanis, K.C. (1966) J.Appl.Mech. 33. 888.
125. Vicille, P. (1899) C.R.Acad.Sci. Paris. 129. 1228.
126. Von Karman, T. and Duwez, P. (1950) J.Appl.Phys. 21. 987.
127. Walsey, R.J., Hoge, K.G. and Cast, J.C. (1969) Review of Sci.Instr. 40. 889.
128. Walsh, E.K. (1971) Trans.Soc.Rheol. 15. 345.
129. Weimer, D.K., Fletcher, C.H. and Bleakney, W. (1949) J.Appl.Phys. 20. 418.
130. White, M.P. and Griffis, L. (1947) J.Appl.Mech. 14. 337.
131. Wood, D.S. (1952) J.Appl.Mech. 19. 521.
132. Zverev, I.N. (1950) Prikl.Mat.Mekh. 14. 295.

APPENDICES


```

DO 40 I = 1,IM
XY(I) = 0.0
XER(I) = 0.0
XSR(I) = 0.0
XSTH(I) = 0.0
XETH(I) = 0.0
XUR(I) = 0.0
XDER(I) = 0.0
XDV(I) = 0.0
40 CONTINUE
XSR(IM+1) = 0.0
DO 45 K = 1, KM
T(K) = 0.0
45 CONTINUE
E1 = E / ((1.0 + GNU) * (1.0 - (1.0 + X2) * GNU))
GNU1 = (1.0 - X2 * GNU) * (1.0 + (X2 - X1) * GNU)
WRITE (HOUT, 50) N1, N2, A0, B0, X1, B0, E7 GNU
50 FORMAT(1H0, 10X, 11HPROBLEM NO., /, 10X, 3HN1 =, 12, 3HN2 =, 12, /,
110X, 13HINNER RADIUS =, F10.4, 3HM .., 10X, 13HOUTER RADIUS =, F10.4,
2 3HM .., /, 10X, 16HCYLINDER LENGTH =, F10.4, 3HM .., /, 10X, 8HDENSITY =,
3 F8.1, 10HKGH/CM3 .., 10X, 16HELASTIC MODULUS =, E13.4, 10HN /SQ.M I,
4 10X, 15HPOISSONS RATIO =, F7.4)
WRITE (HOUT, 55) DT, KM, PD, Q0
55 FORMAT(10X, 14HTIMEINCREMENT =, F12.975HSECS., 10X,
1 16HNO. OF INTERVALS =, I4, /, 10X, 3HPD =, F12.4, 10HN /SQ.M .., 10X,
2 3HQ0 =, E12.4, 10HN /SQ.M .)
C NOW ENTER MAJOR LOOP (TIME CYCLE),
C THE BOUNDARY CONDIONS ARE SPECIFIED AS TIME FUNCTIONS
C BY THE FIRST TWO CARDS WITHIN THE LOOP (0760 AND 0707).
C
DO 95 K = 1, KM
C NOW ENTER MINOR LOOP (CELL CYCLE),
READ (MIN766) P
66 FORMAT(E10.4)
P = P + 1.00E+5
PW(K) = P
Q = Q0

```

```

DO GO I = 1, IM
IF (I.EQ. IM) GO TO 75
XDER(I+1) = (XV(I+1) - XV(I)) * DT / DR
XER(I+1) = XER(I+1) + XDER(I+1)
XSR(I+1) = E1 + (((1.0 * X2 + GNU) * XER(I+1)) + (GNU * (1.0 * X1) * XETH(I)))
XSTH(I) = E1 + ((GNU * XER(I+1)) + ((1.0 * (X2 - X1) * GNU) * XETH(I)))
IF (I=1) 74, 74, 80
74 XSTH(I) = (E * XETH(I) + GNU * (1.0 + (X2 - X1) * GNU) * XSR(I)) / GNU1
XSTH1W(K) = XSTH(1)

```

```

GO TO 80
75 XSTH(I) = (E * XETH(I) + GNU * (1.0 + (X2 - X1) * GNU) * XSR(I+1)) / GNU1
80 XDETH = XV(I) * DT / XR(I)
XSR(1) = -P
XSR(IM+1) = -Q
XETH(I) = XETH(I) * XDETH
AD = ((XSR(I+1) * XA(I+1)) - (XSR(I) * XA(I))) + (XSTH(I) * (XA(I) - XA(I+1)))
XDV(I) = AD * DT / XM(I)
XV(I) = XV(I) + XDV(I)
XDUR = XV(I) * DT
XUR(I) = XUR(I) + XDUR
XURW(K) = XUR(IM)

```

```

N = I
81 CONTINUE
90 CONTINUE
T(K+1) = T(K) + DT
95 CONTINUE
WRITE (MOUT, 97) (K, T(K), XURW(K), XSTH1W(K), PW(K), K=1, KM)
97 FORMAT (1H0, 480 (16, E15, 3, 3E15, 4//))
8 IS THIS LARGE A REPEAT COUNT INTENDED AT ABOUT COLUMN 19, LINE 0123

```

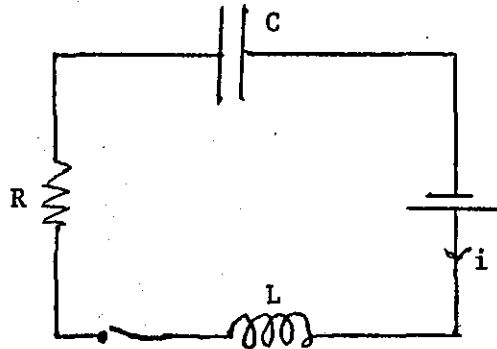
```

WRITE (MOUT, 98)
98 FORMAT (1H1)
WRITE (MOUT, 99)
99 FORMAT (1H1)
CALL UTPAB (T, XURW, 480, 0)
CALL UTPCL
115 STOP

```

APPENDIX 2

EQUATIONS FOR AN LCR CIRCUIT



For a circuit containing a resistance R , self-inductance L , and capacitance C , in which the capacitance has an initial charge Q_0 , the following equations represent the variation in discharge current i with time t :

(i) For $R^2 > \frac{4L}{C}$

$$i = \frac{V}{\sqrt{R^2 - \frac{4L}{C}}} \cdot \exp\left(\frac{1}{2} \frac{R}{L} \cdot t\right) \left[\exp\left(\frac{1}{2} \sqrt{\frac{R^2}{L^2} - \frac{4}{LC}} \cdot t\right) - \exp\left(-\frac{1}{2} \sqrt{\frac{R^2}{L^2} - \frac{4}{LC}} \cdot t\right) \right]$$

where V is the instantaneous voltage across the capacitance.

(ii) For $R^2 = \frac{4L}{C}$

$$i = Q_0 \cdot \frac{R^2 t}{4L^2} \exp\left(\frac{1}{2} \frac{R}{L} t\right)$$

(iii) For $R^2 < \frac{4L}{C}$

$$i = \frac{\frac{V}{L}}{\sqrt{\frac{1}{LC} - \frac{R^2}{4L^2}}} \exp\left(-\frac{1}{2} \frac{R}{L} t\right) \sin \frac{1}{2} \sqrt{\frac{4}{LC} - \frac{R^2}{L^2}} \cdot t$$

For $R^2 < \frac{4L}{C}$ the current in the circuit oscillates and the natural frequency f is given by:

$$f = \frac{1}{2\pi} \sqrt{\frac{1}{LC} - \frac{R^2}{4L^2}}$$

